CELL-SURFACE INTERACTIONS IN A BREAST CANCER MODEL

A THESIS SUBMITTED TO
THE GRADUATE SCHOOL OF NATURAL AND APPLIED SCIENCES
OF
MIDDLE EAST TECHNICAL UNIVERSITY

BY
EZGİ ANTMEN

IN PARTIAL FULFILLMENT OF THE REQUIREMENTS
FOR
THE DEGREE OF DOCTOR OF PHILOSOPHY
IN
BIOTECHNOLOGY

SEPTEMBER 2017

Approval of the thesis:

CELL-SURFACE INTERACTIONS IN A BREAST CANCER MODEL

submitted by **EZGİ ANTMEN** in partial fulfillment of the requirements for the degree of **Doctor of Philosophy in Biotechnology Department, Middle East Technical University** by,

Prof. Dr. Gülbin Dural Ünver _____
Dean, Graduate School of **Natural and Applied Sciences**

Assoc. Prof. Dr. Çağdaş Devrim Son _____
Head of Department, **Biotechnology, METU**

Prof. Dr. Vasıf Hasırcı _____
Supervisor, **Dept. of Biological Sciences, METU**

Prof. Dr. Utkan Demirci _____
Co-supervisor, **Dept. of Radiology, Stanford University, CA, USA**

Examining Committee Members:

Prof. Dr. Aykut Özkul _____
Dept. of Virology, Fac. of Veterinary Med., Ankara University

Prof. Dr. Vasıf Hasırcı _____
Dept. of Biological Sciences, METU

Prof. Dr. Yıldırım Sara _____
Dept. of Medical Pharmacology, Hacettepe University

Assoc. Prof. Dr. Çağdaş Devrim Son _____
Dept. of Biological Sciences, METU

Assist. Prof. Dr. Nihal Terzi Çizmecioğlu _____
Dept. of Biological Sciences, METU

Date: 08.09.17

I hereby declare that all information in this document has been obtained and presented in accordance with academic rules and ethical conduct. I also declare that, as required by these rules and conduct, I have fully cited and referenced all material and results that are not original to this work.

Name, Last Name: Ezgi ANTMEN

Signature:

ABSTRACT

CELL-SURFACE INTERACTIONS IN A BREAST CANCER MODEL

Antmen, Ezgi

Ph.D., Department of Biotechnology

Supervisor: Prof. Dr. Vasıf Hasırcı

Co-Supervisor: Prof. Dr. Utkan Demirci

September 2017, 150 pages

Breast cancer, is one of the most commonly diagnosed cancers, has a high mortality rate. One in every eight women (12.3%) develops breast cancer at some stage of their lives and this is the cause of about 15% of cancer deaths in women and 3% of total deaths. It is therefore important to study the behavior of breast cancer cells. Measurement of the mechanical properties of cancer cells leads to new insights such as that cancer cells are softer than healthy cells. Also, metastatic cancer cells were found to be more than 70% softer than benign cells. In summary, the more deformable the cells are, the more aggressive and invasive they are. This deformation is a result of the inherent properties of the cell and also influenced by the topography of their environment. Topographical cues on a surface influence cell morphology, migration and differentiation. It was found that cancer cells and healthy cells placed on micropatterned surfaces showed differences in their attachment, migration, proliferation and nucleus deformation. The crucial point in cancer studies is to understand the deformation mechanism of cells. Actin fibers of the cytoskeleton and LINC complex proteins are very important for the maintenance of the nuclear shape.

In this study, the main assumption was that the difference in mechanical properties of malignant and benign breast cancer cells could be used as a simple and direct tool in cancer detection. We aimed to compare benign (MCF10A), malignant but noninvasive (MCF7), and malignant and highly invasive (MDAMB231) breast cells in the ability of their nuclei to deform when seeded on surfaces decorated with micro level physical cues. For this purpose, square prism shaped micropillars of

poly(methyl methacrylate) (PMMA) with a specific dimension and gaps (4x4 μm^2 widths with 4 μm gap size) which is optimal for the highest nucleus deformation were used. Quantification of the extent of deformation of cell nuclei was achieved on microscale substrate topography with the help of image analysis software, ImageJ (NIH), and its distribution Fiji. The relation between the nuclear envelope protein Lamin A/C, LINC complex protein Nesprin-2 and deformability of the nucleus was determined on micropatterned surfaces and expression levels of these proteins were quantified by real time quantitative PCR method. It was shown that there was an increase of nucleus deformation by the decrease of Lamin A/C and Nesprin-2. Moreover, the mechanism of the nucleus and cell deformation were studied by using drugs such as cytochalasin D which inhibits actin polymerization. We showed that the deformation of the nucleus of both benign and malignant cells was in a relation with actin filaments and inhibition of the actin polymerization caused a decrease in the deformation capability of the nucleus. Finally, the relation between the inhibition of actin filaments and expression levels of mechanotransduction proteins (Lamin A/C and Nesprin-2) were studied on micropatterned surfaces by using immunocytochemical staining method. It was shown that loss of actin filaments after drug treatment caused increased level of these two proteins and a decrease in the deformation capacity of the nucleus. In summary, it can be said that biomechanical properties (rigidity, elasticity, deformability) of cells can provide useful information about cancer state and they can be viewed as biological markers, which suggest an alternative identification to current proteomic techniques.

Keywords: Cell-surface interactions**,** micropatterns, poly(methyl methacrylate), nucleus deformation, breast cancer, actin polymerization inhibitor, cytochalasin D

ÖZ

MEME KANSERİ MODELİNDE HÜCRE-YÜZEY ETKİLEŞİMLERİ

Antmen, Ezgi
Doktora, Biyoteknoloji Bölümü
Tez Yöneticisi: Prof. Dr. Vasıf Hasırcı
Ortak Tez Yöneticisi: Prof. Dr. Utkan Demirci
Eylül 2017, 150 sayfa

Meme kanseri, en sık saptanan kanserlerden biridir ve yüksek bir ölümlülük oranına sahiptir. Her sekiz kadından biri (% 12.3) hayatlarının bir aşamasında meme kanseri geliştirmektedir ve bu, kadınlarda kanser ölümlerinin yaklaşık% 15'inin ve toplam ölümlerin yaklaşık % 3'ünün nedenidir. Bu nedenle meme kanseri hücrelerinin davranışını incelemek önemlidir. Kanser hücrelerinin mekanik özelliklerinin ölçülmesi, kanser hücrelerinin sağlıklı hücrelere göre daha yumuşak olduğu gibi yeni anlayışlara yol açmaktadır. Ayrıca, metastatik kanser hücrelerinin benign (iyi huylu) hücrelere göre % 70 oranından daha fazla yumuşak olduğu bulunmuştur. Özetle, hücreler ne kadar bozulabilir olabilirse, o kadar agresif ve invaziv olurlar. Bu bozulma, hücrenin kendine özgü özelliklerinin bir sonucudur ve çevrenin topografyasından etkilenir. Yüzeydeki topografik sinyaller hücre morfolojisi, göçü ve farklılaşmasını etkiler. Mikro desenli yüzeylere yerleştirilen kanserli ve sağlıklı hücrelerin bağlanma, göç, çoğalma ve çekirdek bozulmalarında farklılık gösterdiği bulunmuştur. Kanser çalışmalarındaki en önemli nokta, hücrelerin bozulma mekanizmalarını anlamaktır. Hücre iskeletinin aktin filamentleri ve LINC kompleks proteinleri nükleer şeklin korunmasında çok önemlidir.

Bu çalışmada, ana varsayım, kötü huylu (malignant) ve iyi huylu (benign) meme kanseri hücrelerinin mekanik özellik farklarının, kanser tespitinde basit ve doğrudan bir araç olarak kullanılabileceğidir. Biz, benign (MCF10A), malignant ama invaziv olmayan (MCF7) ve malignant ve yüksek invaziv (MDAMB231) meme hücreleri

mikro seviyeli fiziksel sinyaller ile donanmış yüzeylere ekildiklerinde, çekirdeklerinin bozulabilme yetenekleri farkını kulanarak karşılaştırmayı amaçladık. Bu amaçla en yüksek çekirdek deformasyonu için en uygun olan spesifik boyut ve aralıklara sahip (4 μm aralık boyutlu 4x4 μm^2 genişliklerde) poli(metil metakrilat) (PMMA) kare prizma şeklinde mikro sütunlar kullanılmıştır. Hücre çekirdeğinin bozulma derecesinin nicelendirilmesi mikron boyutlu yüzey topografisi üzerinde görüntü analiz yazılımı, ImageJ (NIH) ve dağıtımı Fiji yardımı ile sağlandı. Çekirdek dış kabuk proteini Lamin A/C ve LINC kompleks proteini Nesprin-2 ile çekirdek bozulması arasındaki ilişki mikro desenli yüzeylerde belirlendi ve bu proteinlerin ifade seviyeleri gerçek zamanlı kantitatif PCR yöntemi ile nicelleştirildi. Lamin A / C ve Nesprin-2 azalmasıyla çekirdek bozulmasında bir artış olduğu gösterildi. Ayrıca, çekirdek ve hücre bozulmasının mekanizması, aktin polimerizasyonunu inhibe eden sitokalasin D gibi ilaçlar kullanılarak incelendi. Hem benign hem de malignant hücrelerin çekirdeğinin bozulmasının aktin filamentlerle ilişkili olduğunu ve aktin polimerizasyon inhibisyonunun çekirdeğin bozulma kabiliyetinde azalmaya neden olduğunu gösterdik. Son olarak, aktin filamentlerinin inhibisyonu ile mekanotransdüksiyon proteinlerinin (Lamin A / C ve Nesprin-2) ifade seviyeleri arasındaki ilişki, mikro desenli yüzeyler üzerinde immünositokimyasal boyama yöntemi kullanılarak araştırılmıştır. İlaç uygulanmasından sonra aktin filamentlerinin kaybedilmesinin, bu iki proteinin seviyesinin artmasına ve çekirdek bozulma kabiliyetinde azalmaya neden olduğu gösterilmiştir. Özetle, hücrelerin biyomekanik özellikleri (sağlamlık, esneklik, deforme olabilme) kanser durumu hakkında yararlı bilgiler sağlayabilir ve mevcut proteomik tekniklere alternatif bir tanımlama öneren biyolojik belirteçler olarak görülebilir.

Anahtar kelimeler: Hücre-yüzey etkileşimleri, mikrodesenler, poli(metil metakrilat), hücre çekirdeği deformasyonu, meme kanseri, aktin polimeraz inhibitörü, sitokalasin D

Dedicated to my lovely family

ACKNOWLEDGEMENTS

"Imagination is more important than knowledge. Knowledge is limited. Imagination encircles the world." Albert Einstein

I would like to express my gratitude to my thesis supervisor, Prof. Dr. Vasıf Hasırcı, who has taught me how to use scientific knowledge since my undergraduate education. He has always been an example and a guide to me. Without him, my imagination would have remained limited.

I am deeply grateful to my co-supervisor, Prof. Dr. Utkan Demirci, for his support and guidance. He opened the doors of his laboratory in Harvard-MIT to me, and allowed me to have an experience I could never forget. He has always been supportive of my future plans.

I would like to give my infinite thanks to Prof. Dr. Nesrin Hasırcı. She has always been like a mother to me and has been a role model as a female scientist.

I present my endless thanks to Prof. Dr. Aykut Özkul and Prof. Dr. Çağdaş Son for taking place in my thesis monitoring committee and for their time and patience during my doctorate period. You have always been guides for me.

I would like to extend my gratitude to Dr. Nihal Engin Vrana. He has been the most important guide for me in making decisions about the future. Time and effort he spent on my endless questions were so valuable to me. He is the perfect example of a scientist and a human being.

I give my deepest love and thanks to my lovely family. I would like to thank my brother, Taylan Antmen, for making me feel lucky to have a brother like him. He always encourages me to love science more. I thank my dear father, Ahmet Antmen, for raising me to be a woman who can stand on her own two feet. He is the greatest influence to my perspective on life. I also want to thank my mother, Elif Antmen. I

am so grateful to you for your tenderness, for the joy, energy and hope you give us and all people around you. I am grateful to you for being the best role model as a woman in my life. It would be a great success for me if I could have even half of your personality. I love you all so much. I am so lucky to have you.

I offer my deepest thanks and love to my companion, best friend, and partner in life, Ali Altunsoy. Thank you so much for your endless effort, support and trust you have given me. Without you, my hope and faith for the future would be missing.

One of the things that makes you so real is friendship. I would like to thank Aylin Kömez and Deniz Sezlev Bilecen for always being with me on the rugged path of academic life. Thank you for the endless fun days we spent together and for your valuable friendship. I also thank Uluç and Kıvanç Bilecen for their valuable friendship. I want to thank Celal Elmacı, Ahmet Karaboğa and Ozkan Kayöz for always being my companions while running towards the same aspirations. I also thank Esin Tanya Teso for being such a perfect cousin and friend to me and for her valuable help and support.

I would like to thank all of my lab mates. I especially thank Gökhan Bahçecioğlu for being a valuable friend and a roommate. You were always there for me when I needed a friend. I would like to thank my roommates Cemile Bektaş and Menekse Ermiş Şen for sharing countless days worth remembering. I also thank Menekşe for all the endless days spent on our paper and for being the answer to all problems outside the lab. I want to thank Çağla Mirasyedioğlu for her friendship and endless cheerfulness and energy. I thank Arda Büyüksungur for his help in my earlier times. I thank Gözde Eke, Tuğba Dursun, Esen Sayın, Senem Büyüksungur, Selcen Alagöz, Emre Ergene, Elbay Malikmamadov and Dilara Tamay for their friendship. I also thank Onur Hastürk, a graduate of our laboratory, for his help in AFM imaging and his friendship. I would like to thank the laborer of our group, Zeynel Akın, Ramazan Kavak and Yüksel Güneş for their help and effort throughout these years.

This study was supported by TÜBİTAK and I would like to acknowledge to TÜBİTAK for their support through BİDEB 2211C Ph.D. Scholarship.

TABLE OF CONTENTS

LIST OF TABLES

TABLES

LIST OF FIGURES

FIGURES

LIST OF ABBREVIATIONS

AFM	Atomic Force Microscopy
ALP	Alkaline Phosphatase
BSA	Bovine Serum Albumin
CA	Contact Angle
CLSM	Confocal Laser Scanning Microscopy
CO_2	Carbon Dioxide
DAPI	4', 6-diamidino-2-phenylindole
DMEM	Dulbecco's Modified Eagle Medium
DMSO	Dimethyl Sulfoxide
E	Young's Modulus
ECM	Extracellular Matrix
EDTA	Ethylenediaminetetraacetic Acid
EGF	Epidermal Growth Factor
FAK	Focal Adhesion Kinase
FBS	Fetal Bovine Serum
FITC	Fluorescein Isothiocyanate
LINC	Linker of Nucleus and Cytoskeleton
MW	Molecular Weight
OsO4	Osmium Tetroxide
PBS	Phosphate Buffer Saline
PDMS	Poly(dimethylsiloxane)
PEG	Polyethylene Glycol
Pen/Strep	Penicillin/Streptomycin
PIPES	Piperazine-N, N'-bis(ethanesulfonic acid)
PMMA	Poly(methyl methacrylate)

RGD	Arginine Glycine Aspartic Acid Sequence
RMS	Root Mean Square
SEM	Scanning Electron Microscopy
TCPs	Tissue Culture Polystyrene
UTS	Ultimate Tensile Strength

CHAPTER 1

INTRODUCTION

1.1. The Cell

1.1.1. The Organelles and Organization of a Mammalian Cell

Cells are the smallest unit of a living organism. They have a dynamic nature and undergo different types of intracellular and extracellular events to maintain biological functions such as cell-cell communication, maturation, migration, proliferation, differentiation and apoptosis. Cells adapt themselves to changes in their physiological microenvironment and perform a variety of functions: the synthesis, storage and transport of molecules, the expression of genetic information, and transmission and transduction of signals. They also convert energy from one form to another and respond to external environments by altering their structure (Ingber et al, 1995).

All mammalian cells consist of a membrane, cytoplasm, nucleus and a cytoskeleton. Plasma membrane is a lipid bilayer containing some proteins and polysaccharides. The membrane functions as a barrier and controls the transfer of the molecules between the inside and outside of the cell. Membrane proteins link the membrane to the cytoskeleton, ECM, or other cells. Interior of a cell is the cytoplasm which carries the organelles and a nucleus. Cytoskeleton of a cell is a large protein filament network. Cytoskeleton also defines the cell shape and provides its resistance to deformation and elasticity. Major component of the cell is the nucleus. All nuclei of mammalian cells have a nuclear envelope, nucleoplasm, nuclear lamin and nuclear pore complex (Figure 1.1) (Unal et al, 2014).

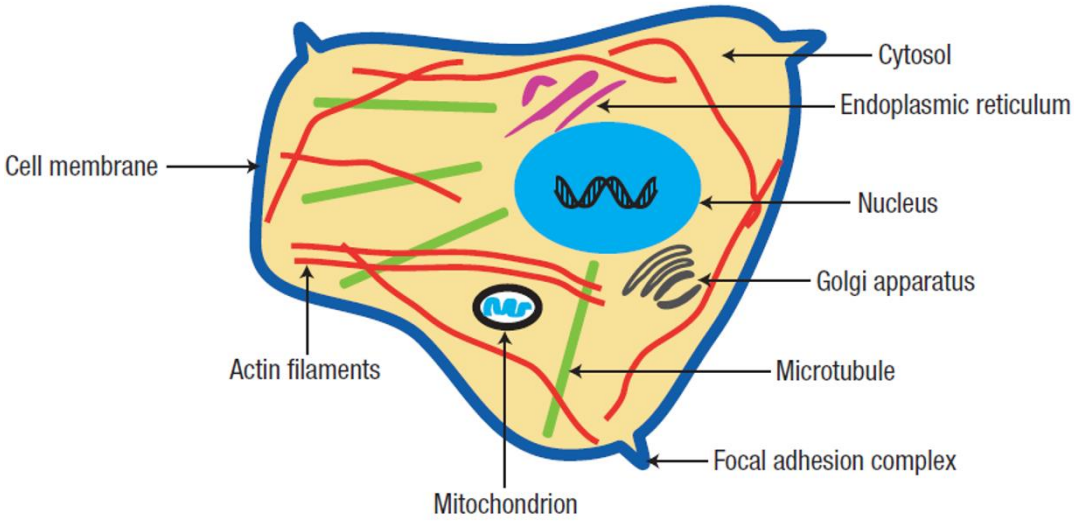

Figure 1.1. Schematic illustration of cellular architecture showing the nucleus and major structural components of the cytoskeleton (Bao and Suresh, 2003).

Cells also undergo mechanical deformation when subjected to external forces and physical constraints. Deformation characteristics of cells can provide valuable information about their biological and structural functions. Most of the biological cells are 1–100 μm in size. The resistance of single cells to physical forces ranges from 10^2 to 10^5 Pa. The deformability of cells is determined largely by the cytoskeleton, whose rigidity is influenced by the mechanical and chemical environments including cell-cell and cell-ECM interactions. (Bao and Suresh, 2003).

The viscoelastic properties of cells are very important for their function and they have been studied using substrates decorated with micro and nanoscale features or using novel approaches such as AFM (Atomic Force Microscopy) either by applying suction or impedance. 2D and 3D topographical cues on a surface influence cell morphology, migration and differentiation. It is known that cancer cells and healthy cells placed on surfaces decorated with micro sized patterns (micropatterned surfaces) show differences in their attachment, migration, proliferation and also nucleus deformation. An important point in cancer studies is to understand the

deformation mechanism of cells and actin fibers of the cytoskeleton are very important in the maintenance of the nuclear shape (Rowat et al, 2008).

In this study, the aim was to study the difference in the stiffness of cancer and healthy cells and to use this information to distinguish them from each other. This difference was then quantified by measuring the extent of nuclear deformation on micropatterned surfaces. All these enabled us to determine the main mechanistic factors controlling the cell shape. Actin inhibitor drugs will be used to specifically study the role of actin on the carcinogenicity.

1.1.1.1. Nucleus and Cytoskeleton

The nucleus is the major component of a eukaryotic cell since it stores the genetic material DNA which provides the characteristics of the cell and its metabolic functions. It has a diameter of about 5 to 15 μm (McGregor et al, 2016). The nucleus is separated from the cytoplasm by a double membrane known as the nuclear envelope (Figure 1.2), which is continuous with the endoplasmic reticulum. The nuclear envelope consists of two phospholipid bilayer membranes and the nuclear lamina. The inner and outer nuclear membranes join at the nuclear pore complexes, which allow nuclear-cytoplasmic transport. Nuclear lamina is a dense protein network consisting mostly of lamin proteins and lamin-associated proteins and underlys the inner nuclear membrane (Burke and Ellenberg, 2002). Lamin binding proteins connect the lamina to the inner nuclear membrane and stabilize the lamina network in addition to connecting lamins to chromatin structures and gene regulatory components (Unal et al, 2014).

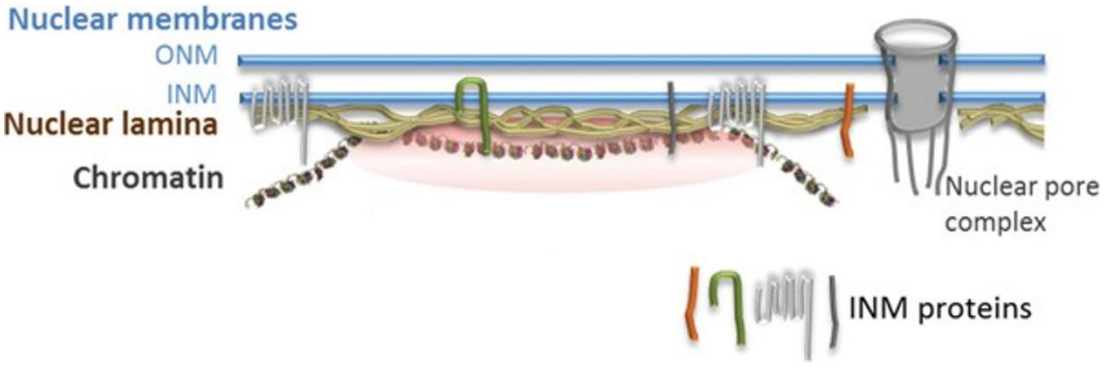

Figure 1.2. Schematic illustration of the organization of the nuclear envelope (NE) and its interaction with chromatin. NE consists of four structural units. The inner (INM) and outer (ONM) nuclear membranes are joined at the nuclear pore complex. The inner nuclear membrane is anchored by transmembrane proteins to the underlying layer of nuclear lamina and to the peripheral chromatin (Collas et al, 2014).

In eukaryotic cells, the cytoskeleton is a network of interconnected filaments and tubules that extend from the nucleus to the plasma membrane. It has three functions: it organizes the contents of the cell, it connects the cell to the external environment, and it generates forces which enable the cell to move and change its shape. There are three main types of cytoskeletal elements: microtubules, microfilaments (actin filaments), and intermediate filaments (Figure 1.3). These proteins control the shape and mechanics of cells. They are organized into networks and resist deformation but they can reorganize in response to external forces. By this way, they take role in the arrangement and maintenance of the integrity of intracellular compartments.

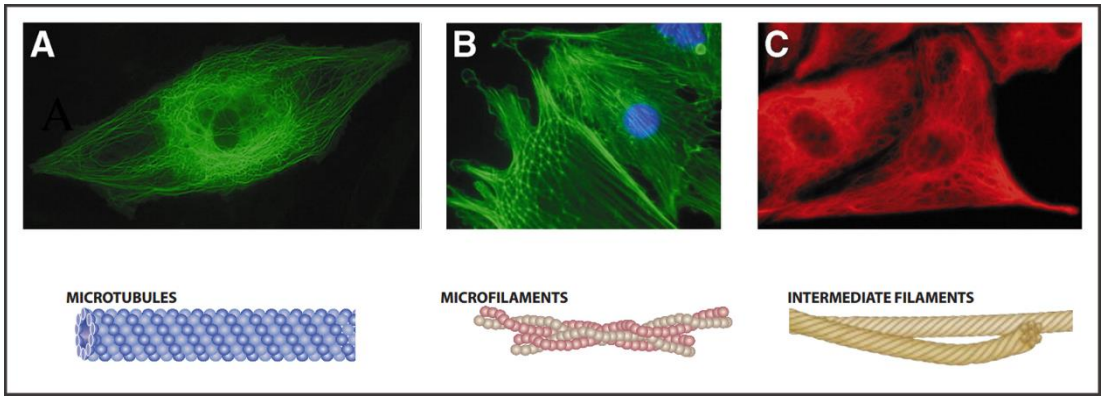

Figure 1.3. Schematic representation of the cytoskeletal elements: A- Microtubules, B- Microfilaments, C- Intermediate filaments (Adapted from Ingber, 1998, 2003).

Microtubules are made of a globular protein called tubulin. Before cell division, the microtubules assemble into a structure called spindle and distributes chromosomes in an order. After the cell division, the spindle disassembles and the microtubules reassemble. When the cell is not dividing, microtubules help the shape of cell maintain and make the organelles move (Dalby, 2005; Fletcher and Mullins, 2010). Actin filaments consist of two types of actin bundles. One type contains closely spaced actin filaments and they support projections in the cell membrane such as filopodia involved in cell sensing and lamellipodia involved in cell crawling. The second type is the stress fibers and composed of more loosely spaced filaments. They are responsible for the contraction. The ability of cells to crawl across substrate surfaces is a function of the actin cytoskeleton. Intermediate filaments are tough protein fibers in the cell cytoplasm. They are around the nucleus and extend out to the cell periphery. The intermediate filaments consist of keratin, vimentin, desmin and nuclear lamins. In cells of mesenchymal origin vimentin is the main intermediate filament protein. The filaments provide mechanical support for the cell and nucleus.

The polymerization and depolymerization of actin filaments and microtubules generate directed forces which change cell shape and guide the organization of

cellular components. Mechanical forces from inside or outside the cell can affect the activity of these regulatory polymers.

1.1.2. Mechanical Properties of Cytoskeleton and Nucleus

Three main cytoskeletal proteins are the microtubules, microfilaments and intermediate filaments. They have several differences such as their mechanical stiffness, assembly, polarity, and the type of molecular motors which they associate with. Microtubules are the stiffest of the three polymers and have the most complex assembly and disassembly dynamics. A microtubule can grow and shrink rapidly. This dynamic instability enables the microtubule cytoskeleton to reorganize. Actin filaments are much less rigid than microtubules. However, there are several crosslinkers which bind to actin filaments and make them highly organized, stiff structures (Fletcher and Mullins, 2010). Both actin filaments and microtubules are polarized polymers and they provide a suitable path for motor proteins which move preferentially in one direction. For microtubules, motor proteins are dynein or kinesin families, whereas, for actin filaments, they are myosin proteins. Microtubule-associated motors play a role in the assembly of the microtubule in interphase. Actin-associated myosin motors have a role in the alignment of actin filaments in stress fibers and enable the cells to contract and sense their external environment (Dalby, 2005). Intermediate filaments are the least stiff of the three types of cytoskeletal polymer and they resist tensile forces much more effectively than compressive forces. They can be crosslinked to each other by proteins called plectins. Many cell types assemble intermediate filaments in response to mechanical stresses and form a network which helps cells to resist shear stress (Flitney et al, 2009). Nuclear lamins are one of the widely expressed intermediate filaments and they contribute to the mechanical integrity of the eukaryotic nucleus (Dalby, 2005).

The nuclear interior is less well defined. Within the nucleoplasm, DNA is wrapped by histones which are organized into chromatin fibers. These fibers are organized into chromosomes in prophase and in the phases beyond prophase of mitosis.

Nuclear stiffness varies from as low as 0.1 to 10 kPa depending on the cell type and the method of measurement. The nucleus is significantly stiffer than the surrounding cytoplasm. Several structural proteins are also found in the nuclear interior such as nucleoplasmic lamin A and lamin C proteins, actins, myosin and spectrins (Dahl et al, 2008). Lamins provide the majority of the structural and mechanical support of the nucleus. Lamin binding proteins can further stabilize the lamina and connect it to the nuclear membrane and chromatin structures. The lamina is stiff load bearing element necessary for the structural integrity of the nucleus. A-type lamins are the main contributors to nuclear stiffness. In addition to the nuclear lamina, the nuclear interior also contributes to the mechanical behavior of the nucleus. Chromatin itself is also thought to provide mechanical stability to the nucleus. Chromatin structures have a more viscous nature than the lamina network and stretch elastically. Chromatin will also deform plastically under high mechanical stress (Gruenbaum et al, 2005; Dahl et al, 2008).

1.1.2.1. Cell Adhesion

Cells adhere to ECM with focal adhesion complexes and to neighboring cells with junctional complexes. Focal adhesion complexes consist of integrins and cytoskeleton-associated proteins such as talin, vinculin, α-actinin, paxillin, and focal adhesion kinase. Focal adhesion kinases connect the cytoplasmic tails of integrins with F-actin. Mechanical forces can be transmitted across the membrane through integrins (Zhu et al, 2000). Binding of integrin to ECM changes the shape and composition of the cytoskeleton. Forces are generated upon contraction of cytoskeleton and rigidity of ECM contributes to the conformational changes in integrin receptors and adhesion of cells (Arnaout et al, 2007). After cell adhesion, spreading occurs by integrin mediated adhesions. Actin polymerization is affected by integrin-ECM binding and membrane resisting to the external forces. Cell spreading is characterized by the competition between polymerization and depolymerization rate of actins (Figure 1.4) (Li et al, 2014).

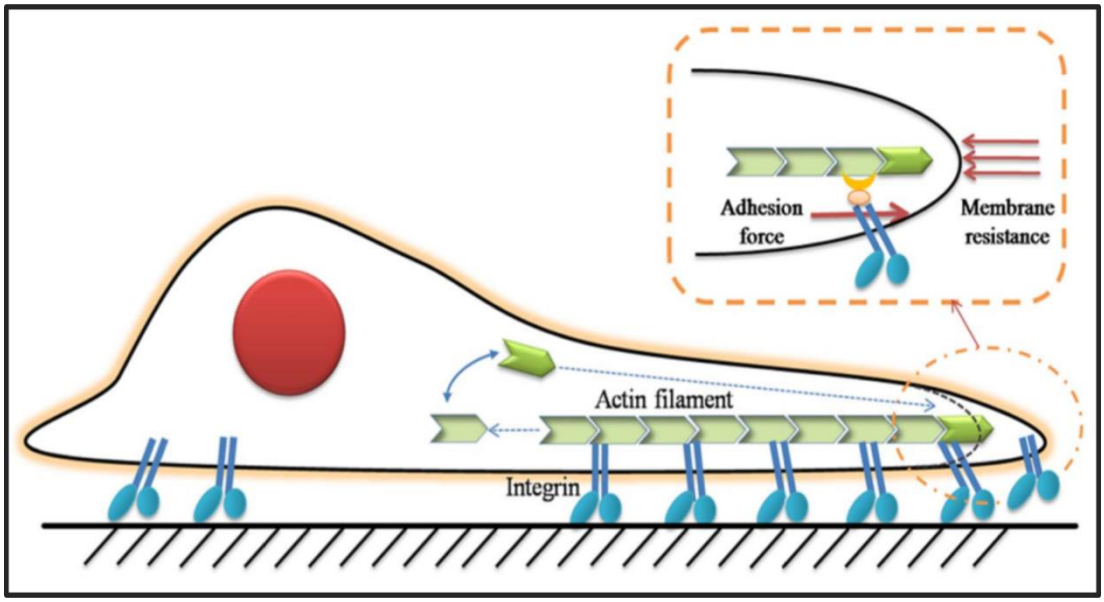

Figure 1.4. Schematic representation of cell spreading and migration over a substrate. The chemical process of actin assembly is affected by the integrin-ECM binding force and membrane resistance (Li et al, 2014).

1.1.2.2. Cell Mobility

Cell mobility and migration involve rapid changes in the dynamics of actin filaments and in the formation and disassembly of cell adhesion sites. These changes in the actin cytoskeleton and cell adhesion sites lead to the generation of membrane protrusions and traction forces. External stimuli that control cell motility are transmitted through the integrins that bind to ECM proteins (Mitra et al, 2005). During movement of cells through 3D substrates, the stiffness and density of the ECM become an additional force against the cell movement. Migrating cells can overcome these constraints by proteolytic ECM degradation, and by elastic and plastic deformations of the cell body. As a result, translocation of cells through 3D substrates is dependent on the deformability of the cell body and dynamic changes in the actin cytoskeleton (Friedl et al, 2011). In Figure 1.5, a summary of this actin dependent movement of the cells is given (Mattila and Lappalainen, 2008).

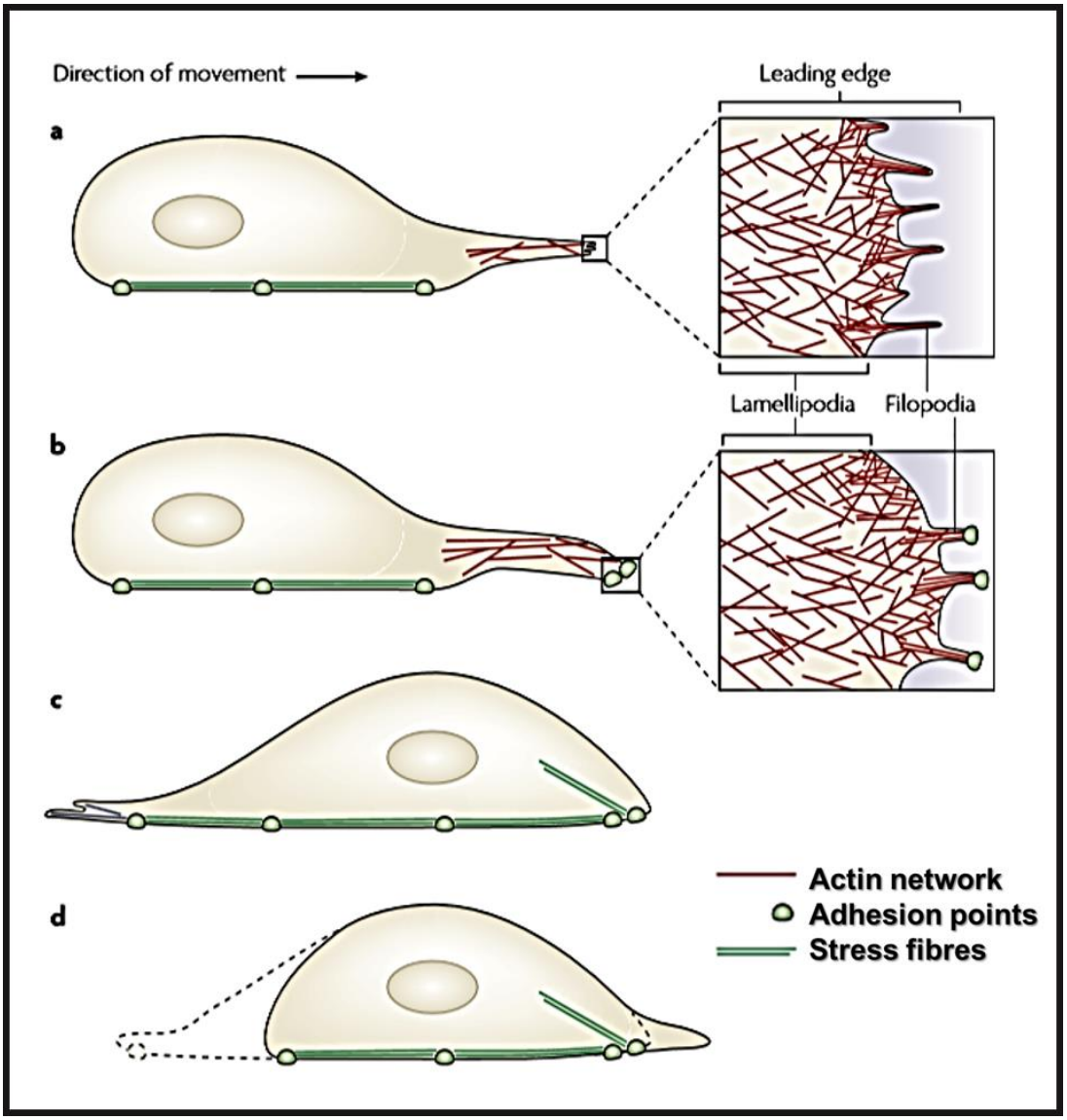

Figure 1.5. Schematic illustration of cell movement. Cell migration is dependent on actin filament structures. A- Motility is initiated by actin-dependent protrusion of the leading edge which is composed of lamellipodia and filopodia. B- New adhesions are formed under the leading edge. C- Next, the nucleus and the cell body are translocated through actomyosin-based contraction forces. D- Then, retraction fibers pull the cell forward and adhesions of the cell disassemble (Mattila and Lappalainen, 2008).

On the other hand, Figure 1.6. shows cytoskeletal organization and dynamics during migration in confined 3-D environments. Mechanism of the cytoskeleton translocating the nucleus through confined spaces includes: pushing (with actomyosin contraction at the posterior of the nucleus), pulling (with actomyosin contraction facilitated by intermediate filaments), pulling (with microtubule associated motors) and rotation (with microtubule-associated motors) (McGregor et al, 2016).

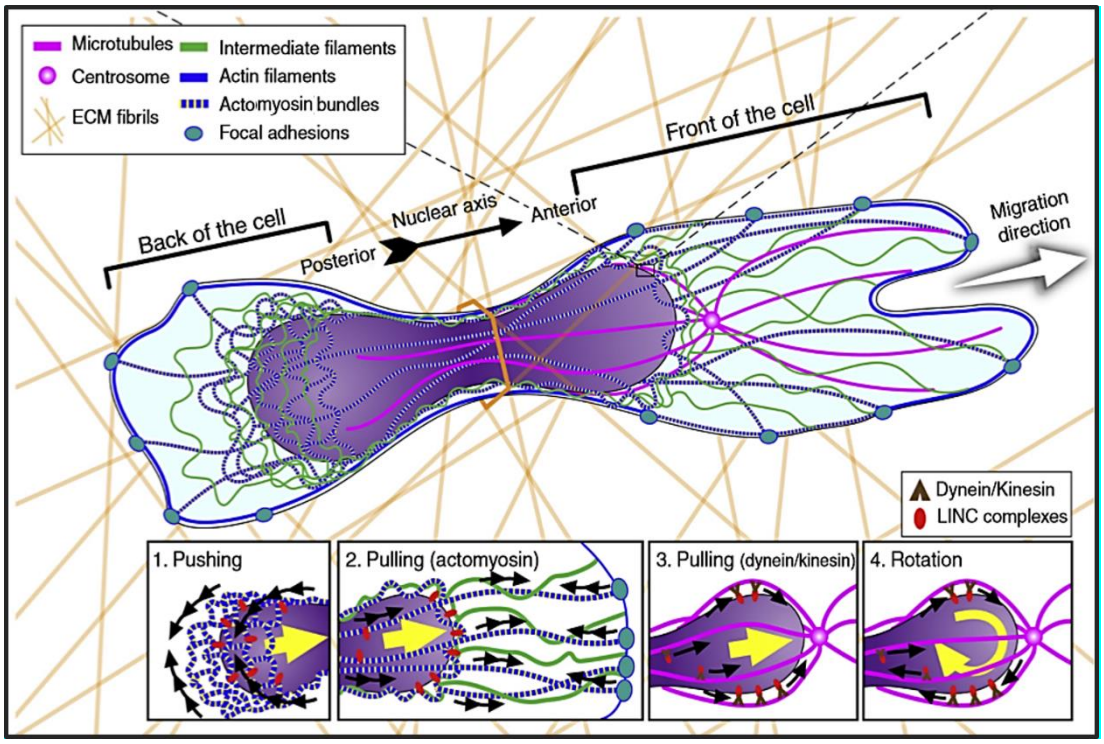

Figure 1.6. Cytoskeletal organization and dynamics during migration in confined 3-D environments (adapted from McGregor et al, 2016).

1.2. Mechanotransduction

Interactions of cells with the extracellular matrix (ECM) and the neighboring cells trigger various responses that have essential roles in the regulation of the behavior

and fate of the cell. ECM constitutes the physical and chemical microenvironment, provides a site for anchorage of cells, guides cell migration during embryonic development and wound repair and it plays other key roles in tissue morphogenesis. In addition, the ECM is responsible for the transmission of environmental signals to cells and affects proliferation, differentiation and death of a cell (Geiger et al, 2001). To grow, living organisms must sense, respond, and adapt to their physical environments at the molecular, cellular, tissue, organ and organism levels. Cells respond to mechanical cues by initiating signaling events that result in adaptations in cytoskeletal architecture and gene expression (Uzer et al, 2016).

Adhesion on the ECM is achieved by all types of adherent cells regardless of differences in their morphology, size and subcellular distribution. The adhesion of the cells is achieved by using integrins and influences the organization of the actin cytoskeleton at the cell interior (Figure 1.7.A and 1.7.B) (Mitra et al, 2005; Isermann and Lammerding, 2013; Tsimbouri, 2015). The extracellular ligands that these cellular adhesion molecules attach to include fibronectin, vitronectin and various collagens. The best characterized adhesions are the focal adhesions (Figure 1.7.B) (Geiger et al, 2001). Focal adhesions link the plasma membrane of the cell and the extracellular matrix and play a critical role in sensing the mechanical cues and in regulating the response of signaling pathway.

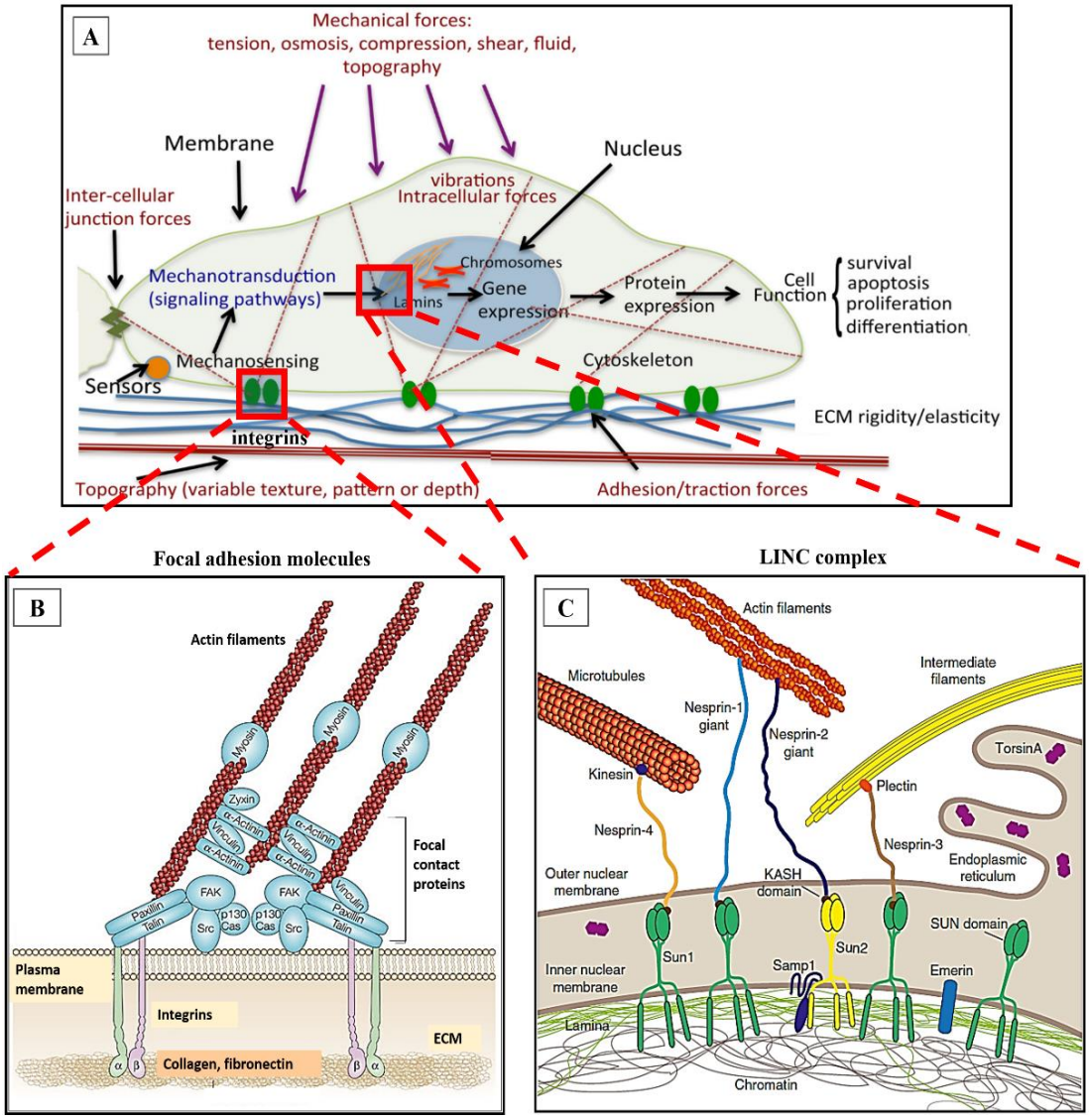

Figure 1.7. Schematic diagram of cell adhesion to a substrate and mechanotransduction. A) Schematic diagram of mechanical stimulation of cells. B) Focal contacts. C) Schematic overview of LINC complex proteins and their connections to the cytoskeleton and interior of the nucleus. (Adapted from Mitra et al, 2005; Isermann and Lammerding, 2013; Tsimbouri, 2015).

The nuclear envelope separates the nuclear and cytoplasmic compartments and serves as a mechanosensory element regulating both biochemical and physical

interaction of the nucleus with cell cytoskeleton, cell membrane and ECM (Uzer et al, 2016). It is clear that mechanical forces are important in the function of tissues and cells. Mechanotransduction is the process by which cells convert mechanical stimuli into biochemical signals. It enables cells to sense their physical environment and to respond by adjusting their structure and function. Mechanotransduction has roles in the regulation of blood pressure, remodeling of bone, maintenance of muscle and perception of touch and sound. Cell growth, migration and gene expression are influenced by mechanotransduction in most cell types (Dalby, 2005). Cells utilize a variety of mechanosensitive elements to sense applied forces and substrate stiffness including conformational changes in proteins at focal adhesions and inside the cytoskeleton (McGregor et al, 2016).

Molecular components that have a role in mechanotransduction and involved in nuclear mechanics and migration in confined environments are presented in Figure 1.7.C (Mitra et al, 2005; Isermann and Lammerding, 2013; Tsimbouri, 2015). A central role in this mechanosensory process has been attributed to lamins. Lamins are nuclear intermediate filaments and they are the major components of the nuclear lamina which is a dense protein network underlying the inner nuclear membrane. They are extended parts of the LINC (linker of nucleoskeleton and cytoskeleton) complex which enables force transmission across the nuclear envelope (Isermann and Lammerding, 2013). The LINC complex itself is composed of two protein families: SUN domain proteins at the inner nuclear membrane and KASH domain proteins at the outer nuclear membrane (Figure 1.7.C). SUN domain proteins interact with the nuclear lamina, nuclear pore proteins and other nuclear proteins at the nuclear interior; in the cytoplasm and KASH domain proteins can bind to all major cytoskeletal filament networks, including actin filaments (through the actin-binding domain of the giant isoforms of nesprin-1 and -2), intermediate filaments (by interaction of nesprin-3 with the cytoskeletal linker plectin), and microtubules (by kinesin and dynein motor proteins binding to nesprin-1, -2, -4 and KASH5) (Isermann and Lammerding, 2013). Many lamin binding proteins also interact with chromatin, particularly with silenced heterochromatic form, and the lamins have

been shown to bind to DNA directly. These interactions complete a continuous physical linkage through which deformations can be transmitted from the cell exterior to chromatin (Swift and Discher, 2014).

1.2.1. Mechanism of Nucleus Deformation

Forces applied on the cell surface result in cell responses including the reorganization of cytoskeletal elements, actin microfilaments, intermediate filaments, microtubules and nuclear structures (Dahl et al, 2008). The rigidity, or deformability, of a cell nucleus as is primarily determined by (1) chromatin as well as the nucleoskeletal organization and (2) expression and assembly of lamins as part of the nuclear lamina (Krause and Wolf, 2015).

Even though the nucleus is the stiffest cellular organelle and is 2-10 times stiffer than the surrounding cytoskeleton, extracellular forces and strain lead to clearly detectable nuclear deformations (Guilak, 1995; Maniotis et al, 1997; Guilak et al, 2000; Caille et al, 2002). Micropipette aspiration of isolated nuclei shows that nuclei exposed to shear stress have a reduced height and increased stiffness (Deguchi et al, 2005). Atomic Force Microscopy (AFM) has also been used to investigate the elastic modulus of nuclei in cells and similarly it was found that nuclei in cells under shear stress were stiffer than nuclei of control cells (Mathur et al, 2007). Studies focusing on nuclear shape and structure have revealed strong correlations between the changes in shape and cellular phenotype. Deformation of nuclear morphology, such as the increase in nuclear size, changes in nuclear shape, and loss of nuclear domains are often used to identify cancerous tissue (Zink et al, 2004). Studies of breast cancer cells show a stronger correlation between nuclear morphology and cancer than between cellular morphology and cancer (Bissell et al, 1999; Paszek et al, 1999). Many cancer types are correlated with changes in the expression of nuclear structural proteins. For example, lamins A and C are overexpressed in ovarian cancer cells compared to control cells, and increased levels of lamin B in prostate cancer strongly correlate with tumor existence (Coradeghini et al, 2006; Hudson et al, 2007).

Decrease in nuclear stiffness can also be an indicator of increased mobility of tumor cells and metastasis potential (Dahl et al, 2008). As a summary, lamins are important structures in the study of the relation between nuclear structure and cellular function.

1.3. Biomaterials Used in Cell-Material Interactions

1.3.1. Types of Substrate Materials

Biomaterials are defined as 'materials intended to interface with biological systems to evaluate, treat, augment or replace any tissue, organ or function of the body' (O'Brien, 2011). There are four types of biomaterials used as substrate materials in the studies of cell-surface interactions and tissue engineering. These are metals, ceramics, composites, polymers.

Metals are mechanically strong, tough, and ductile materials. Metallic substrates are typically used as substitutes for hard tissue replacement such as total hip and knee joints, bone plates and screws, spinal fixation devices and dental implants. Titanium (Ti) and its alloys are the most commonly used metals for dental implants. However, prosthetic components of the implants are made from gold alloys, stainless steel, and cobalt-chromium and nickel-chromium alloys. Corrosion is one of the disadvantage of metallic substrates since it may cause release of dangerous metal ions causing eventual failure and removal of implants in tissue engineering applications. Another disadvantage is the stress shielding and weakening of the surrounding tissue (Katti, 2004).

Ceramics are hard and have high compressive strength. They have similar physical properties with the mineral components of the bone. However, due to their ionic bonding within the crystals, they are brittle and they exhibit low tensile and impact strengths. As a result, they are very sensitive to notches or microcracks which propagate to fracture (Katti, 2004). Alumina, zirconia and pyrolitic carbon are some of the ceramics used as biomaterials in applications such as orthopedic and dental

implants. Titania is mostly used in the fabrication of micro and nanoscale surface structures to study cell-surface interactions.

Polymers can be both synthetic and natural. They can be easily processed to form complex shapes. Their surface properties are important in biological applications since they can be modified physically, chemically, or biochemically. They are extensively used in biomedical applications such as implantable medical devices, prostheses, dental materials, contact lenses, drug delivery systems and scaffolds for tissue engineering applications. Due to the various properties of polymeric materials, types of polymers will be shown in detail in the next section.

Composites contain two or more distinct constituent materials on the microscopic or macroscopic size scale. Many natural structures such as bone, wood, dentin, cartilage and skin are composite materials. They can provide more desirable material properties than homogeneous materials; the resultant product has much improved properties than the individual components. Some biomedical applications of composites are dental filling, bone cements and orthopedic implants with porous surfaces. In addition to these, biodegradable polymer-calcium phosphate based ceramic composites have been widely investigated as scaffold materials for bone tissue engineering applications.

1.3.2. Natural Polymers

Natural polymers can be components of the ECM such as collagen, fibrinogen, hyaluronic acid and glycosaminoglycans (GAGs). They are biocompatible and have mechanical properties similar to those of native tissues. Natural biomaterials can also be derived from plants, insects, or animals (e.g. cellulose, chitosan, silk fibroin, etc.) and they can provide favorable microenvironments for the cells (Naderi et al, 2011). They are used in many applications since they are mostly biocompatible and provide favorable environment for cell-biomaterial interactions. For example, collagen coupled with osteogenic factors such as bone morphogenetic proteins or

hydroxyapatite were shown to enhance bone tissue incorporation and widely used bone tissue engineering applications, fibronectin induces cell attachment and spreading, and it is generally incorporated onto the surface of biomaterials, fibrin has been used as cell delivery matrix as the composites of other natural substrates such as alginate or hyaluronic acid in cartilage and skin tissue engineering applications, silks were shown to exhibit high tensile strength and elasticity and also support stem cells adhesion, proliferation and differentiation, making them promising scaffolds for skeletal and connective tissue engineering applications, alginate, hyaluronic acid and chitosan exhibit a wide range of properties and physiological functions, and offer a variety of biomedical applications (Naderi et al, 2011). However, using natural materials rather than synthetic materials include restricted control over their chemical properties and the control of their degradation rates, sterilization and purification are challenging (O'Brien, 2011).

1.3.3. Synthetic Polymers

Various synthetic polymers have been used as substrates including poly(glycolic acid) (PGA), poly(lactic acid) (PLA) and their copolymers (PLGA), poly(p-dioxanone) and poly(methyl methacrylate) (PMMA). Some of these polymers are biodegradable. They can be fabricated with a designed architecture and most are biocompatible (Naderi et al, 2011). These properties make synthetic polymeric materials highly suitable for medical uses. They however have several drawbacks such as poor bioactivity (e.g., polyethylene glycol, PEG) and acidic byproducts (e.g., PGA, PLA, or PLGA). Modification of physical and chemical properties of these materials can be a solution to these problems since they can be easily controlled (Gunatillake and Adhikari, 2003). The application of biodegradable biomaterials for artificial implants have two major advantages. They do not have to be removed after use by a secondary surgery since most degradation products can be excreted from the body through natural pathways and they may lead to a better recovery of the biological system due to the progressive loss of mechanical strength of the material

while the tissue is gaining strength through regeneration (Piskin, 1995). Biodegradable synthetic polymers such as PGA and PLA have been used in many applications including sutures, drug delivery systems and orthopaedic fixation devices such as pins, rods and screws. Among the synthetic polymers, the polyesters have been attractive for these applications because of their enzymatic and hydrolytic degradation, degradation products being natural metabolites and ability to control their degradation rates through chemical modification and monomer choice (Gunatillake and Adhikari, 2003). On the other hand, nondegradable polymers are biologically stable and they can perform during the life time of the patient. For example, PMMA is mainly used as bone cements in hip and knee replacements (Dhandayuthapani et al, 2011).

1.3.3.1. Poly(methyl methacrylate) (PMMA)

Poly(methacrylates) are polymers of the esters of methacrylic acids. The most commonly used among them is poly(methyl methacrylate) (PMMA). It is the polymerized form of methyl methacrylate (Figure 1.8).

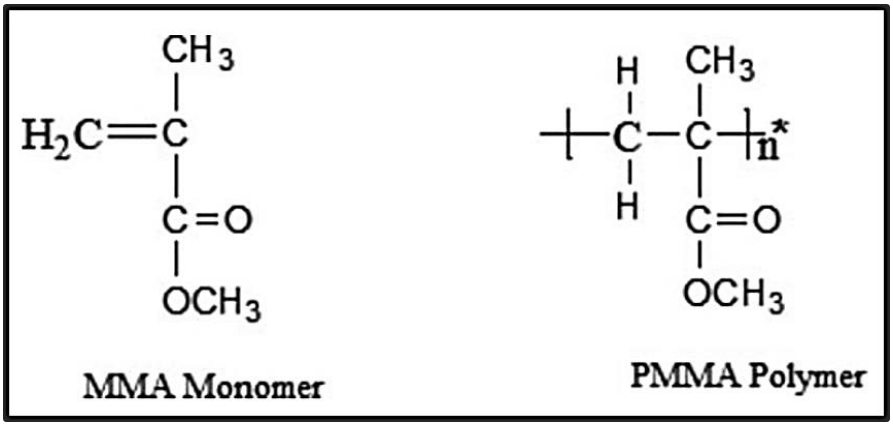

Figure 1.8. Structure of methyl methacrylate (MMA) and poly(methyl methacrylate) PMMA (Ali et al, 2015).

Poly(methyl methacrylate) (PMMA), known as the plexi glass, is an amorphous thermoplastic. It was first used in clinics as a dental device. It is biocompatible and it is easy to manipulate so it has been used commonly in other medical applications such as bone cement, contact and intraocular lenses, screws for fixation of bone and skull defects, repair and stabilization of vertebrae in osteoporotic patients. It has high rigidity, optical transparency, low density and high impact strength. It exhibits low water absorption. These properties of PMMA make it suitable to use in biomedical studies and viewing under the microscope imaging systems and also in microfluidics devices. (Punet et al, 2015).

PMMA can be produced from its monomer using different techniques of polymerization. The monomer undergoes addition polymerization reactions through free radical or ionic initiators and in solution, suspension, and emulsion techniques (Ali et al, 2015).

1.3.3.1.1. Physical, Chemical and Mechanical Properties of PMMA

PMMA is one of the amorphous polymers that belongs to the acrylate family. It has a density of 1.20 g/cm^3 at room temperature. It has a high resistance to sunshine exposure. It has very high thermal stability. It also possesses very good optical properties, with a refractive index of 1.490, and a high degree of compatibility with human tissue. PMMA swells and dissolves in many organic solvents. It also has poor resistance to many other chemicals due to its easily hydrolyzed ester groups. PMMA has a high Young's Modulus and a low elongation at break and it is one of the hardest thermoplastics with high scratch resistance (Ali et al, 2015). Due to its properties, PMMA has very wide application in science and biotechnology.

1.4. Modification of Surface Properties of Substrate Materials

The surface properties of materials in contact with biological systems affect cell-material interactions. Surface characteristics of material on micro and nano scales effect the structure and function of cells and proteins at biointerfaces in vitro. In order to obtain appropriate mechanical properties, durability, and functionality of materials, design, synthesis, and fabrication of biomaterials and devices should be optimized. Materials can be surface-modified by using biological, mechanical, or physicochemical methods. Examples of methods include micro and nano patterning of surfaces with various lithographic techniques and chemical modification of surfaces.

1.4.1. Chemical Modification

The interactions between the biological environment and biomaterials take place on the material surface and the biological response from living tissues to biomaterials depends on the surface properties such as chemical composition. Surface modification of biomaterials is used to improve the function and lifetime of the biomaterials used in medical components (Chu et al, 2002). For example, most synthetic polymers are hydrophobic and their surface should be modified to obtain a hydrophilic surface for the intended use. Chemical surface modification of biomaterials can be performed in two ways: by immobilization of certain molecules directly on the biomaterial surfaces and by changing the surface properties of the materials such as chemical composition, hydrophilicity/hydrophobicity, surface charge and roughness by using several techniques. Examples of these techniques include chemical vapor deposition (CVD), plasma vapor deposition (PVD), grafting techniques, self-assembled monolayers (SAMs), attachment of polymer chains and biomolecules, chemical oxidation by reactive solutions and ionized gas treatment. Among these, protein immobilization and plasma treatment are the most commonly used methods:

Two main classes of proteins can be immobilized on biomaterial surfaces. First group proteins are cell adhesive proteins derived from ECM such as fibronectin, laminin, vitronectin and collagen. These proteins can promote cell adhesion and enhance cell attachment. Adhesive peptides containing the Arg–Gly–Asp (RGD) sequence are also used widely and they function as a binding domain to the cell integrins. The second group includes growth factors. Immobilized growth factors can modulate cell behaviors such as proliferation and differentiation. To covalently immobilize protein molecules on the chemically inert polymeric biomaterials, reactive groups such as hydroxyl, carboxyl and amino groups are used firstly as coupling sites (Ma et al, 2007).

On the other hand, plasma surface modification is another chemical surface modification technique. Plasma is a complex mixture composed of energetic free radicals, ions, electrons, atoms, and molecules sustained by an external energy source. Plasma treatment introduces polarized groups such as hydroxyl, carboxyl, amino and sulfate groups on polymer surfaces using different reaction gases such as air, NH_3, SO_2, CO_2, O_2 or other organic compounds (Ma et al, 2007). Plasma treatment can produce highly inert surfaces consisting of fluorinated hydrocarbons, covalent bonds of bioactive molecules that inhibit cell attachment, and covalent bonds of very hydrophilic groups to improve the biocompatibility of the surface (Chu et al, 2002). By using different plasma modification methods and changing the operating conditions, such as the type of discharge, reactor geometry, flow rates, pressure, and gas species, a variety of surface chemistries can be obtained. In this study, oxygen plasma treatment of PMMA will be used to introduce covalent bonds of hydrophilic groups to PMMA surface in order to make it more compatible with the cells.

1.4.2. Physical Modification: Surface Topography

Another way of surface modification is changing the topography of the surface. Micro and nanofabrication techniques are used to change the topographies of

materials surfaces. Modifications in surface features haven been widely used for in vitro cell biology studies in order to manipulate cell adhesion and cell responses or to give surfaces sensor capabilities. The topographies either mimic typical shapes and feature sizes found in the natural environment of cells or expose them to artificial geometries. Since the size of cells and the size of adhesion proteins and their ligands are in the nanometer to micrometer scale, modifications of this level are required on the substrates. Common architectures used in the fabrication of surface topographies are pores, gratings, wells, pits, cones, posts, pillars, grooves or meshlike structures that can either be organized in a regular or irregular manner (Ermis et al, 2016; Hasturk et al, 2017; Greiner et al, 2016).

In order to create substrates with surface topographies, there are several methods such as photolithography, hot embossing, surface cracking, replica molding, phase separation micro molding, electron and focused ion beam lithography, stereolithography, direct laser writing and etc.

Photolithography uses light, a photomask and a photosensitive material (photoresist) to create a pattern in the micrometer range. The thickness of the layer of photoresist determines the height of the structures. The pattern of the photomask will determine the later dimensions of a surface structure. This method can be combined with other procedures such as physical or chemical vapor deposition in order to obtain nano scale topographies. The surface structures made by photolithography are used as a master structure for further processing.

Hot embossing also replicates micro and nanofeatures of master substrates. A thermoplastic material is pressed on the mold at an elevated temperature to form the topography of the features in the plastic. Similar to hot embossing, in soft lithography, features down to around 10 nm can be replicated.

Another method is surface cracking. It provides controlled cracks on a surface of a material and surface micro and nano structures.

Replica molding is a soft lithography technique and it uses an elastomeric soft material to replicate patterns. Micrometer-sized topographies can be produced by this method.

Phase separation micromolding is an alternative, less common microfabrication technique for structured substrates. It consists of separating a polymer solution in two phases. The phase containing the polymer solidifies by forming the replicate of the surface topography (Dhowre et al, 2015).

In Figure 1.9, a summary of the fabrication techniques including photolithography, and soft lithography is given:

	Photolithography	Soft lithography			
		Microcontact printing	Microtransfer molding	Molding in capillaries	Scanning probe lithography
Resolution	37 nm	35 nm–1 μm	250 nm	50 μm	20–30 nm
Scheme of the technique	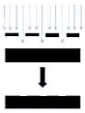	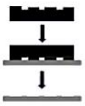	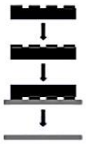		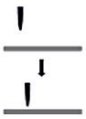
Most advantageous feature(s)	Precise control of the features	Simplicity Flexibility Allows for multipattern Applied to nonplanar surfaces	Applied to nonplanar surfaces Allows to generate 3D structures Pattern large areas	Allows to produce different patterns in a parallel fashion The use of wet patterns – broaden applications Creation of gradients	Precise control of the added groups
Most disadvantageous feature(s)	Polymers added with photosensitive compounds	Structural constraints of the stamp Low control of the ligand density	Microstructures have a thin film between the raised features	Patterned geometries limiting	Limited to a low range of patterned sizes

Figure 1.9. Micro and nano fabrication techniques (Coutinho et al, 2011).

1.5. Cell-Substrate Interaction Studies

Cells interact with their environment in several ways: 1) They generate and resist mechanical stress; 2) they secrete and sense signals; and 3) they create and identify electrical signals. The interactions of cells with their extracellular environment are mediated by cell surface receptors. ECM is a complex consisting of glycoproteins, polysaccharides, proteins, low molecular weight compounds, electrolytes and water. The interaction between the cell and ECM plays a crucial role in tissue homeostasis, mechanics and functionality. As a result, interactions of cells with biomaterial surfaces within the organism are critically important for both the cell and the organism. When cells are removed from the organism and transferred to an *in vitro* environment, they lose their specific functions and ability to differentiate due to the absence of the three dimensional tissue architecture. In order to maintain the phenotypes of cells and mimic the natural environment *in vitro*, substrates should be designed by considering the desired purpose of the study of cell-material interactions (Michaelis et al 2011). In addition to substrate properties, cell type is also a determining parameter in cell-material interactions.

1.5.1. Role of Substrate Properties in the Study of Cell-Substrate Interactions

Biocompatibility of surfaces is closely related to the response of cells that are in contact with the substrate surface. Implant coatings or modifications are commonly used to control cell attachment and spreading by means of tailored topography and chemistry (Dhowre et al, 2015). Cells interact with their microenvironment via receptors located on their membranes. Binding of antibodies or antigens to these receptors creates a receptor response. Integrins are one of these receptors and bind specifically to an arginine-glycine-aspartic acid (RGD) tripeptide sequence found in cell adhesive proteins such as fibronectin, vitronectin, laminin and collagen. Through these receptors, cells can attach to solid surfaces (Roach et al, 2007). Cells sense their surroundings using projections called lamellipodia in epithelial cells and fibroblasts or pseudopodia in neutrophils. At the ends of these projections, there are

smaller hair like structures called filopodia, composed of actin filament bundles and they have a role in sensing ECM and substrate surface. If filopodia could find a suitable binding site, cells can localize on the substrate by triggering several signaling pathways (Roach et al, 2007). As a result, chemical properties of substrates have significant importance in cell-material interactions (Dhowre et al, 2015). Substrates with engineered properties affect cellular function and processes. Three surface properties have been identified as the main determinants of cell behavior and cell fate: surface chemistry, surface topography and surface elasticity (or stiffness). The latter two are both physical characteristics and will therefore be classified together in this study.

1.5.1.1. Influence of Substrate Chemistry

The surface chemistry of an implanted material can be modified to improve cell adhesion and spreading. Surfaces have been modified with various functional groups such as methyl, hydroxyl, amino and carboxyl. The methyl and hydroxyl surfaces represent neutral hydrophobic and hydrophilic functional groups whereas amino and carboxyl surfaces show negatively and positively charged characteristics, respectively (Roach et al, 2007). Moreover, cell adhesion on surfaces containing amine functional groups has been shown to increase when compared with other functionalities such as carboxyl (negatively charged), methyl (hydrophobic) and hydroxyl (neutral and polar) groups. As the surface of cells is typically negatively charged, the presence of positive surface charges often promotes cell adhesion. Similarly, moderately hydrophilic molecules tend to promote cell adhesion to a surface (Dhowre et al, 2015). Chemical properties such as charge and wettability have been shown to affect cell adhesion or phenotype and functionality of mesenchymal stem cells (Hasturk et al, 2016). In addition to natural surface chemistry, proteins, peptide sequences (e.g. RGD) and carbohydrates have been immobilized to control cell behavior. RGD peptide sequence especially promotes integrin mediated cell adhesion to artificial surfaces (Dhowre et al 2015).

1.5.1.2. Influence of Substrate Topography

Cell shape, migration and adhesion can be influenced by surface topography of a substrate. Micron to nanometer scale topographies are smaller than the size of a cell and in the similar size range with the topography created by ECM proteins, such as collagen, fibronectin, and laminin fibers (Wang and Carrier, 2011). This size range of substrate topography may influence cell behavior at the cellular level as shown in Figure 1.10 (Greiner et al, 2016).

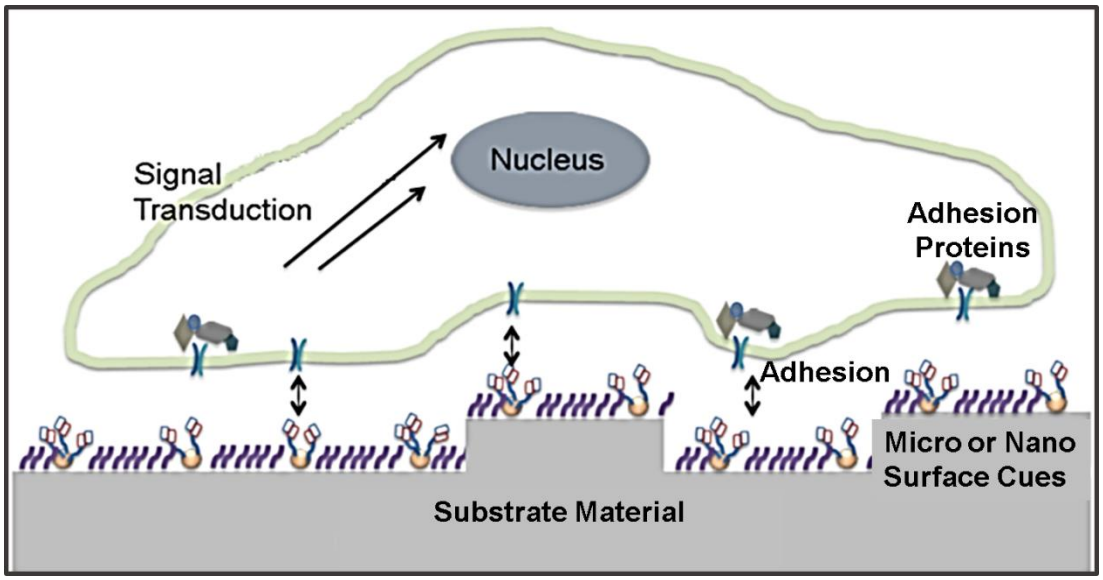

Figure 1.10. Schematic illustration of cell interaction with a micro and nanostructured surface. The surface is structured with a micropattern with dimensions corresponding to the size of cells. Adhesive receptors interact with nano surface features in the nanometer range (Greiner et al, 2016).

Harrison was the first to observe the interaction between a topography of substrate and cellular tissue when investigating spider silk fibers in 1911. Later, in 1964, it was first proposed that cells react to the topography and their environment (Curtis and Varde, 1964). Since then, several studies have shown that many cell types react

strongly to microtopography (Flemming et al, 1999; Curtis and Gadegaard, 2006; Hasirci and Kenar, 2006; Ermis et al, 2016; Hasturk et al, 2016). On patterned surfaces, changes in cell adhesion (Matsuzaka et al, 2003; Recknor et al, 2004), alignment (Clark et al, 1987, 1990; Recknor et al, 2004), morphology (cytoskeletal organization) (Wojciak-Stothard et al, 1995; Flemming et al, 1999), proliferation (Keselowsky et al, 2007), vitality (Chen et al, 1997) and gene expression and differentiation (Watt et al, 1988; Bruinink and Wintermantel, 2001; Hasturk et al, 2016) have been reported. Novel micro and nano fabrication approaches and technologies enabled the development of complex surface features with controlled pattern, periodicity, shape, and dimensional properties (Barthes et al, 2014). Several top down and bottom up techniques such as phase separation, self assembly, thin film deposition, chemical vapor deposition, chemical etching, nanoimprinting, photolithography, scanning probe lithography, and electron beam lithography (Hasirci et al, 2006) were used to produce micro and nanoscale structured environments. In these studies, mostly microgrooves were used to control cell behavior. Groove features were arranged as repeating patterns with equal groove and ridge widths. The majority of cell types cultured on these topographies aligned along the major axis of grooves and their alignment and orientation enhanced on decreasing groove width and increasing groove depth to dimensions comparable to that of the cells. Other types of topographical features include pillars, wells, and pits (Nikkhah et al, 2012). In a study fibroblast cells were cultured on PDMS pillars fabricated by soft lithography and the dimension of the pillars, such as height and spacing, were shown to influence the morphology of cell. Decreasing pillar height led to cells exhibiting morphologies as on flat surfaces indicating that shallow channels do not possess the restrictive ability (Ghibaudo et al, 2009).

Aside from chemical modification, surface roughness or micro and nanoscale three dimensional (3D) structures were shown to enhance the intrinsic hydrophobic nature of some surfaces and increased the water contact angles. The basis of topographically induced superhydrophobicity was first explained in 1936 by Wenzel who proposed that a liquid completely fills the gaps on a rough surface that it is in contact with and

the surface roughness emphasizes the intrinsic wetting tendency towards reduced or enhanced contact angle. In 1944, Cassie and Baxter suggested that water forms incomplete contact with a rough surface as air is trapped between the liquid and the solid and bridging the gaps always results in an increase in contact angle. On surfaces that display simple roughness, wetted (Wenzel) and bridging (Cassie-Baxter) states are easy to define, but complex roughness may exhibit a mixture of two states. On many surfaces, a transition from Cassie-Baxter to Wenzel state is possible, and the resistance to transition depends on the intrinsic hydrophobicity and the distance between and the shape of topographic features.

While the previous studies showed the influence of substrate topography on cell morphology and adhesion, the response of cells to microscale topographies is highly dependent on the cell type, in addition to the geometry and dimension of the features on the substrate.

1.5.2. Role of Cell Type in the Study of Cell-Substrate Interactions

ECM shows various degrees of stiffness depending on the type of the tissues as shown in Figure 1.11.

The stiffness and nanotopographical characteristics of the ECM may change in different tissues and also in disease and healthy states of the cells of various tissue types. For example, the stiffness of mammary cells decreases during breast cancer. Lung stiffness is higher in fibrotic tissues than under normal conditions. Moreover, fibroblasts respond to increases in matrix stiffness and ECM stiffening can promote fibrosis (Yang et al, 2017). Cells respond to the mechanical properties of the substrates they interact with. Mouse myoblasts show actomyosin contractility only on substrates with a stiffness similar to normal muscle, but not on softer (gel) or stiffer (glass) substrates. Furthermore, the neurogenic, myogenic, and osteogenic differentiation of human mesenchymal stem cells (hMSCs) can be induced by substrates with stiffnesses similar to brain, muscle, and collagenous bone tissues,

respectively. (Yang et al, 2017). There are more examples of various cell and tissue types showing distinctive characteristics on substrates with changing properties:

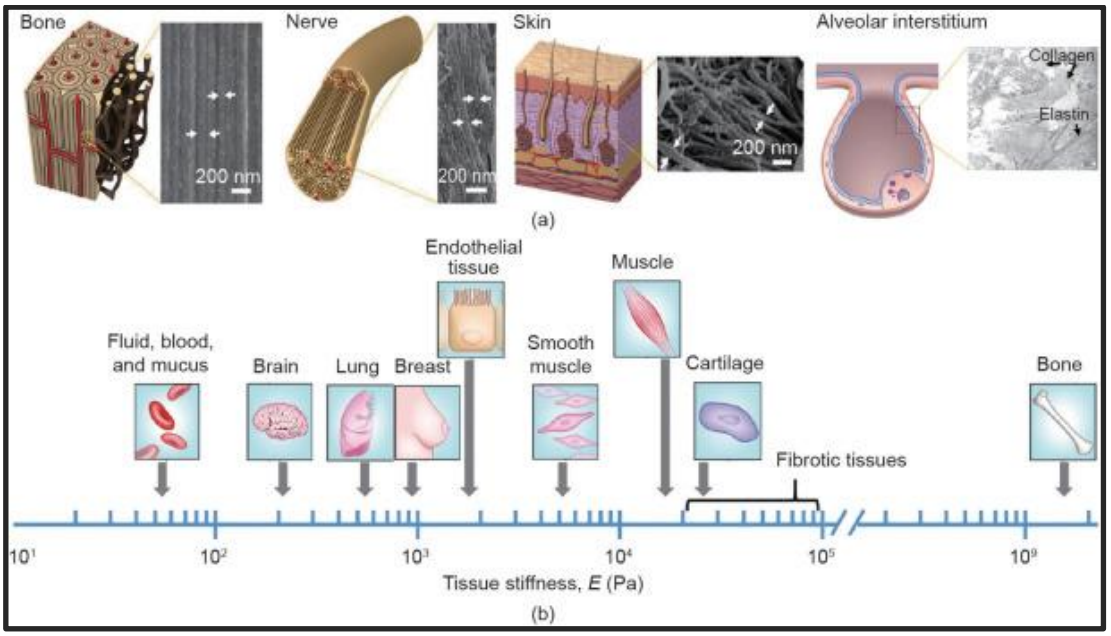

Figure 1.11. Biophysical characteristics of human tissues. A- Nanoscale structures in various tissues. B- Stiffness of various human tissues (Yang et al, 2017).

Fibroblasts in collagen gels show distinct morphologies from those cultured on tissue culture plastic that they lack F-actin stress fibers in collagen gels. On the other hand, fibroblasts on constrained collagen gels can generate stress fibers (Halliday and Tomasek, 1995).

Endothelial cells on collagen gels or fibrin gels show a decrease in network-like structures on stiffer gels. Softer substrates allow cells to form long capillary like tube structures. On stiffer gels, endothelial cells from human umbilical vein are more spread, have larger lumens and exhibit less branching compared with the same cells on soft gels (Sieminski et al, 2004).

Muscle cells also exhibit substrate dependent behavior, too. They are able to spread on both soft and stiff substrates but they show contraction only on substrates with intermediate stiffness closer to that of the muscle. The modulus of healthy muscle tissue is an intermediate range of stiffness, so this behavior of muscle cells is reasonable (Georges and Janmey, 2005).

On the other hand, the most commonly used cell type in tissue engineering is stem cells (SCs). Stem cells can be categorized into two main groups: embryonic stem cells (ESCs) and adult stem cells (ASCs). It was shown that topography affects the differentiation ability of SCs. Human MSCs can differentiate into osteoblasts under the influence of only micro or nanotopography of culture substrates (Hasturk et al, 2016). Another example is that human mesenchymal stem cell shape was observed to be rounded when entrapped in 3D hyaluronic acid hydrogel and elongated when seeded onto fibrous scaffolds or 2D biodegradable elastomer (Barthes et al, 2014).

Finally, the state of healthiness of cells has also important effects on their activities. Cells in diseased state show different behavior on substrates than in the healthy state. The most important example of this phenomenon is the difference between the behavior of cancer and healthy cells on various substrates with topography or different chemistry. Diverse properties of cancer cells on substrates will be discussed in detail in the next part of this study.

1.5.2.1. Cancer and Mechanics of Cancer Cells

Cancer is a disease where cells proliferate uncontrollably and form tissue which does not have the normal organization. Cancer cells do not require an external inducing signal to proliferate. They fail to sense signals that restrict cell division. They often change their attachment to surrounding cells or the extracellular matrix, they divide more rapidly and exhibit inappropriate immortality. Tumors arise with great frequency but they have low risk to their host because they are localized and of small size. These are called as benign tumors. The cells composing benign tumors may

function like normal cells. In contrast, cells composing a malignant tumor, or cancer, usually grow and divide more rapidly than normal, fail to die at the normal rate or invade nearby tissue without a significant change in their proliferation rate. When these tumors progress, the cells invade surrounding tissues, get into the circulatory system, and establish secondary areas of proliferation, a process called metastasis. Most malignant cells eventually acquire the ability to metastasize. Thus the major characteristics that differentiate metastatic (or malignant) tumors from benign ones are their invasiveness and spread (Lodish et al, 2003). Cancer cells also create their own signals for sustained growth and duplication and transmit them between proteins through a process commonly referred as signal transduction. The signals are transmitted back and forth between the ECM and the cell interior, including the cytoplasm and nucleus, through the integrins and focal adhesions that bind the cell to the ECM. Moreover, altered protein structures change the ability of cancer cells to contract or stretch by influencing their mechanics of deformation. (Suresh, 2007).

1.5.2.1.1. Breast Cancer

Studies have shown that breast carcinomas can be divided into 5 similar subgroups using immunohistochemical (IHC) analysis by antibody markers (including ER, PR, HER2, Ki-67, CK5/6 and EGFR) (Subik et al, 2010). These subgroups have different properties in terms of gene expression profiling, clinical outcomes, responses to therapy and patterns of metastasis (Subik et al, 2010). Among these molecules, Ki-67 protein is strictly associated with cell proliferation. During interphase, the antigen is within the nucleus, whereas in mitosis most of the protein is relocated to the surface of the chromosomes. It is present in the nuclei of cells in the G1, S, and G2 phases of the cell division cycle as well as in mitosis however quiescent or resting cells in the G0 phase do not express the Ki-67 antigen (Scholzen and Gerdes, 2000). Since the Ki-67 antigen is present in all proliferating cells (normal and tumor cells), the presence of this structure can be used as a reference marker to determine the “growth fraction” of a given cell population. Growth is the overall increase in cell number and

it is defined as the number of cells gained by proliferative activity and cells lost by apoptosis or necrosis. Proliferative activity results from cell cycling and is defined by the speed of the cell cycle and the proportion of cells committed to the cycle (growth fraction). On the other hand, doubling time of a tumor is defined by both cycle time and growth fraction (Van Diest et al, 1998; McDonald et al, 2016). As a result, Ki-67 is directly related to the proliferative activity of a cell but the doubling time of cells do not have to correlate with the proliferative activity or the expression of the Ki-67 antigen. For this reason, antibodies against the Ki-67 protein can be used as diagnostic tools in several types of neoplasms (Scholzen and Gerdes, 2000).

Other important cancer markers are nuclear lamina component, Lamin A/C and LINC complex components. It was found that all LINC complex components, SUN1, SUN2, and Nesprin-2, were downregulated in human breast cancer tissues (Matsumoto et al, 2015). Since the LINC complex and nuclear lamina have a role in the organization and mechanical stiffness of the nucleus, loss of LINC complex and nuclear lamina proteins reduces nuclear and cellular rigidity and consequently increases tissue fluidity, an important property for invasiveness of the cancer. Also, structural defects of the nucleus in cancer cells have been explained by the loss of Lamin A/C. In a study, it was shown that the loss of Lamin A/C in breast cancer tissue was accompanied by the loss of LINC complex components (Matsumoto et al, 2015). Importantly, all breast cancer patients showed decreased expression levels of at least one of the four components of LINC complex (Matsumoto et al, 2015).

1.5.2.2. Deformability of Cancer Cells and Their Nuclei

In the last decade, studies on the connection between the biophysical properties of cells and the progression of cancer have significantly increased (Suresh, 2007). It is widely accepted that to understand the malignancy of cancer cells, knowledge of the mechanical properties of cancer cells and their microenvironment is required. Biomechanical properties (rigidity, elasticity, deformability) of cells can provide useful information about cancer state and they can be viewed as biological markers,

which suggest an alternative to current proteomic techniques in the identification of cancer (Guck et al., 2005). It has been shown that even though tumor tissues are relatively stiff (due to their stiff ECM), their cells are softer in comparison to healthy counterparts (Coceano, 2015). They are able to spread within the ECM into the blood stream and this eventually leads to infiltration of the tissues, a process of spreading from the primary tumor site in order to establish secondary sites. (Lekka et al, 1999; Huang et al, 2005). Cells sense and adapt to changes in the surrounding environment that are formed by other cells and the extracellular matrix (ECM). Extracellular environment exerts biochemical and physical stimuli on the cells which respond to these stress through many cellular events such as stiffening, softening, maturation, calcium influx, morphological changes, generation of traction forces or focal adhesions (Discher et al, 2005), as well as disease states such as cancer (Suresh, 2007).

The intracellular components of cells such as cytoskeletal proteins, cytoplasm and membrane contribute to the mechanical properties of cells and tissues. The nucleus of cell provides a degree of structural stiffness and plasticity (Dahl et al., 2008; Guilak et al, 2000). On the other hand, the rigidity or deformability of a nucleus is primarily mediated by chromatin as well as nucleoskeletal organization and expression and assembly of lamins as part of the nuclear lamina (Krause and Wolf, 2015). In recent years, many studies have reported altered nuclear envelope composition in various cancers as well as breast cancer. The structure and composition of the nucleus, particularly the nuclear envelope, have a significant role in cellular mechanics and function and it determines nuclear deformability and fragility. Changes in the composition of nuclear envelope could contribute to cancer progression and a softer and more lobulated nucleus cause cancer cell invasion through dense tissues where cells pass through constricted areas smaller than diameter of a nucleus. Furthermore, the physical coupling between the nucleus and the cytoskeleton is critical for cytoskeletal organization and cell polarization and this may affect migration of cancer cells (Denais and Lammerding, 2014).

Maintaining the cell shape is crucial to perform biological functions. Cell shape is also determined and controlled by cellular attachments with the surrounding extracellular matrix (Lecuit and Lenne, 2007). Besides the stiffness of cell and nuclei, viscoelasticity of them also plays a key role in defining the mechanical properties of a living cell (Kollmannsberger and Fabry, 2011). Cells and their nuclei behave like viscoelastic materials, presenting both solid and fluid characteristics. Due to these properties, they deform in a time dependent manner that mechanical stresses relax under constant deformation or deformation increases over time as a result of a constant load (Kollmannsberger and Fabry, 2011). Viscoelasticity plays a significant role in cellular processes, and therefore should be taken into account in studying cancer cell mechanics (Guck et al., 2005; Suresh, 2007) Mechanical properties of breast cancer cells have been intensely studied in the recent years (Li et al, 2008; Subik et al, 2010; Rother et al, 2014; Coceano, 2015; Geltmeier et al, 2015; Calzado-Martin et al, 2016). In a study, malignant breast cells (MCF-7) were found to have an apparent Young's modulus significantly lower (1.4–1.8 times) than their non-malignant counterpart (MCF-10A) (Li et al, 2008). Both confocal and AFM images showed a significant difference in the organization of their actin structures, which directly contributes to cell elasticity (Li et al, 2008). Softening of the cytoskeleton allows increased replication and motility of cancer cells and cells contract more easily because they are more stretchable and deformable (Coceano, 2015). As a summary, mechanical properties of the breast cell lines which are used in this study are given in Table 1.1.

Table 1.1. Properties of human breast cell lines (Calzado-Martin et al, 2016; Subik et al, 2010).

Name of human breast cell line	Cell type	Disease	Biological characteristics	Young's Modulus (kPa)	Doubling time (h)	Ki-67 expression (%)
MCF-10A	epithelial	fibrocystic disease	• benign	0.7	16	30
MCF-7	epithelial	adeno-carcinoma	• non invasive • malignant • derived from metastatic site	0.5	29	90
MDA-MB-231	epithelial	adeno-carcinoma	• highly invasive • malignant • derived from metastatic site	0.3	38	100

1.5.2.3.Quantification of Cell and Nucleus Deformations

Cell-material interactions lead to different results in diseased and healthy cells. Interaction between the diseased cells and surfaces with microtopographical features have a significant importance in the study of the cancer since deformability extent of cells on these surfaces can be quantified and this helps study the intrinsic differences between various cell categories. There are several methods for the quantification of this deformability and the most common conventional techniques in cell mechanics are: atomic force microscopy (AFM), optical tweezers, micropipettes and confocal and fluorescence microscopy.

AFM is a scanning probe microscopy tool for imaging and it has been widely used in cell mechanics studies (Rother et al, 2014; Unal et al, 2014; Geltmeier et al, 2015). The mechanical properties including the elasticity, viscoelasticity and plasticity cells can be quantified using AFM force measurements. Elastic modulus and viscosity can be used as indicators of cellular differentiation (Unal et al, 2014).

Optical tweezers manipulate dielectric particles by focusing a laser on a diffraction limited point through a microscope objective. The size of the particles that can be trapped in optical tweezers range from 20 nm to several micrometers. These could be organelles, cells and polymeric and mineral (polystyrene or silica) micro and nano spheres (Neuman and Nagy, 2008).

Micropipettes are used for the mechanical analysis of cells and the working principle is applying vacuum (suction) to a small portion of a cell and measurement of the deformation of the cell membrane. The automated micropipettes can be used together with a video microscopy system. Membrane deformation, membrane area and cell volume and isolated nucleus of cell can be measured at a nano scale resolution (Unal et al, 2014).

Optical microscopy tools have been commonly used in studies of cell mechanics. High resolution imaging and 3D volume construction are needed for cell deformation and strain measurements. Fluorescence and confocal microscopes are used with live cell imaging functions in the study of cell mechanics. 3D reconstructions of the cells can be obtained and cellular deformations can be evaluated on micro and nano scale topographic surfaces. The viscoelastic mechanical properties of cells can be analyzed using these microcopies. After the imaging of cells on substrates, various image analysis software such as ImageJ or Matlab can be used to quantify the deformability of nucleus and cell (Ermis et al, 2016; Hasturk et al, 2016).

1.6. Aim, Approach and Novelty of the Study

In this study, main assumption was that the difference in the stiffness of malignant and benign breast cancer cells can be used as a tool in cancer detection with the help of surface topography, cell and nucleus deformation and quantification. To achieve this, the first aim was to distinguish malignant cells from benign cells by using the extent of nuclear deformation induced by the micropatterned surfaces. Second, the mechanism of nucleus deformation was studied by using drugs that inhibit the

synthesis of actin cytoskeleton. By the relation between cell deformability and carcinogenicity, these inhibitor drugs could be used as a cancer treatment agent by inhibiting deformability property of breast tumor cells. Third, relation between the deformability of nucleus and the expression of mechanotransduction proteins (Lamin A/C, Nesprin-2 and actin filaments) was used as a simple method for the detection and discrimination of breast cancer cells on micropatterned surfaces by showing an increase of nuclear deformation by decrease of the expression levels of these proteins.

Breast cancer cell lines was used as a model in this project to study the differences between benign and malignant tumor cells. Although there have been several studies on the discrimination of breast cancer cells, it is novel to compare benign (MCF10A), malignant but noninvasive (MCF7), and malignant and highly invasive (MDAMB231) breast cells by using differences between the ability to deform their nuclei on micropatterned surfaces.

As the substrate material, poly(methyl methacrylate) (PMMA) was used in this study. PMMA is very useful for microscopy imaging studies because of its excellent optical transparency and it is also biocompatible. It was processed to obtain micropatterned surfaces. There are several lithographic micro- and nanofabrication methods to produce ordered structures such as grooves, wells, pits and pillars. Photolithographic technique used in this study was the UV photolithography, in which a photocurable resist such as SU-8 that was crosslinked upon UV radiation and it was used to fabricate the positive-tone of the transparent regions of the photomask on the substrate. The patterns obtained on the original wafer by photolithography were transferred to polymer surfaces by the molding process. In this study, PMMA micropatterned surfaces was designed with micropattern and gap dimensions (4x4 μm^2 with 4 μm gap size) which are optimal for making the cell slip in between the pillars which lead to nucleus deformation.

The cells were studied for their attachment, proliferation, and nuclear deformation. An engineered surface modification provides the enhancement of biocompatibility

and biofunctionality while the bulk properties stay unchanged. When the surface chemistry of a polymeric substrate is not suitable for certain biological goals, the surface chemical modification can be used. In this study, oxygen plasma treatment was used for the modification of polymer surfaces because it produces oxygen-rich functional groups including hydroxyl, carbonyl and carboxyl and, as a result, wettability of PMMA was increased.

Next, in order to observe the mechanism of deformation in nucleus of cells, cytoskeletal element, basically actin which was predicted to be the main structure controlling deformation, was destabilized by using chemicals such as cytochalasin D (inhibitor of actin polymerization). By this act, deformation of the nucleus of both benign and malignant cells was initiated or inhibited and the role of these molecules in nucleus deformation was understood. This was a key to detect cancer cells. As indicated before, drug treatments on cytoskeletal elements have been used commonly to understand the mechanism of cancer however observing the effect of inhibitor drugs on benign and malignant cells and making comparison between them on micropatterned surfaces is novel. Finally, the relation between the actin filaments, mechanotransduction proteins (Lamin A/C and Nesprin-2) and deformability of the nuclei of the cells was investigated by the help of the drugs and this information was also help us understand the mechanism of nuclear deformation.

In summary, biomechanical properties (rigidity, elasticity, deformability) of cells provide valuable information about cancer state and they can be used as an alternative identification method to current proteomic techniques in cancer detection.

CHAPTER 2

MATERIALS AND METHODS

2.1. Materials

Silicon wafers were produced by Dr. Pu Chen using MEMS technology at Prof. Utkan Demirci's Bio-Acoustic MEMS in Medicine Laboratory, at the Canary Center at Stanford for Cancer Early Detection (Palo Alto, CA). Dulbecco's Modified Eagle Medium (DMEM) High Glucose, DMEM:F12 1:1 mixture, DMEM High Colorless, Pen-Strep (10.000 $U.mL^{-1}$ Penicillin and 10.000 $U.mL^{-1}$ Streptomycin), and L-glutamine (200 mM in 0.85% NaCl solution) were obtained from Lonza (Switzerland). Sylgard 184 Silicone PDMS polymer and Sylgard 184 Curing agent were bought from Dow Corning Company (UK). Poly(methyl methacrylate) (PMMA; with molecular weights MW= 120,000 and 996,000), Trypsin-EDTA (0.25%), amphotericin-B (0.25 $\mu g.mL^{-1}$), potassium chloride (KCl), bovine serum albumin (BSA), piperazine-N,N'-bis(ethanesulfonic acid (PIPES) were purchased from Sigma-Aldrich (USA). Fetal bovine serum (FBS) was from Biowest (France). Chloroform and ethanol were obtained from Avantor J.T. Baker (USA). Alamar Blue® Cell Viability Assay, Alexa Fluor® 488 conjugated phalloidin, ethidium bromide (10 $mg.mL^{-1}$), dimethyl sulfoxide (DMSO), NucleoCasette was from ChemoMetec (Denmark). 4',6-diamine-2-phenylindole dihydrochloride (DAPI) and DRAQ5 were bought from Cell Signalling Technology (USA). Sodium chloride (NaCl), potassium dihydrogen phosphate (KH_2PO_4) and disodium hydrogen phosphate (Na_2HPO_4) were obtained from Merck Millipore (Germany). Osmium tetroxide (OsO_4) (4%) was bought from Polysciences (USA) and Triton-X 100 was purchased from PanReac Applichem (Germany). RevertAid First Strand cDNA Synthesis Kit, Ambion DNA-free™ DNA Removal Kit, SYBR™ Green PCR Master Mix, Quant-iT™ PicoGreen™ dsDNA Assay Kit were purchased from Thermo

Fisher Scientific (USA). Marker specific primers were synthesized by Sentegen (Turkey).

2.2. Methods

2.2.1. Preparation of Micropatterned PMMA Films

2.2.1.1. Preparation of Silicon Wafers Designed with Micropillars

SU-8 micropillar arrays chips were fabricated at Prof. U. Demirci's Bio-Acoustic-MEMS in Medicine (BAMM) Laboratory, Stanford University (USA) using standard photolithography procedures (Figure 2.1). The square prism pillars were designed with 8 μm height with an area of 4x4 μm^2 (P4) and a gap of 4 μm (G4). Pattern designs were printed on a custom-designed photomask (Fineline Imaging, CO). A control wafer with no pillars was used as unpatterned control (UC).

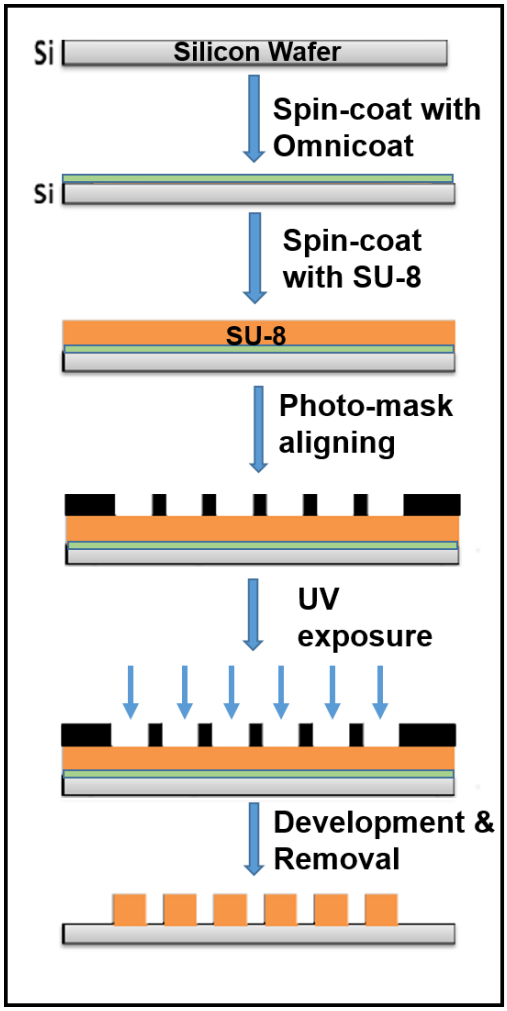

Figure 2.1. Fabrication of SU-8 micropillars

2.2.1.2. Preparation of Polydimethylsiloxane (PDMS) Templates

Negative copies of the wafers were molded using polydimethylsiloxane (PDMS), prepared from Sylgard 184 silicone polymer and Sylgard 184 curing agent (Dow Corning Company, UK) mixed in a ratio of 10:1 (w/w). The silicone prepolymer mix was poured onto the patterned surface of the wafer in a petri plate, vacuum was applied for 45 min and then heated (70 °C, 4 h). After cooling, the formed PDMS structure was peeled off from the wafer producing a negative copy of the original (Figure 2.2.A).

2.2.1.3. Preparation of PMMA Replicas of the Silicon Wafers

PDMS negative mold was used to make polymer films of poly(methyl methacrylate) (PMMA) (mw~120000 and 996000) (Sigma, Germany). Solvent casting method was used to produce PMMA replicas of the original silicon wafers by using the PDMS negatives. PMMA solution (10% w/v in chloroform) was poured onto the PDMS mold and air dried for 12 h at room temperature for the evaporation of chloroform. Dry films were then peeled off from the PDMS molds and stored at room temperature until use. To prepare smooth surfaces, unpatterned PDMS molds were used (Figure 2.2.B).

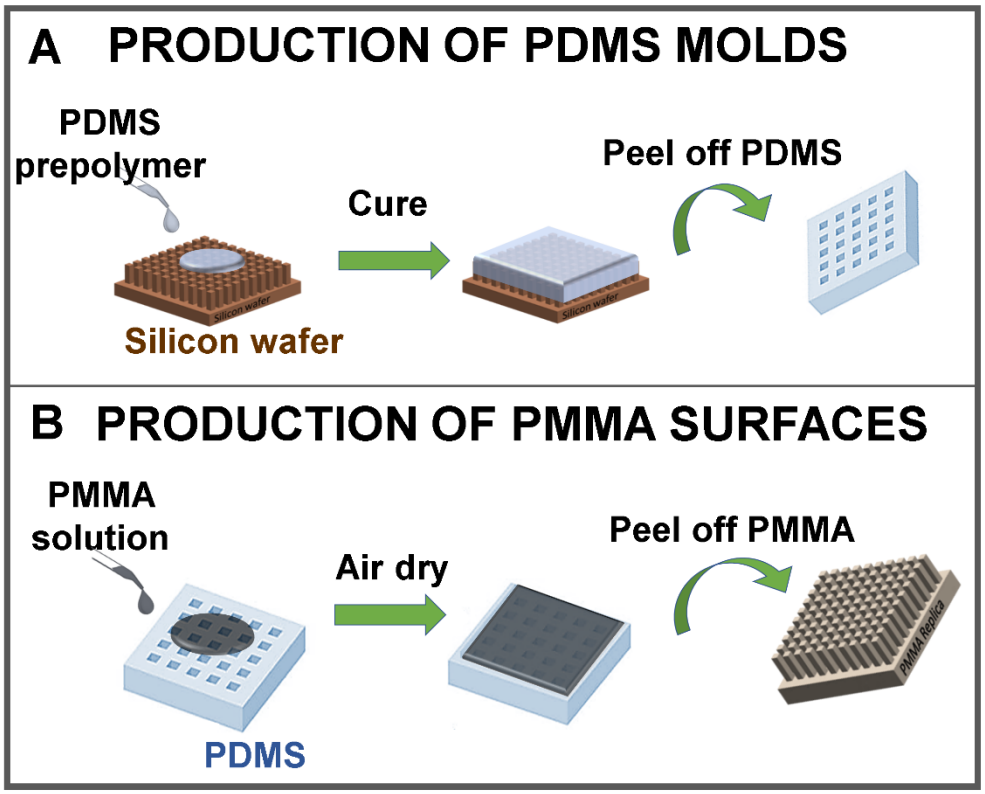

Figure 2.2. Schematic presentation of the fabrication of PMMA films decorated with micropillars. A- Production of PDMS molds of the original silicon wafers, B- Production of PMMA replicas of the original silicon wafers using the PDMS molds and solvent casting method.

2.2.2. Oxygen Plasma Treatment of Micropatterned PMMA Films

Surfaces of PMMA films were modified by oxygen plasma treatment. Films were placed in the plasma reaction chamber (Femto 40 kHz, Diener Electronic, Germany) and the plasma pressure was maintained at 20 mbar by the introduction of the oxygen gas at a controlled rate. The power was set to 100 W and the films were exposed to oxygen plasma for 10 min. After the plasma treatment was stopped, the gas flow was continued for 10 min for the termination of the created reactive groups. One set of smooth and micropatterned samples treated at 100W, 10 min were then immediately used in contact angle measurements and the other set was used in in vitro studies.

2.2.3. Characterization of PMMA Films

2.2.3.1. Mechanical Properties

2.2.3.1.1. Tensile Testing

Tensile tests of PMMA samples were conducted with Shimadzu AGS-X universal test machine (Japan). PMMA films for mechanical testing were prepared by solvent casting of PMMA (Mw = 120000 and 996000) solutions (10%, w/v) in chloroform in a glass petri dish. Five tensile specimens (10 mm wide x 50 mm long x 0.10-0.15 mm thick) were cut from the cast PMMA sheets. PMMA strips with a gauge length of 20 mm were attached, and a uniaxial tensile load was applied to the specimen at a pulling rate of 1 $mm.s^{-1}$. Force and elongation values were recorded and the stress and strain graphs were plotted using the values calculated with the following equations:

$$\text{Stress } (\sigma) = F/A \quad (1)$$

$$\text{Strain } (\varepsilon) = \Delta l/l \quad (2)$$

where F is the force (N), A is the crosssectional area (width x thickness, mm^2), Δl the change in length (mm) and l the initial length (mm). Ultimate tensile strength (UTS)

of the samples was defined as the highest stress value on the stress-strain curve. The tensile moduli (Young's Modulus, E) were calculated as the slope of these curves using the following equation:

$$E = \sigma/\varepsilon \quad (3)$$

where σ is the stress (MPa) and ε the strain in the elastic region (Figure 2.3).

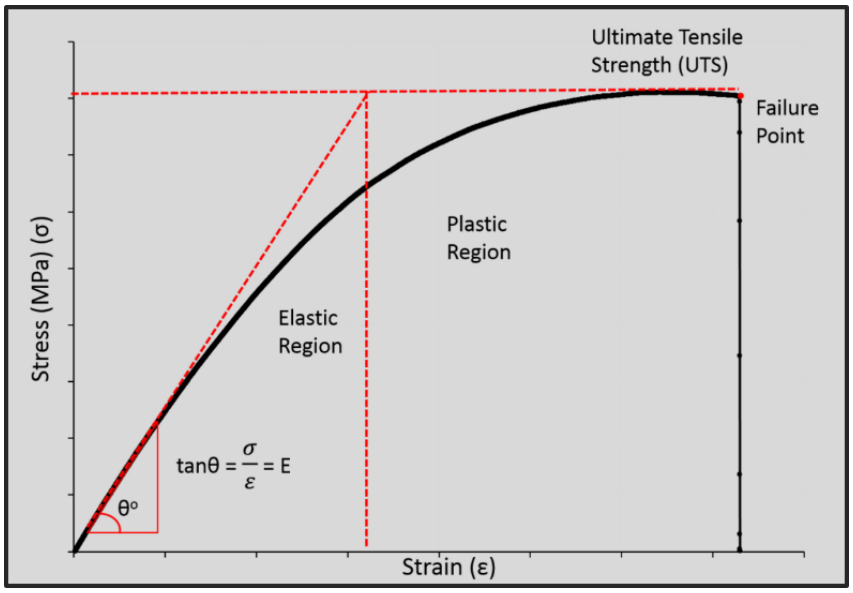

Figure 2.3. The representative stress-strain curve of the PMMA film tested under tension.

2.2.3.2. Microscopy

2.2.3.2.1. Scanning Electron Microscopy (SEM) Analysis

Surface features of the PMMA films were examined with SEM (400D Field Emission SEM, USA). Films were coated with Au-Pd under vacuum and micrographs of top and side view were taken. Pillar and gap dimensions of the films were measured using the SEM micrographs and the image analysis software ImageJ (NIH).

2.2.3.2.2. Atomic Force Microscopy (AFM) Analysis

The surface morphology of untreated and oxygen plasma treated smooth PMMA surfaces were examined with an atomic force microscope (Universal SPM, Ambios Technology, Korea) in intermittent tapping mode. The mean surface roughness and the average height of three sample surfaces from each group were measured, and 2D and 3D wavemode micrographs were recorded.

2.2.3.3. Contact Angle

Contact angles untreated and oxygen plasma treated PMMA films were measured by the static sessile drop method using a goniometer (Attension, Biolin Scientific, Sweden) (n=3). The measurements were made with distilled water with a drop volume of 7 μL.

2.2.3.4. X-Ray Photoelectron Spectroscopy (XPS)

X-ray photoelectron spectroscopy (XPS) analysis was carried out on a PHI 5000 VersaProbe (Japan) spectrometer with an argon ion gun and employing Al monochromatic X-ray source. The electron take off angle was 45° and the pass energy was 187.850 eV for survey spectra. XPS analyses were done at Central Laboratory, METU.

2.2.4. *In Vitro* Studies

2.2.4.1. Culture of Breast Cell Lines: MCF10A, MCF7, MDAMB231

MCF-10A cells were cultured in DMEM/F12 medium (Sigma, USA) supplemented with 5% fetal bovine serum (FBS) (Lonza, USA), EGF 20 ng/mL (Sigma), insulin 10

μg/mL (Sigma), hydrocortisone 0.5 mg/mL (Sigma), cholera toxin 100 ng/mL (Sigma) and 100 units/mL penicillin (Sigma, USA).

MCF-7 cells were cultured in DMEM low glucose medium (Lonza, USA) supplemented with 10% fetal bovine serum (FBS) (Lonza, USA), 100 U/mL penicillin (Sigma, USA).

MDA-MB-231 cells were cultured in DMEM high glucose medium (Lonza, USA) supplemented with 10% fetal bovine serum (FBS) (Lonza, USA), 100 U/mL penicillin (Sigma, USA).

The cells were cultured in tissue culture polystyrene (TCPS) flasks at 37°C in a humidified atmosphere with 5% CO2. The cells were removed from the culture flasks with Trypsin-EDTA, diluted to 0.05% from a 0.25% stock in PBS.

2.2.4.2. Seeding of Cells

Micropatterned and unpatterned control PMMA films were sterilized by exposing both sides to UV in a laminar flow hood for 25 min. Cells were seeded at a desired density (50,000 cells/film) suspended in 100 μL of the growth medium of choice per film (ca 64 mm^2). After allowing the cells to adhere to the surfaces for 5-6 h, 2 mL of growth medium was added into each well and plates were incubated at 37 °C and 5% CO2. Tissue culture plates were also seeded as control surfaces in addition to unpatterned control PMMA films at the same cell density.

2.2.4.3. Determination of Cell Metabolic Activity by Alamar Blue Assay

Cell numbers were determined upon 24, 48, 72 h culture duration for proliferation with the Alamar Blue cell viability assay. The films were washed with PBS twice and incubated in 500 μL Alamar Blue solution (10% in DMEM High Glucose colorless supplemented with 100 U/mL Pen-Strep) for 2 h at 37 °C and 5% CO_2.

After incubation, 200 µL of the Alamar Blue solution was transferred into a 96 well plate and the absorbances of the transferred solutions were determined at 570 nm (λ_1) and 595 (λ_2) with a plate reader (Multiscan Spectrum, Thermo Scientific, USA). The absorbances were converted to percent reduction by using the equation shown in Appendix A. Two technical replicates and three biological replicates were used for each group of measurements.

2.2.4.4. Determination of Cell Number by PicoGreen DNA Quantification Assay

PicoGreen Assay (Quant-IT PicoGreen dsDNA assay kit, Invitrogen) is used for the quantification of DNA content. This assay determines the amount of DNA in the sample, from which cell number in the sample can be estimated. After culturing the cells on smooth and micropatterned PMMA and tissue culture plates for 24 h, the cells were resuspended in 350 µL of RLT lysis buffer (RNeasy mini kit, Qiagen). All samples were vortexed for 15 s, and centrifuged for 1 min at 13,000 rpm. Then, 10 µL of the sample was diluted 10X in DNase free water. Finally, 5 µL of this diluted sample was diluted in 195 µL working buffer (199 µL of the Quant-IT dsDNA buffer and 1 µL Quant-IT dsDNA reagent prepared for each sample), after which the sample was shortly vortexed and incubated at room temperature for 5min. The DNA concentration was then measured with the fluorometer by exciting at 485 nm and measuring the fluorescence intensity at 520 nm. All samples were prepared in triplicate. The linearity of the DNA measurements was evaluated for the RLT lysis buffer with a final buffer dilution of 400X·by preparing calibration curve (Appendix B). DNA standard concentrations in the measurement solution were 10, 25, 50, 100, 250 and 500 ng/mL.

2.2.4.5. Live-Dead Cell Viability Assay

Viability of the cells on seeded films and tissue culture plates was determined with Live-Dead cell viability assay. After 24 h culture, medium was discarded and

samples were washed 3 times and they were double stained with calcein (2 µM in PBS) and ethidium homodimer-1 (4 µM in PBS) (Molecular Probes, USA). After washing with PBS, samples were examined by fluorescence microscopy.

2.2.5. Influence of Actin Inhibitor Drugs

2.2.5.1. Dose Optimization with Alamar Blue Assay

Actin cytoskeleton inhibitor drugs Cytochalasin D (inhibits actin polymerization by capping filaments binding to monomers and is selective for actin) and Jasplakinolide (stimulates actin polymerization and inhibits growth of breast cancer cells by disrupting F-actin fibers by blocking FAK signaling pathway) (Figure 2.4).

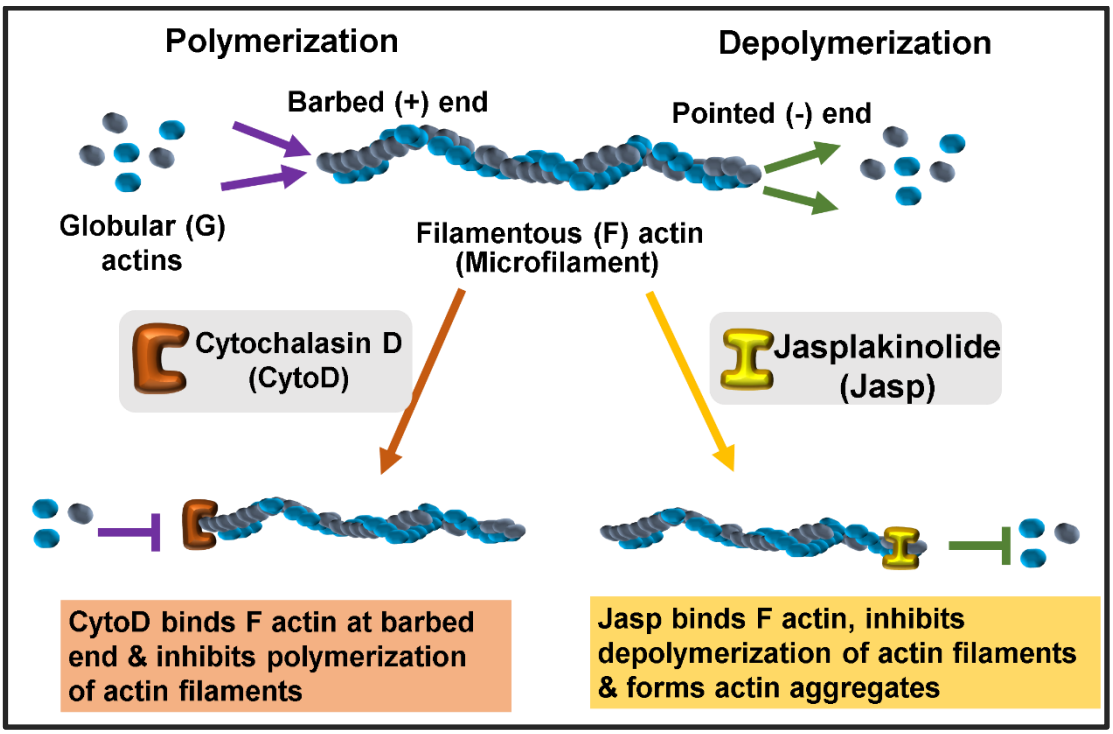

Figure 2.4. Scheme of actin polymerization/depolymerization and working mechanisms of actin inhibitor drugs (Cytochalasin D and Jasplakinolide).

Serial dilutions of these chemicals were used on three cell cultures. Concentrations for both drugs were prepared by dissolving them in dimethyl sulfoxide (DMSO). Final concentrations of both drugs in 1 mL of culture medium were 0, 0.01, 0.05, 0.1, 0.5, 1, 5, 10 μM of Cytochalasin D and 0, 0.01, 0.05, 0.1, 0.5, 1, 5 μM of Jasplakinolide. Amount of DMSO for the highest concentration of drugs (CytoD: 10 μM and 5 μM Jasp) in culture medium was 0.22 % and (v/v) 0.18 % for CytoD and Jasp, respectively. Control samples without drugs were prepared with the same highest amount of DMSO for both drugs. Cell were cultured for 24 h (day 1) on tissue culture plate (TCPS) and micropatterned films (P4G4) and then drugs were used on the cells for another 24 h (day 2). Inhibitory dose of Cytochalasin D and Jasplakinolide on the cell viability before and after drug treatment was determined by Alamar Blue assay as given in detail in Section 2.2.4.3 above.

2.2.5.2. Nuclear Deformation

Actin cytoskeleton inhibitor drugs Cytochalasin D and Jasplakinolide were used on cell seeded TCPS and P4G4 films. Effect of these chemicals on nuclear deformation of three cell lines was observed and quantified under fluorescence microscopy as given in detail in Section 2.2.6. below.

2.2.6. Microscopy

2.2.6.1. Scanning Electron Microscopy (SEM)

Cell seeded micropatterned and smooth films as SEM specimens were washed twice with PIPES (piperazine-N,N'-bis(ethane sulfonic acid)) buffer (Sigma Aldrich, USA), and fixed in 4% paraformaldehyde solution for 5 min. After washing with PIPES buffer, the samples were stained with 1% osmium tetroxide (OsO_4) (Sigma Aldrich, USA), washed twice with PIPES buffer and dehydrated by immersing in an ethanol series. Cell seeded and unseeded films were coated with Au–Pd under vacuum and examined with the SEM (400F Field Emission SEM, USA).

2.2.6.2. Fluorescence and Confocal Microscopy

Cell seeded samples were removed from the growth medium and washed twice with PBS, the cells were fixed in 4% paraformaldehyde and permeabilized with 1% Triton-X 100 solution (Applichem, Germany). After washing with PBS twice, films were incubated in BSA blocking solution (1%, w/v, in PBS) at 37 °C for 30 min. Films were then incubated in Alexa Fluor 488® labeled Phalloidin solution (1:50 dilution in 0.1% BSA in PBS) for 1 h at 37 °C. Samples were incubated for 5 min at room temperature with DAPI (Invitrogen, USA) or DRAQ5 (Abcam, UK) for the staining of nucleic acids. Films were washed twice with PBS and stored in 12 well plates in 1 mL PBS solution at 4 °C and the plates were wrapped in aluminum foil for light protection until analysis.

Fluorescence micrographs of the cells were obtained using an upright fluorescence microscope under 350 nm, 488 nm, 550 nm or 630 nm LED sources and appropriate filter sets (Zeiss Axio Imager M2, Germany).

Confocal micrographs of the cells were obtained using an upright Confocal Laser Scanning Microscope (CLSM) under 488 nm, 532 nm, 630 nm lasers (Leica DM2500, Germany).

2.2.6.3. Immunocytochemistry (ICC)

Samples were prepared for fluorescence and confocal microscopy. Then, they were incubated for 1 h at 37 °C with Alexa Fluor 532 Phalloidin (Invitrogen, USA) for staining of the actin cytoskeleton. For Lamin A/C, Nesprin-2 and Ki-67 imaging antibodies specific to these proteins (Anti-Nesprin-2 ab57397, anti-Lamin-A ab8980 and anti-Ki67 ab8191 antibodies, Abcam, UK) were used according to manufacturer’s directions.

2.2.7. Digital Analysis of Cell Nuclear Deformation

Fluorescence micrographs of the nuclei of cells upon 24, 36, 48 and 72 h culture duration were analyzed by using the image analysis software ImageJ (NIH) and its distribution Fiji to determine the "perimeter", "area", "circularity" (Eqn. 4) and "roundness" (Eqn. 5) of cell nuclei. ImageJ (NIH) uses the following equations to calculate circularity and roundness (Schindelin et al, 2012; Schindelin et al, 2015):

$$\text{Circularity} = 4\pi \times \frac{[\text{Area}]}{[\text{Perimeter}]^2} \quad (4)$$

$$\text{Roundness} = 4 \times \frac{[\text{Area}]}{\pi \times [\text{Major axis}]^2} \quad (5)$$

"Circularity" value of 1 indicates a perfect circle. As the value approaches 0, it indicates an increasingly elongated polygon. The perimeter of a circle is $p = 2\pi r$ and the area is $a = \pi r^2$.

"Roundness" is 1 for a circle and approaches 0 for elongated objects. The major axis of a circle is $p = 2r$ and the area is $a = \pi r^2$.

Nuclear deformation values were calculated from 100 cell nuclei per surface.

2.2.8. Quantification of Expression Levels of Proteins Based on the Intensity of ICC Staining

Confocal micrographs of the samples stained with antibodies specific to Lamin A/C, Nesprin-2 and Ki-67 were analyzed by using image analysis software Fiji. Original images were in Red (R), Green (G), Blue (B) format. Image preprocessing was applied to obtain gray scale (8 bit) images. "Lookup table" of Fiji was changed to "HiLo". Then the contrast was adjusted. The minimum pixels were increased until the background becomes blue in the image. Background subtraction was done using "rolling ball algorithm". The pixel value should be set to at least the size of the largest object that is not part of the background. From the "set measurements" panel,

"mean gray value" was chosen. Finally, the intensity of the antibody specific stain was measured and a mean gray value (sum of the gray values of all the pixels in the selection divided by the number of pixels) was obtained for each micrograph.

2.2.9. Quantitative Real Time Polymerase Chain Reaction (qRT-PCR) Studies for Lamin A/C, Nesprin-2 and Ki-67

2.2.9.1. Isolation of Total RNA

RNA isolation was performed by using RNeasy Micro Kit (Qiagen, Germany) according to manufacturer's protocol. Briefly, $5x10^5$ cells were disrupted with buffer RLT (350 µL) by vortexing and was added into QIAshredder spin column for homogenization and centrifuged (14000 rpm, 2 min). Ethanol (70%, 350 µL) was added and transferred to an RNeasy MinElute spin column and centrifuged (10000 g, 15 sec). The spin column was washed with RW1 buffer (700 µL), RPE buffer (500 µL), ethanol (80%, 500 µL). The RNA was eluted from the membrane by centrifugation (14000 rpm, 1 min) with nuclease free water (14 µL). Finally, the RNA sample was incubated at 65°C for 10 min and treated with DNase I to clean the DNA.

2.2.9.2. DNase I Treatment

DNase I treatment was performed using DNA-freeTM kit (Ambion, Invitrogen, Germany). Briefly, RNA solution contaminated with DNA (10 µL) was incubated with DNAse I buffer (1 µL) and rDNase I (1 µL) at 37°C for 30 min. Then DNase inactivation reagent (1 µL) was added to the solution and incubated for 2 min at room temperature, mixed occasionally during the incubation. Lastly, the solution was centrifuged (10000 g, 5 min) and the supernatant was taken into a DEPC treated tube and stored at -80°C until used. RNA concentrations were measured by Nanodrop 2000C (Thermo Scientific, USA).

2.2.9.3. First Strand cDNA Synthesis by Reverse Transcription PCR (RT-PCR)

First-strand cDNA synthesis via RT-PCR was performed with 1 µg RNA from each sample with RevertAid First Strand cDNA Synthesis Kit (Thermo Fisher Scientific, USA) and a thermal cycler (iCycler, BIO-RAD, USA) with the oligo$(dT)_{18}$ primers supplied with the kit. The reverse transcription step was run for 60 min at 42 °C, followed by reaction termination for 5 min at 70 °C.

2.2.9.4. Primer Design

Primers were synthesized for GAPDH, Ki-67, Lamin A/C, Nesprin-2 genes by Sentegen (Sentegen, Turkey) according to the sequences given in Table 2.1.

Table 2.1. Primer sequences for qRT-PCR analysis. F: forward primer, R: reverse primer.

Marker		**Primer (5' – 3')**	**Amplicon Size (bp)**	**NCBI Accession #**	**Reference**
GAPDH	F	AATCCCATCACC ATCTTCC	155	NM_001289 745.1 (transcript variant 3)	Matsumoto et al, 2015
	R	GCAGAGATGATG ACCCTTT			
Nesprin-2	F	GGAGAAAGTTGG TTTCAAAAACTC	76	NM_182914 .2 (transcript variant 5)	Matsumoto et al, 2015
	R	AAAGTGGGCTGA TCCTGTTTT			
Lamin A/C	F	AGCAAAGTGCGT GAGGAGTT	62	NM_170707 .3 (transcript variant 1)	Matsumoto et al, 2015
	R	AGGTCACCCTCC TTCTTGGT			
Ki-67	F	ATTGATCGTTCC TTCAGGTATG	134	NM_002417 .4 (transcript variant 1)	Bie et al, 2011a, 2011b, 2012
	R	TCATCAGGGTCA GAAGAGAA			

2.2.9.5. Quantitative Real Time PCR (qRT-PCR)

qRT-PCR reactions were performed by using the SybrGreen Quantitative RT-PCR kit (Sigma Aldrich, Germany) according to the manufacturer's instructions. The reactions were run by the Corbett Rotor-Gene 6000 (Qiagen, Germany). Melting curves for each gene were analyzed to ensure specific amplicon replication, and all reactions were performed in triplicates and each reaction was included no template control. The reactions were optimized for each primer and gene for the efficient qRT-PCR reactions. Samples were assayed in duplicate, and the Ct (threshold cycle) values for Lamin A/C, Nesprin-2 and Ki-67 were normalized to that of the housekeeping gene GAPDH. Gene expression levels of the cells cultured on TCPs were normalized to control cell type MCF10A. Gene expression levels of the cells cultured on smooth PMMA were normalized to the cells cultured on TCPs while the expression levels of the cells cultured on micropatterned PMMA films were normalized to that on smooth PMMA according to the following equations:

$$\Delta C_t\,(\text{control}) = C_t\,(\text{control}) - C_t\,(\text{reference}) \quad (6)$$

$$\Delta C_t\,(\text{treated}) = C_t\,(\text{treated}) - C_t\,(\text{reference}) \quad (7)$$

$$\Delta\Delta C_t = \Delta C_t\,(\text{treated}) - \Delta C_t\,(\text{control}) \quad (8)$$

$$\text{Normalized treated gene expression level} = 2^{(-\Delta\Delta Ct)} \quad (9)$$

2.2.9.6.Agarose Gel Electrophoresis of DNase Treated RNA Samples

For the preparation of agarose gels, 50X stock Tris-Acetate-EDTA (TAE) buffer (121 g of Tris and 37.2 g of EDTA, 28.55 mL of glacial acetic acid in distilled water) were used. It was diluted to 1X buffer by addition of distilled water. 1X TAE was used to prepare 1% agarose gel (Sigma Aldrich, Germany). 1 µL of ethidium bromide solution (AppliChem, Germany) was added to the gel and mixed for the

homogenous distribution of ethidium bromide. The gel solution was poured onto the tank and the comb will be placed on it. After the gel is solidified, the comb was removed and 1X TAE buffer was added to the electrophoresis tank. Then the samples were loaded into the wells by mixing the samples with 6X gel loading solution (Fermentas, Germany) together with 100 bp DNA ladder (Sigma Aldrich, Germany). Samples were run under 100 V potential difference for 45 minutes.

2.2.10. Statistical analysis

All quantitative data in this study were expressed as mean ± standard deviations with n≥2 unless otherwise stated. Statistical analysis was performed by one-way ANOVA (analysis of variance) test followed by Tukey's test for normally distributed data and Kruskal-Wallis test for non-normally distributed data. *p*-values less than 0.05 were considered statistically significant.

CHAPTER 3

RESULTS AND DISCUSSION

3.1. Characterization of PMMA Films

3.1.1. Mechanical Properties of PMMA Films

Mechanical property of a material is a very important parameter affecting the cell behavior on substrates. Balance between scaffold mechanical properties and architecture is important for cell attachment, adhesion and migration since surface roughness and material stiffness are the main parameters that affect the response of cells to substrates (O'Brien, 2011). For this reason, mechanical properties of the PMMA films (Mw: 120000 and 996000) were measured under tensile conditions. Young's Modulus (E) and Ultimate Tensile Strength (UTS) determined from the curves obtained during tensile test are presented in Figure 3.1. PMMA with lower molecular weight (Mw: 120000) had a Young's Modulus (E) of around 850 MPa and an Ultimate Tensile Strength (UTS) around 25 MPa whereas PMMA with higher molecular weight (Mw: 996000) had a higher E (1200 MPa) and UTS (40 MPa). In general, when the molecular weight of polymers are higher, they have higher rigidity, strength and stiffness (Kawaguchi et al, 2011). In a study, the influence of molecular weight on mechanical properties of PMMA was explained by the entanglement of the polymer chains and the increase in the molecular weight led to an increase in the entanglement of the chains, a decrease in the viscosity of polymer chains and finally an increase in the UTS and E values (Landel and Nielsen, 1993). In the literature, PMMA was accepted as a polymer with high Young's Modulus as was found in this study and it is stated that this high Young's Modulus makes PMMA one of the hardest thermoplastics with high a scratch resistance (Ali et al, 2015).

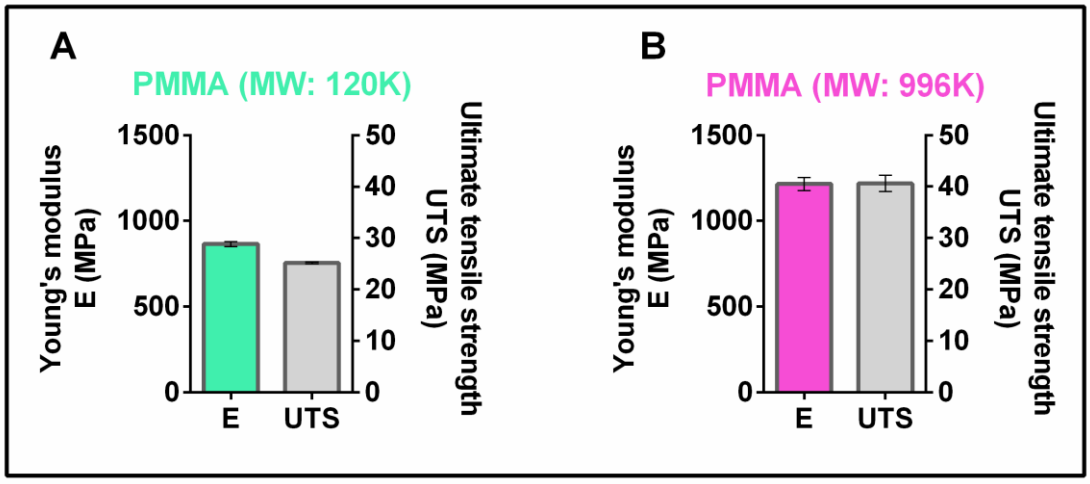

Figure 3.1. Young's Modulus and Ultimate Tensile Strength of solvent cast PMMA films with two different PMMA polymers with molecular weights A- 120K and B- 996K.

3.1.2. SEM

Micropillar arrays with 8 µm tall, 4x4 μm^2 area and 4 µm gap (P4G4) pillar organization and unpatterned (smooth) control (UC) were prepared on PDMS molds using the original wafer as the main template (Notation: P stands for the length of one side of the square pillar top (µm), G stands for interpillar distance (µm)). SEM micrographs of the top and side views of surface micropillar structures are shown in Figure 3.2.A. The pillar dimensions on the PMMA films were measured with ImageJ (NIH) software and it was found that PMMA films produced on PDMS molds had dimensions very close to those of the original wafer (Figure 3.2.B).

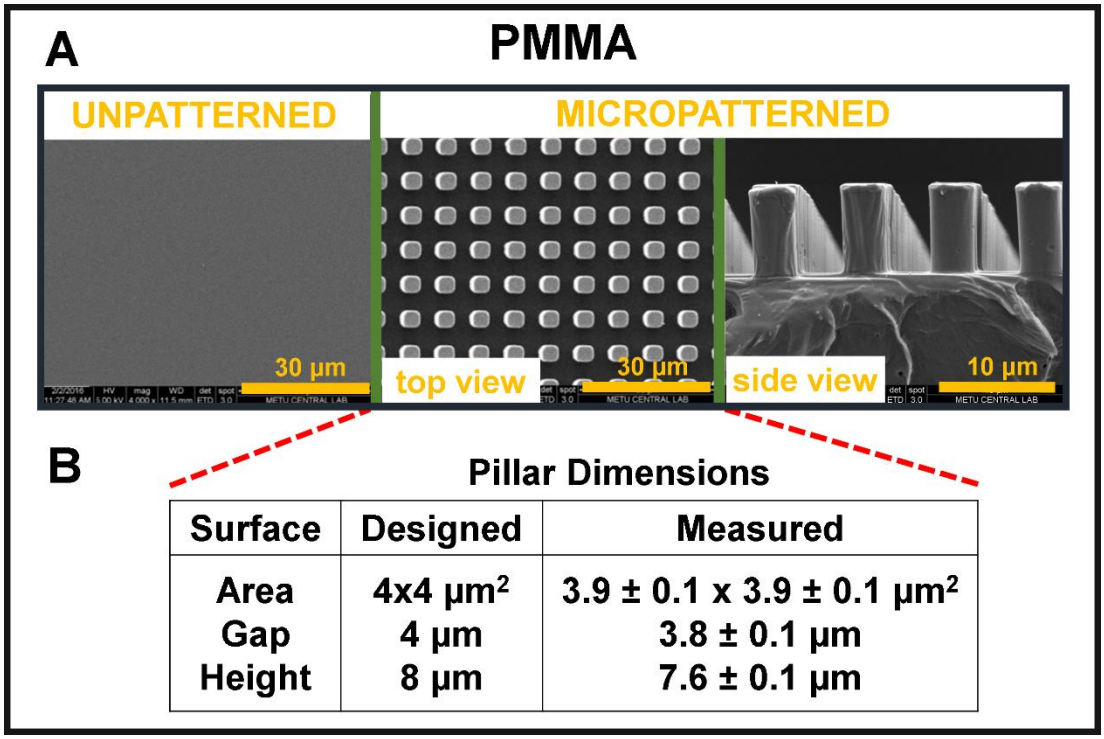

Surface	Designed	Measured
Area	4x4 µm²	3.9 ± 0.1 x 3.9 ± 0.1 µm²
Gap	4 µm	3.8 ± 0.1 µm
Height	8 µm	7.6 ± 0.1 µm

Figure 3.2. Characterization of PMMA films using SEM. A- SEM micrographs of (i) unpatterned and (ii) P4G4 patterned surfaces. (iii) side view of micropatterned P4G4 surface. B- Designed and obtained pillar dimensions of PMMA films.

3.1.3. AFM

PMMA was treated with oxygen plasma to modify its surface chemistry and increase its hydrophilicity. Oxygen plasma creates active centers on the surface because of the reaction with the excited ions and radicals of oxygen. Preparation conditions of 100 W for 10 min was used as was reported to be enough to saturate the surface with oxygen (Ozcan and Hasirci, 2007). The surface topography of untreated and plasma treated PMMA films were studied with AFM (Figure 3.3.A and B). The morphology of pristine PMMA was significantly different than the plasma treated PMMA; oxygen plasma treated surface was rougher than the untreated sample indicating that plasma treatment induces not just chemical but also morphological modifications on the surface. In addition to the introduction of new functional groups, some low MW

molecules (present or newly added) are removed from the polymer surface and this results in etching of the surface and resultant increase in surface roughness (Cvelbar et al, 2003; Vesel and Mozetic, 2012). AFM micrographs, root mean square (RMS) values and average heights support these observations (Figure 3.3.C). Upon treatment, the average height increased from 33.1 to 55.0 nm and RMS deviation increased from 6.4 to 15.9 nm, showing an increase in surface roughness.

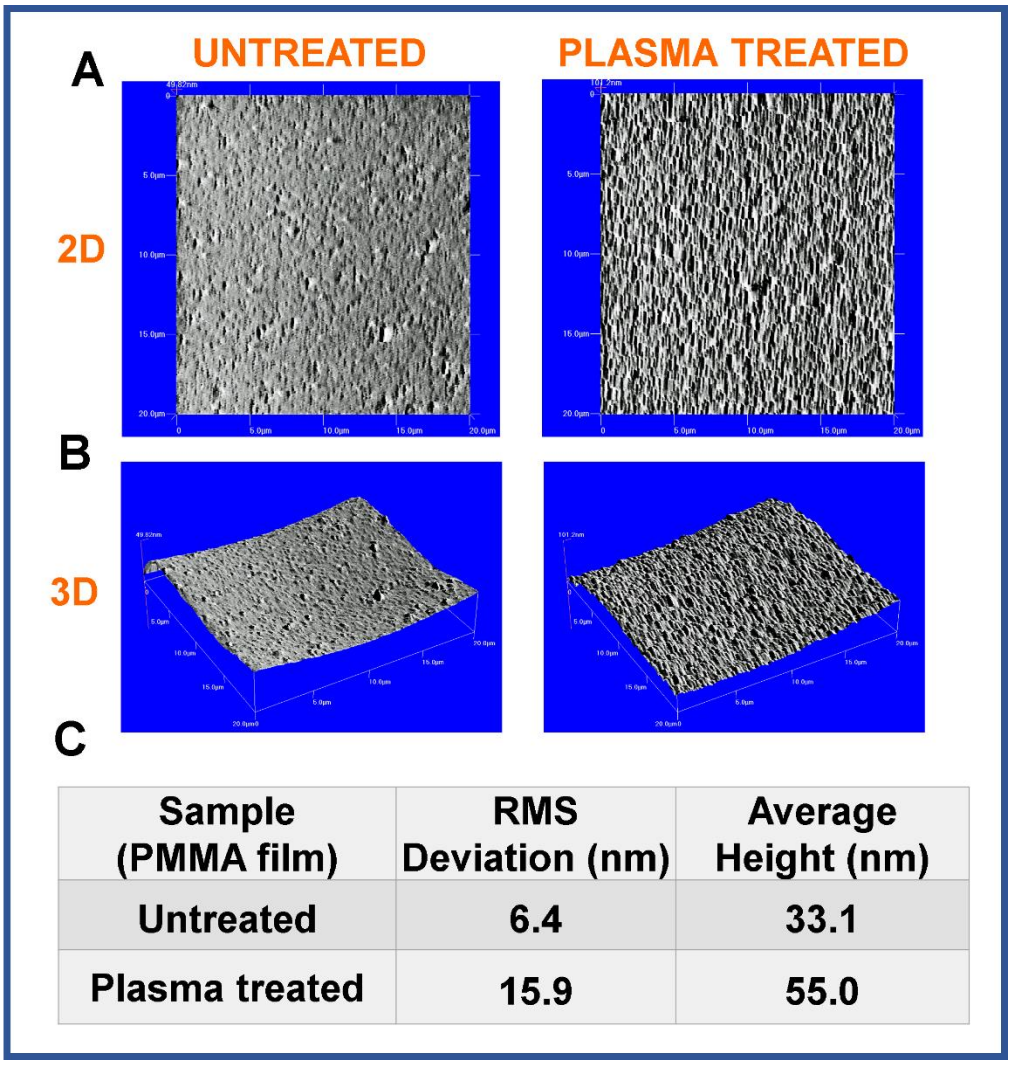

Sample (PMMA film)	RMS Deviation (nm)	Average Height (nm)
Untreated	6.4	33.1
Plasma treated	15.9	55.0

Figure 3.3. AFM micrographs of unpatterned PMMA films. A- 2D and B- 3D micrographs of untreated (left) and oxygen plasma treated (right) surfaces. C- Root mean square (RMS) and average height values obtained from the AFM.

3.1.4. Water Contact Angles

The water contact angle values were determined to investigate the influence of roughness or patterns on the wettabilities of oxygen plasma treated PMMA films. It was observed that after oxygen plasma treatment, contact angles of PMMA surfaces decreased to 14.5° and 14.7° for unpatterned and micropatterned films from their original values of 89.3° and 132.1° respectively (Figure 3.4). On the plasma treated surfaces, water droplets spread immediately and wetted the surface completely. This significant decrease upon plasma treatment is a result of increase in the polar or ionic oxygen groups (Chai et al, 2004). These values are in good agreement with the earlier reports on O_2 plasma treated PMMA surfaces decorated with microchannels (Yuan et al, 2009). On the other hand, change in wettability is also a result of the changes in the surface roughness. Contact angles of untreated micropatterned substrates (132.1°) were much higher than that on the untreated smooth surface (89.3°), suggesting that the micropillar features decreased the wettabilities of the substrates. This was expected, because the surface texture, or roughness up to a certain value, is known to enhance the intrinsic hydrophobicity of substrates and this is used to produce superhydrophobic (C.A. > 150°), highly water repellent, antifouling surfaces (Roach et al., 2008). Surface wetting and roughness relation was explained by Wenzel and Cassie-Baxter. They stated that the water droplets form equilibrium shapes to minimize the surface free energy at the solid-liquid interface resulting due to surface texture (Shirtcliffe et al., 2005). This superhydrophobicity phenomenon was first explained in 1936 by Wenzel and it was proposed that a liquid completely fills the gaps on a rough surface where it contacts. In 1944, Cassie and Baxter suggested that water forms incomplete contact with rough surfaces because air is trapped between the liquid and the substrate and this results in an increase in contact angle. On surfaces with simple roughness (roughness complexity is defined as the ratio between mean spacing and mean depth of the roughness motifs), Wenzel and Cassie-Baxter states are easy to distinguish, but complex roughness (such as roughness of micro and nano patterned substrates) may exhibit a mixture of two states. On many surfaces, a transition from Cassie-Baxter to Wenzel state is possible,

and the resistance of transition depends on the intrinsic chemical hydrophobicity and the distance between and the shape of topographic features.

In summary, to study the influence of 3D surface cues and wettability on cell morphology and behavior, four different surfaces were used in this study; untreated and smooth surfaces as controls, oxygen plasma treated smooth surfaces to study the effect of wettability, micropatterned untreated and oxygen plasma treated (100W, 10 min) surfaces to study the effect of surface topography.

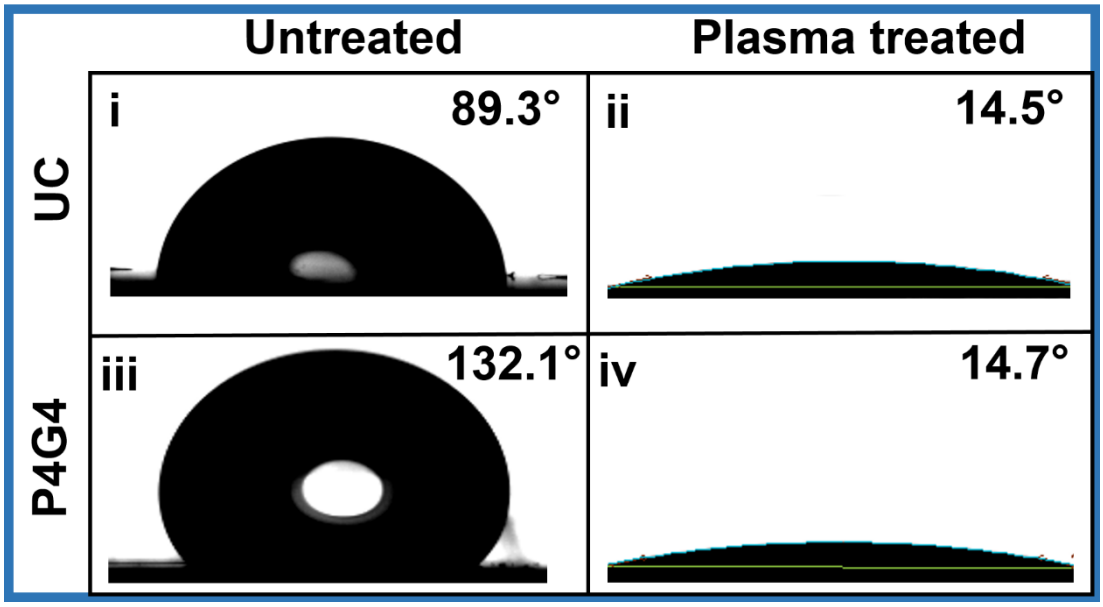

Figure 3.4. Contact angle measurements of the films. Water sessile drops on oxygen plasma treated and micropatterned (P4G4) surfaces and their controls are shown.

3.1.5. XPS

X-Ray Photoelectron Spectroscopy (XPS) is a method that determines the presence and amount of atoms on surfaces. In this study, it was used to determine the polymeric surface chemical composition after plasma treatment. Results in Figure 3.5, show an increase in oxygen to carbon ratio on the oxygen plasma treated PMMA films regardless of the pattern presence. The lowest ratio was observed with films

which were not treated with oxygen plasma supporting the contact angle results reported above.

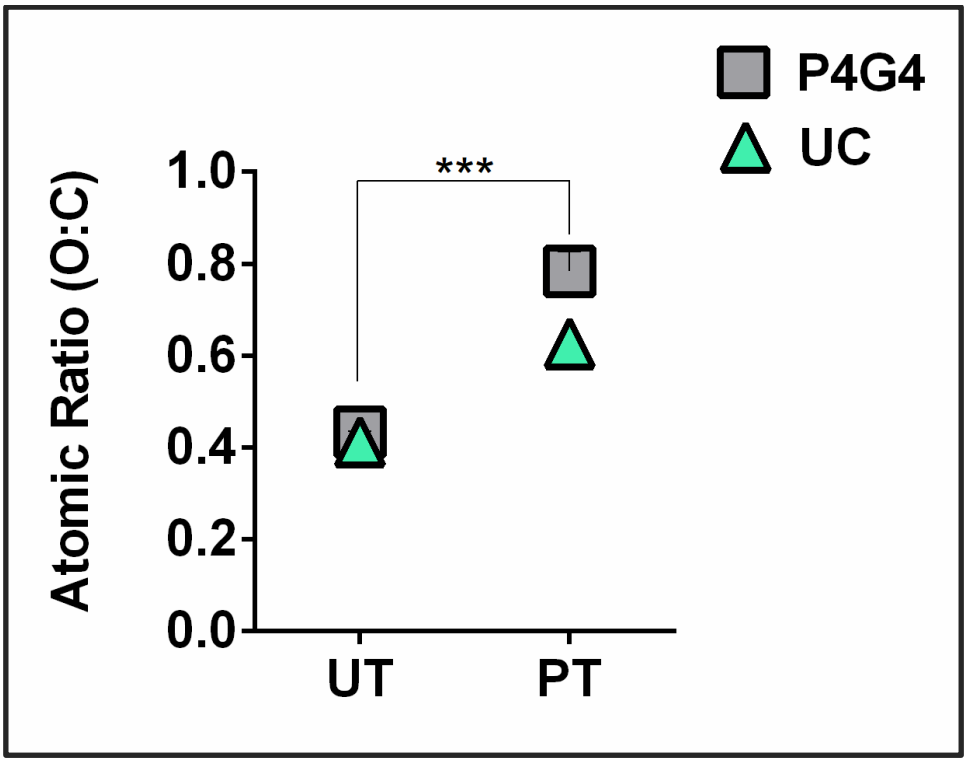

Figure 3.5. XPS analysis of the films. Oxygen:Carbon (O:C) atomic ratio determined using the XPS spectra of the O_{1s} and C_{1s} core level peaks of oxygen plasma treated and micropatterned (P4G4) films and their controls. (Plasma treatment: 100 W, 10 min).

3.2. *In vitro* Studies

Benign (MCF10A) breast epithelial cells, malignant but noninvasive (MCF7), and malignant and highly invasive (MDAMB231) breast cancer cells were seeded on micropatterned (P4G4) and oxygen plasma treated PMMA films. Adhesion and deformability behavior of the cells on these surfaces were studied by using Scanning Electron Microscopy (SEM) and fluorescence microscopy. Proliferation, metabolic

activity and viability of cells were studied by using Alamar Blue assay, PicoGreen DNA quantification assay and Live-Dead cell viability assay, respectively.

3.2.1. SEM

The 3 breast cells MCF10A, MCF7 and MDAMB231 were seeded on plasma treated and micropatterned (P4G4) PMMA films. They were cultured for 24 h. SEM micrographs of the cells seeded on these films are presented in Figures 3.6 and 3.7. When pristine (Figure 3.6) and oxygen plasma treated (Figure 3.7) surfaces were compared, higher spreading was observed on the plasma treated surfaces while the cells were more circular on untreated surfaces. Also, on plasma treated surfaces, they showed more filopodia. Moderately wettable or hydrophilic surfaces are preferable for cell adhesion and proliferation (Ozcan and Hasirci, 2007). Thus, a higher number of filopodia on the plasma treated surface suggests enhanced adhesion and migration of the cells compared to that on the untreated surface. Furthermore, filopodia are rich in activated cell adhesion molecules such as integrins and cadherins, and enable cells to probe their environment and migrate by acting as sites for signal transduction (Mattila and Lappalainen, 2008). A similar influence of increased hydrophilicity on the spreading of cells and the number of filopodia was reported on thermally oxidized silicon surfaces. Cells grown on hydrophilic surfaces were reported to spread well and exhibit areas of dense filopodia extensions while the cells grown on hydrophobic counterparts were much smaller and had less filopodia (Ranella et al, 2010). Therefore, it is clear that surfaces with optimal hydrophilicity exhibit better cell attachment and plasma treated films had the optimal hydrophilicity (C.A. 10º-40º) (Webb et al, 1998; Khorasani et al, 2008) for cell adhesion as shown in Figure 3.7. When the three cells were compared, it was observed that MDA-MB-231 cells, the invasive cancerous breast cells, were more circular and smaller than the other two.

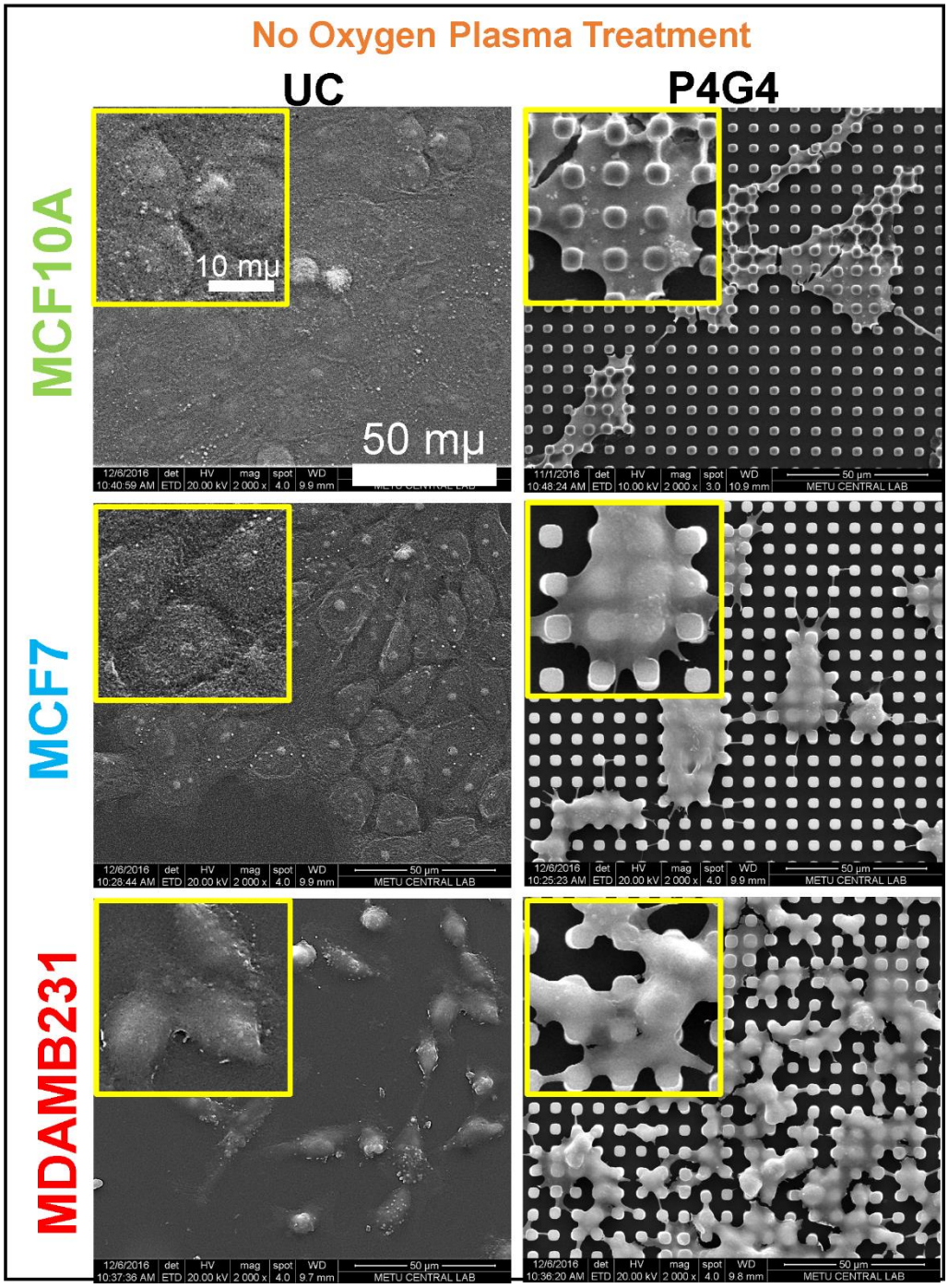

Figure 3.6. SEM micrographs of MCF10A, MCF7 and MDAMB231 cells on untreated unpatterned (UC) and P4G4 PMMA films. The upper left insets show a higher magnification of the micrographs. (Time: 24 h, Cell seeding density: 50000, Scale bars are same for all: 50 μm, insets: 10 μm).

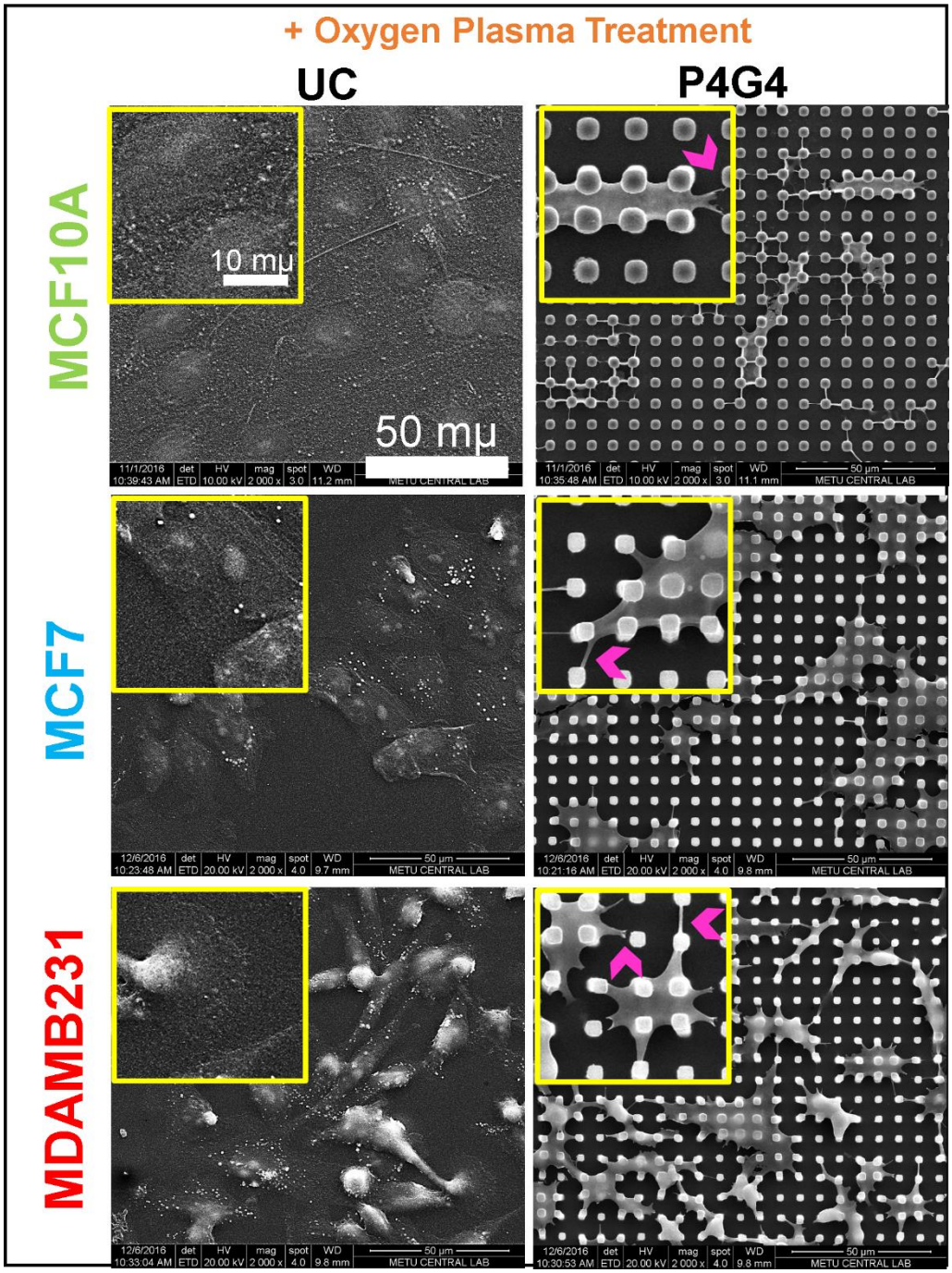

Figure 3.7. SEM micrographs of MCF10A, MCF7 and MDAMB231 cells on oxygen plasma treated unpatterned (UC) and P4G4 PMMA films. The upper left insets show a higher magnification of the micrographs. Pink chevrons show filopodia of the cells. (Time: 24 h, Cell seeding density: 50000, Scale bars are same for all: 50 μm, insets: 10 μm).

3.2.2. Fluorescence Microscopy

Fluorescence micrographs shows actin cytoskeleton (Figures 3.8, 3.9 and 3.10) and nuclei (Figures 3.11, 3.12 and 3.13) of the cell lines on plasma treated (PT) and micropatterned (P4G4) PMMA surfaces and their controls. On untreated surfaces cells attached as clusters and there was not so much interaction between the cell groups whereas they scattered to the surface uniformly on plasma treated P4G4 and smooth surfaces in any of the cells (Figures 3.8, 3.9 and 3.10). This is a result of moderate hydrophilicity of the surface provided by plasma treatment as explained before.

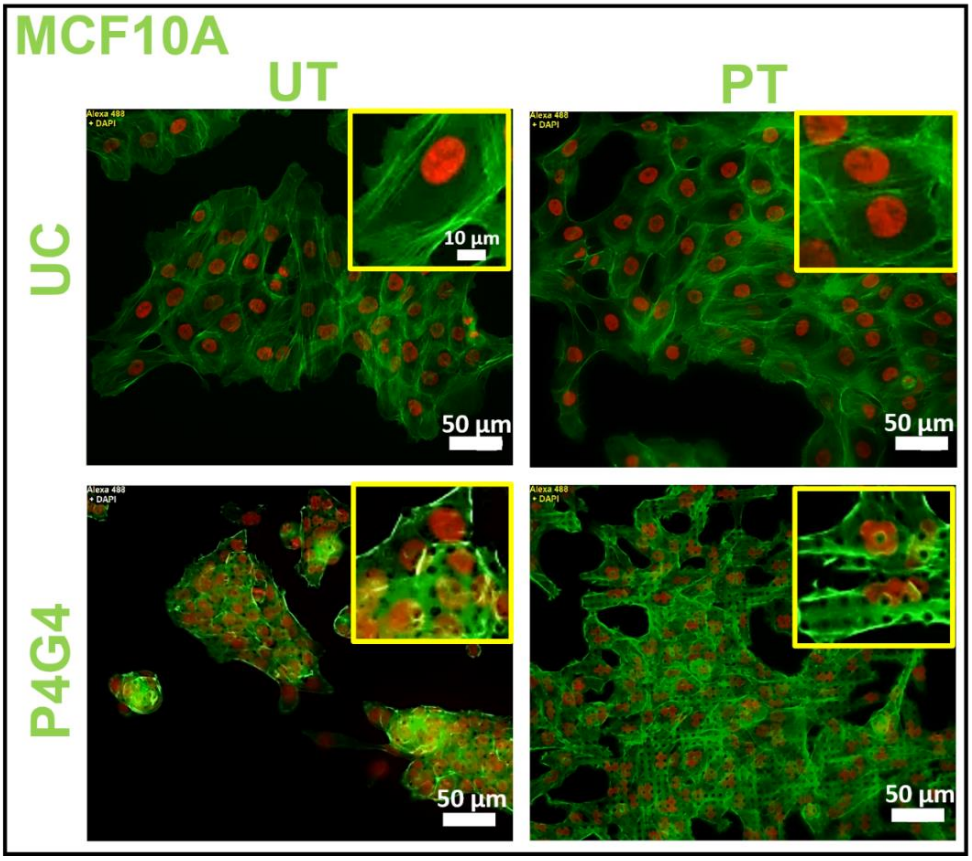

Figure 3.8. Fluorescence micrographs of actin cytoskeleton (green) and nuclei (red) of MCF10A cells. They are seeded (50000 cells/film) on untreated (UT) and plasma treated (PT), unpatterned (UC) and P4G4 PMMA films for 24 h. (Green: Alexa Fluor 488 Phalloidin, Red: DAPI, Scale bars: 50 µm, insets: 10 µm).

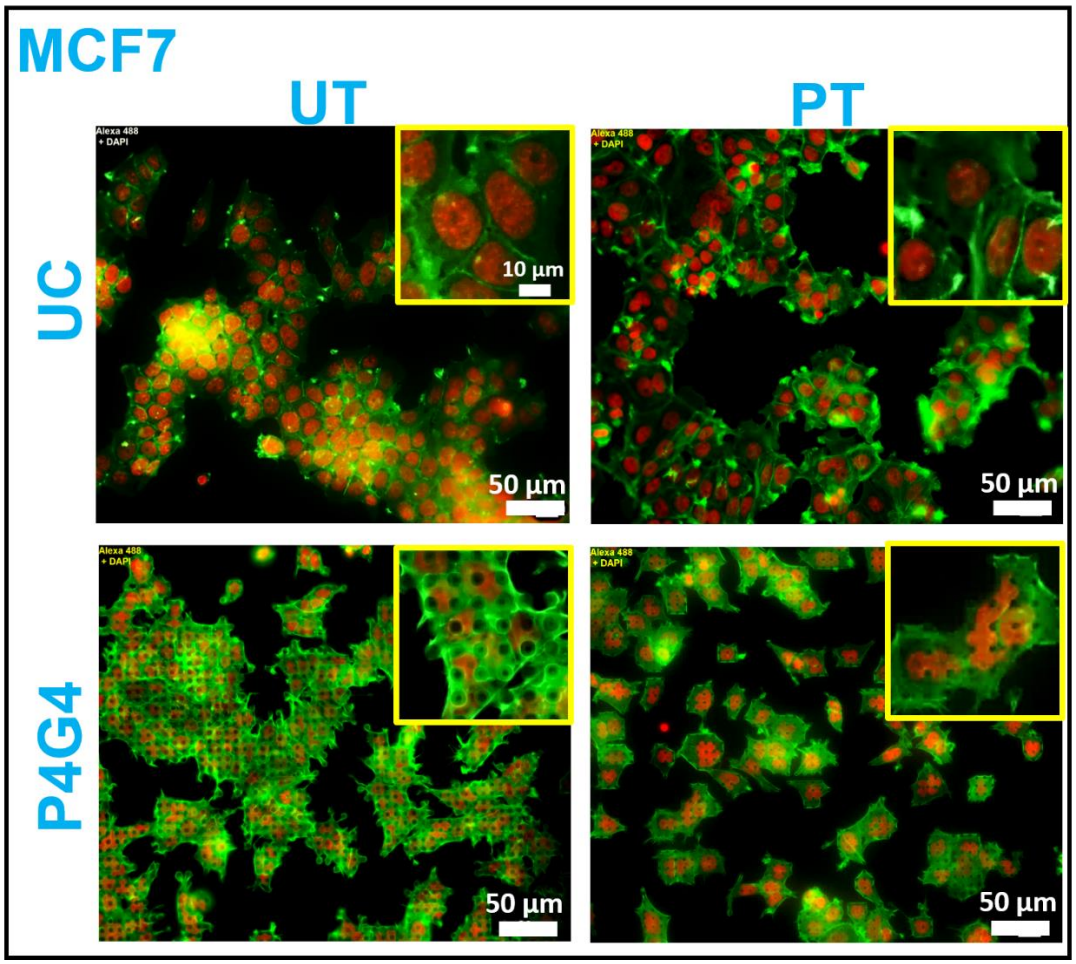

Figure 3.9. Fluorescence micrographs of actin cytoskeleton (green) and nuclei (red) of MCF7 cells. They are seeded (50000 cells/film) on untreated (UT) and plasma treated (PT), unpatterned (UC) and P4G4 PMMA films for 24 h. (Green: Alexa Fluor 488 Phalloidin, Red: DAPI, Scale bars: 50 µm, insets: 10 µm).

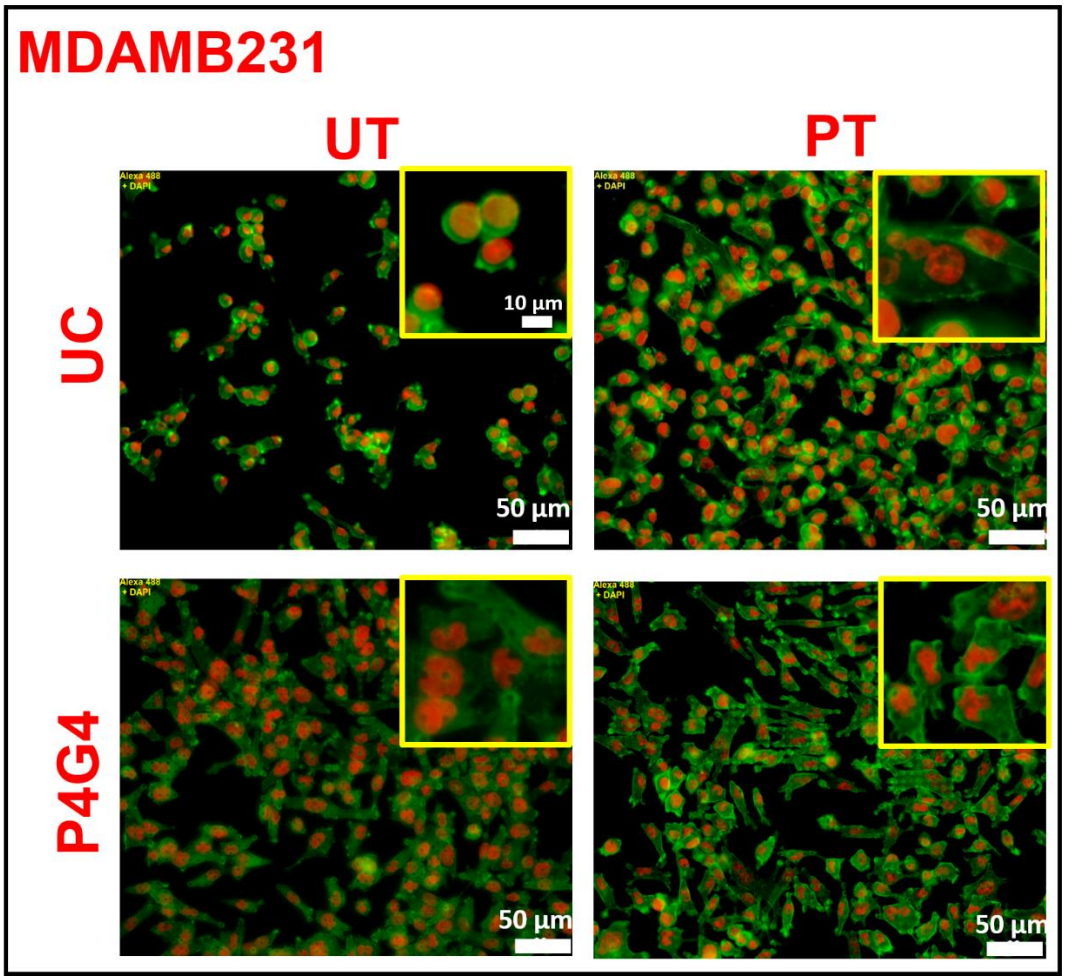

Figure 3.10. Fluorescence micrographs of actin cytoskeleton (green) and nuclei (red) of MDAMB231 cells. They are seeded (50000 cells/film) on untreated (UT) and plasma treated (PT), unpatterned (UC) and P4G4 PMMA films for 24 h. (Green: Alexa Fluor 488 Phalloidin, Red: DAPI, Scale bars: 50 µm, insets: 10 µm).

When the nuclear deformability of the cells were compared, both MCF-7 (Figure 3.12) and MDA-MB-231 (Figure 3.13) showed nucleus deformation on micropatterned (P4G4) films, plasma treated or not. However, MCF10A benign cells (Figure 3.11) showed nucleus deformation only on plasma treated P4G4 surfaces whereas there was no nucleus deformation on untreated P4G4 surfaces. It is known that this deformability difference in between the different cells with different

malignancy is mainly a result of differences between stiffness of the cells (Guck et al., 2005). Moreover, the mechanical properties and stiffness of the cell as a whole reflect contributions from the nucleus, microtubule and intermediate filament networks, actin cytoskeleton, membrane, and are additionally influenced by interactions with the pericellular ECM (Staunton et al, 2016). In a study, average Young's Modulus of the three cell lines were given as; 0.7 kPa, 0.5 kPa and 0.3 kPa for MCF10A, MCF7 and MDAMB231 cells, respectively showing that cancer cells are softer than healthy cells and invasive cancer cells are softer than non-invasive cells (Calzado-Martin et al, 2016). These correlation between the stiffness and invasiveness of the tumor cells explains the reason of decreasing deformation of nuclei from cancer to benign cell. However, there were not significant differences between the two malignant cells (invasive MDAMB231 and noninvasive MCF7). Moreover, it seems that oxygen plasma treatment plays a role and enable cells attach and spread better and deform. Thus, the difference between the cells is more apparent when the surfaces are not oxygen plasma treated. As a conclusion, untreated P4G4 PMMA surfaces can be used to detect malignant and benign breast cells. On the smooth films, nuclei of cells were elliptical or circular for all three cells.

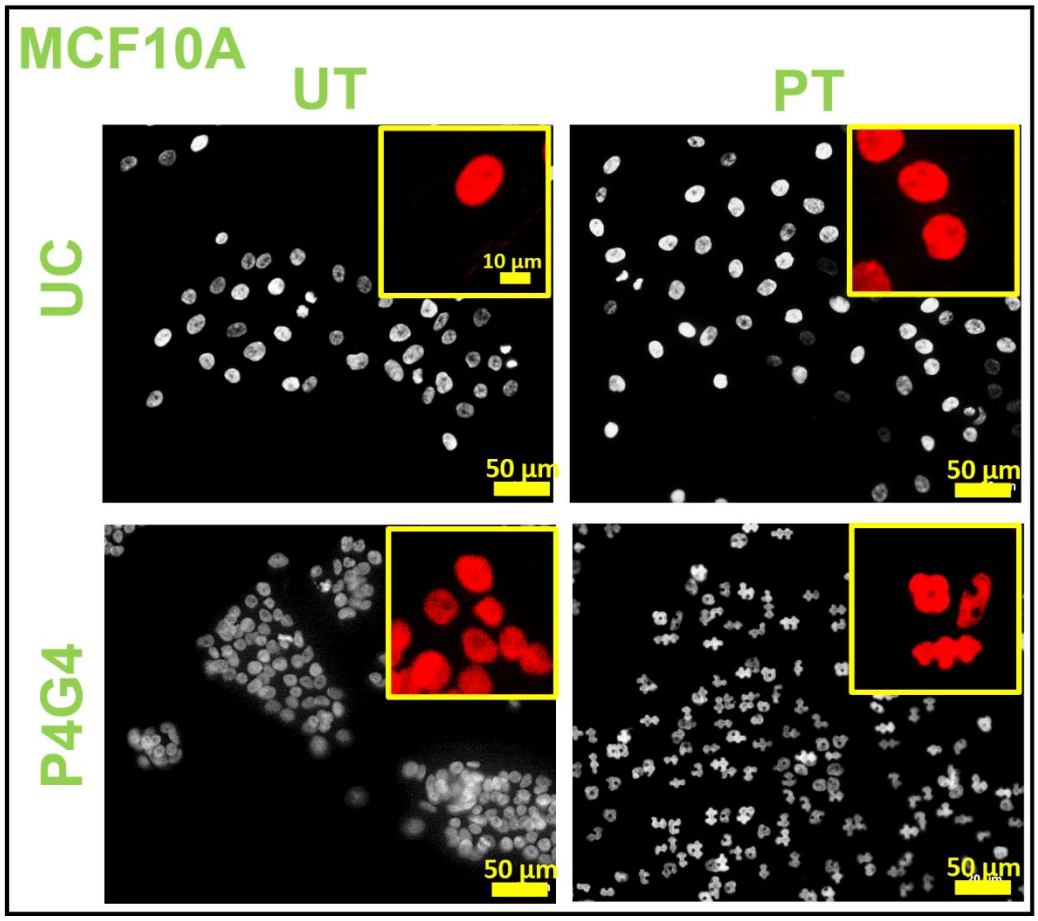

Figure 3.11. Fluorescence micrographs of nuclei of MCF10A cells. They are seeded on untreated (UT) and plasma treated (PT), unpatterned (UC) and P4G4 PMMA films for 24 h. (Nucleus stain: DAPI, Cell seeding density: 50,000 cells/sample, Scale bars: 50 µm, insets: 10 µm).

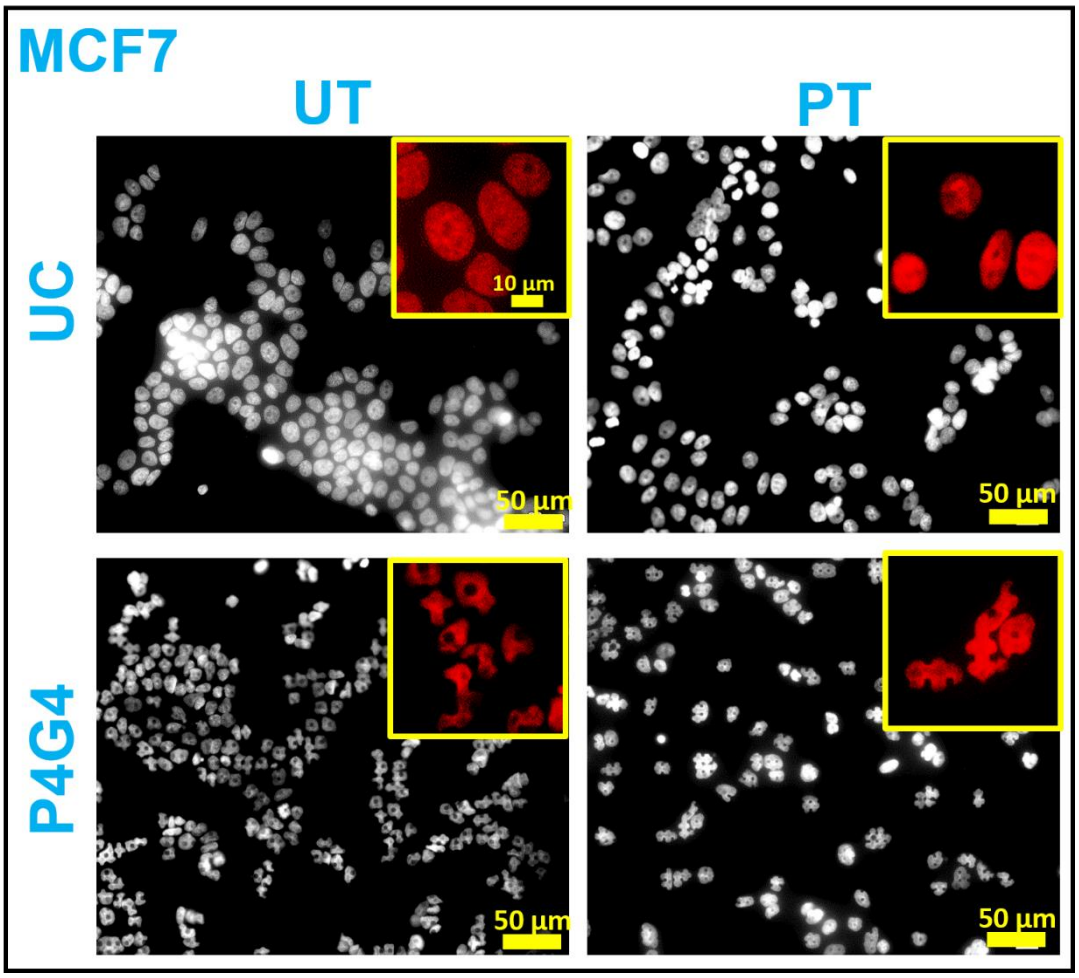

Figure 3.12. Fluorescence micrographs of nuclei of MCF7 cells. They are seeded on untreated (UT) and plasma treated (PT), unpatterned (UC) and P4G4 PMMA films for 24 h. (Nucleus stain: DAPI, Cell seeding density: 50,000 cells/sample, Scale bars: 50 µm, insets: 10 µm).

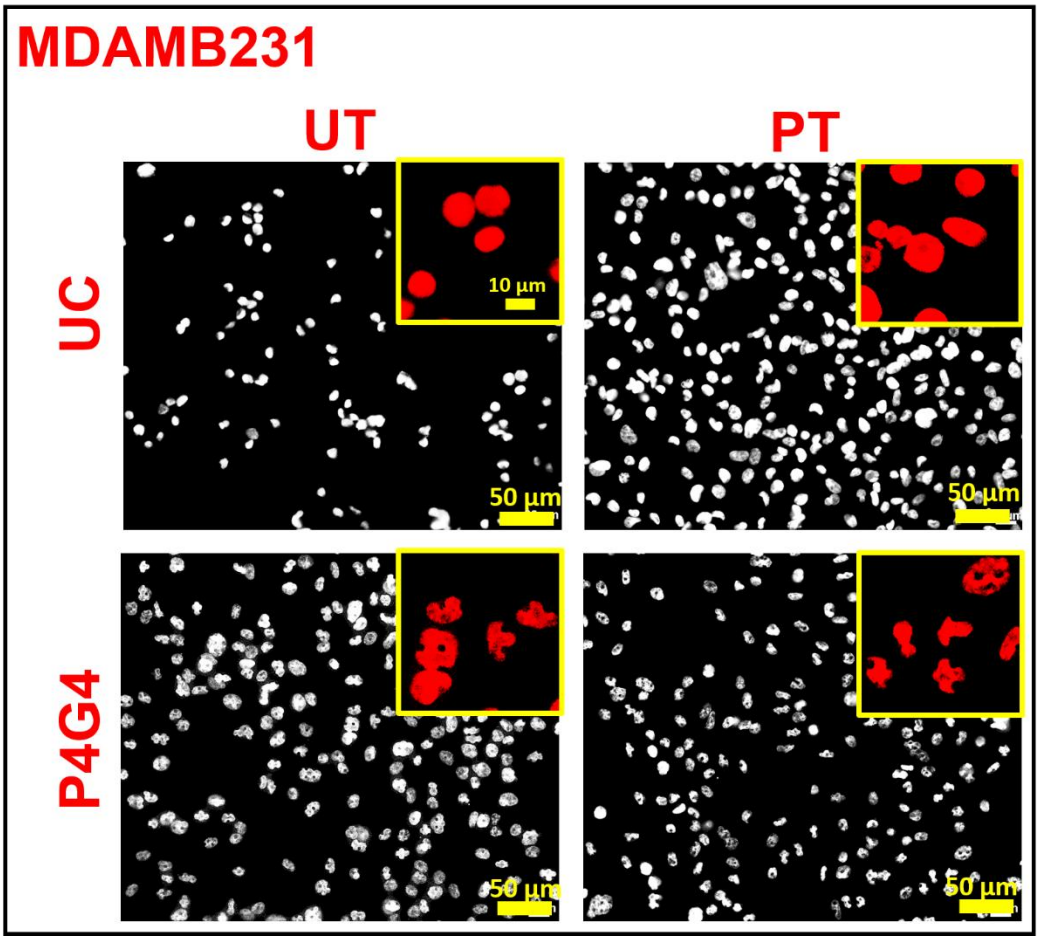

Figure 3.13. Fluorescence micrographs of nuclei of MDAMB231 cells. They are seeded on untreated (UT) and plasma treated (PT), unpatterned (UC) and P4G4 PMMA films for 24 h. (Nucleus stain: DAPI, Cell seeding density: 50,000 cells/sample, Scale bars: 50 µm, insets: 10 µm).

3.2.3. Proliferation, Metabolic Activity and Viability of Cells

In order to study the effect of PMMA and micropatterns on cell proliferation and metabolic activity, Alamar Blue assay, PicoGreen DNA quantification assay and Live-Dead cell viability assay were used. TCPS and unpatterned PMMA films were used as controls.

3.2.3.1. Proliferation of Cells

In the literature, it is shown that nano and micropatterns affect cell proliferation and the extent of this effect depend on the cell type (Green et al, 1994; Dalby et al, 2004; Miller et al 2004; Bettinger et al, 2009). However, there is no consensus on how this effect will be. A few studies reported an increase in cell number on a patterned substrate while some other studies reported a decrease (Popat et al, 2007). A number of parameters such as micropattern dimensions, chemistry, mechanical properties and cell types were found to be influential. In this study, cell numbers were calculated from the DNA content of cells using PicoGreen DNA quantification assay (Figure 3.14). A single human diploid cell contains approximately 7 picograms of DNA and the DNA content obtained from the cells are divided by 7 in order to calculate cell number (Chomczynski et al, 1997; Serth et al, 2000; Melnikov et al, 2005; Kumar et al, 2013; Macaulay and Voet, 2014). Tests showed that PMMA causes a decrease in cell number when compared to TCPS. Micropatterns, on the other hand, caused an increase in cell number when compared to smooth PMMA (Figure 3.14). Many researchers have studied proliferation behavior of cells on micro and nanostructured surfaces and showed proliferation rate increase on microstructures compared to smooth surfaces (Moroni et al, 2009; Kim et al, 2010; Nagayama et al, 2015) and explained this behavior by the increasing number of attachment sites on micropatterned surfaces (Moroni et al, 2009; Kim et al, 2010). Decrease in proliferation in benign MCF10A cells seeded on P4G4 or smooth PMMA surfaces was more distinct than in the malignant cells when compared to the ones on TCPS. In a study, this difference between the proliferation of benign and malignant cells was explained as a result of deformation of nuclear lamins on micropatterned surfaces. Deformation in nuclear lamins caused a stress-induced inhibition in cell proliferation but this occurred rarely in cancer cells with already deformable nuclei (Nagayama et al, 2015). Proliferation on PMMA is lower than on TCPS and it was earlier shown that PMMA had an inhibitory effect on cell proliferation and metabolic activity by causing cells to arrest at G_0-G_1 phases of the cell cycle (Zambonin et al, 1998; Latz et al, 2000; Evans et al, 2004; Schulze et al, 2013; Ermis, 2016).

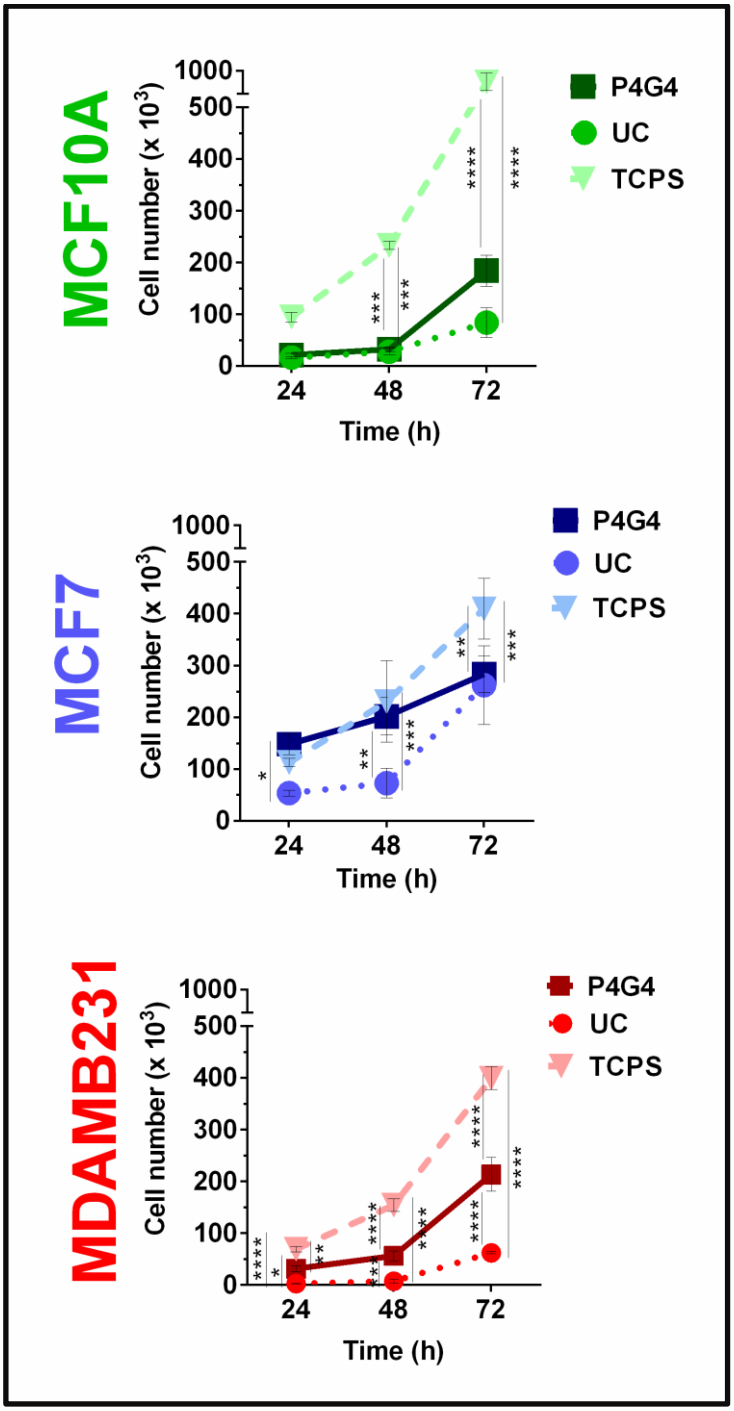

Figure 3.14. Cell proliferation on P4G4 surfaces as determined by PicoGreen DNA quantification assay. Numbers of three breast cells are shown for a period of 48 h culture durations. (Cell seeding density: 50,000 cells/sample).

3.2.3.2. Metabolic Activity of Cells

Metabolic activity of the cells were studied by reduction (%) from Alamar Blue assay (Figure 3.15). In summary, metabolic activity of the cells was lower on all surfaces for 24 h due to adhesion being low. After 24 h, metabolic activity of cells increased on TCPS but this increase was the highest for MCF10A. This can be a result of different doubling times of the cells; MCF10A: 16 h, MCF7: 29 h and MDAMB231: 38 h. On the other hand, on PMMA surfaces, metabolic activity of the cells were low for the whole culture duration. Reason of the low metabolic activity on smooth and P4G4 PMMAs was the effect of both the nature of PMMA itself and the deformation of the cells. PMMA was known to arrest cells at stationary (G_0/G_1) of the cell cycle (Ermis, 2016) and also changes in cell and nuclear shape have an effect on the chromatin condensation and elongated or deformed nuclei was shown to cause a chromatin condensation and decreased proliferation rate of cells (Versaevel et al, 2012).

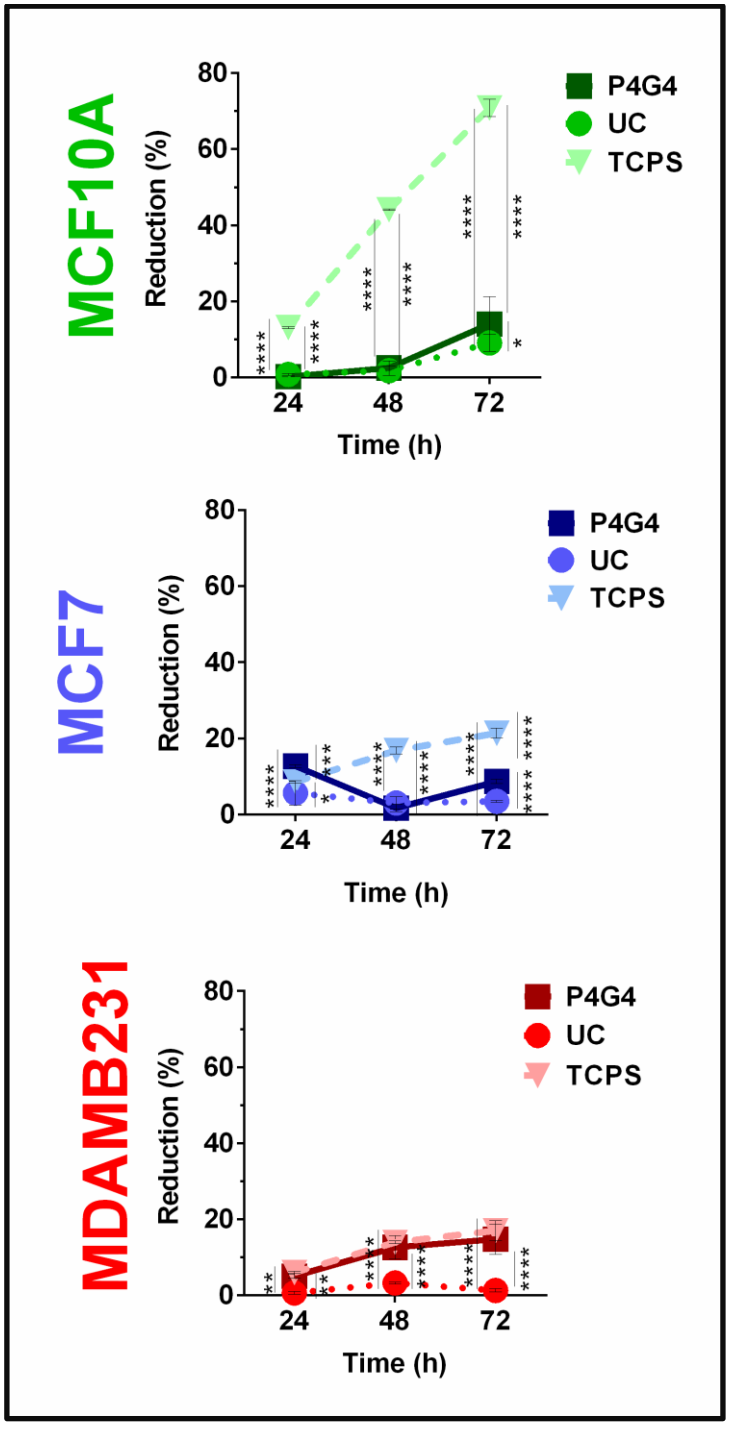

Figure 3.15. Cell metabolic activity as determined by Alamar Blue Assay on P4G4 PMMA. Metabolic activity of cells is shown by Reduction (%) (Cell seeding density: 50,000 cells/sample).

3.2.3.3. Viability of Cells

Live-Dead cell viability assay was used to show that all the cells used in PicoGreen DNA quantification and Alamar Blue assays were alive (Figures 3.16-3.18). Calcein and Propidium Iodide (PI) solutions were used to stain live and dead cells, respectively. Since calcein only stains viable cells and emits a strong green fluorescence, micrographs showing only green cells and no red cells means all cells are viable. All micrographs (Figures 3.16-3.18) showed only viable cells for the three days the cells spent on TCPS and PMMA surfaces.

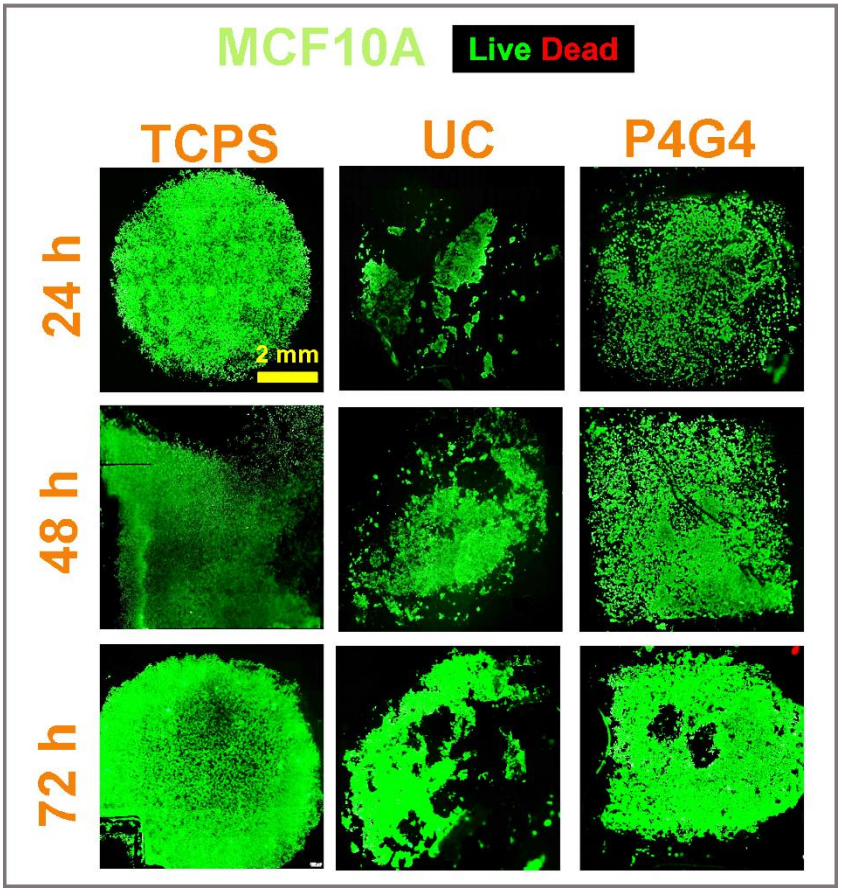

Figure 3.16. Live-Dead assay of MCF10A cells. Cells on the TCPS, unpatterned (UC) and micropatterned (P4G4) PMMA surfaces were stained for Live-Dead assay using Calcein (green, Live) and Propidium Iodide (red, Dead) upon 24, 48 and 72 h culture duration (Cell seeding density: 50,000 cells/sample, Scale bars: 2 mm).

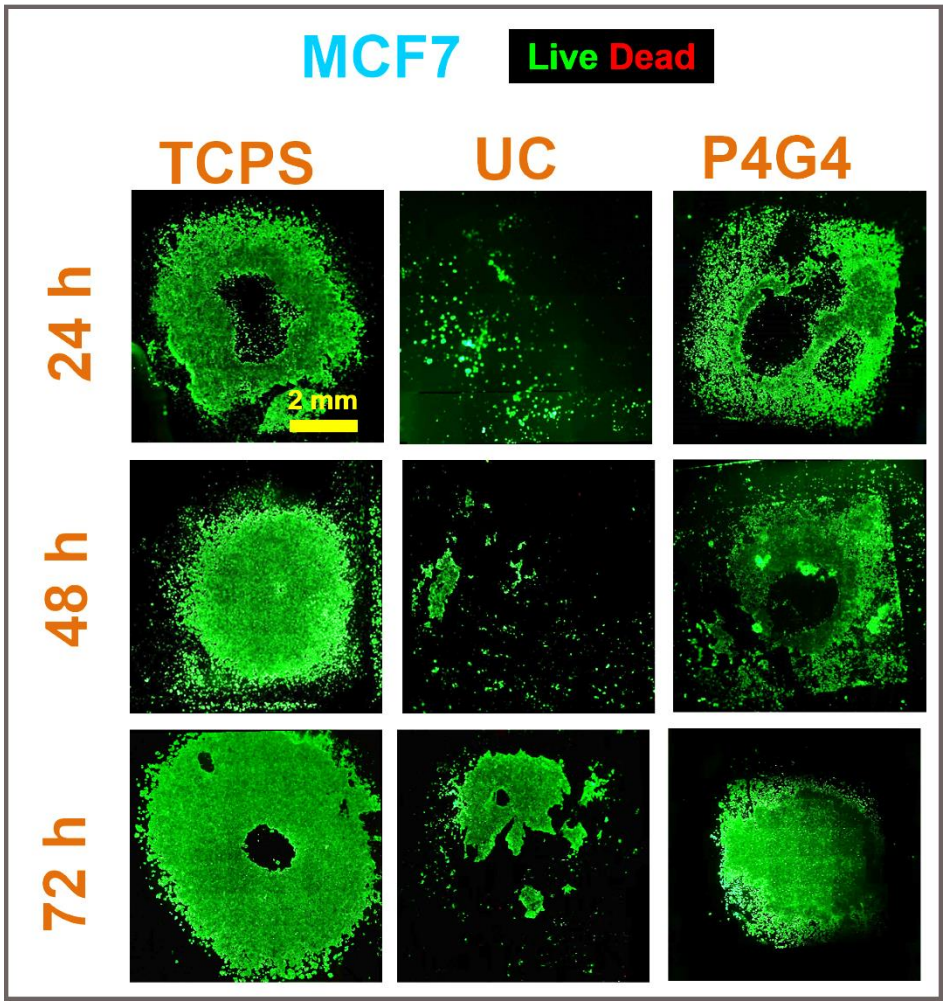

Figure 3.17. Live-Dead assay of MCF7 cells. Cells on the TCPS, unpatterned (UC) and micropatterned (P4G4) PMMA surfaces were stained for Live-Dead assay using Calcein (green, Live) and Propidium Iodide (red, Dead) upon 24, 48 and 72 h culture duration (Cell seeding density: 50,000 cells/sample, Scale bars: 2 mm).

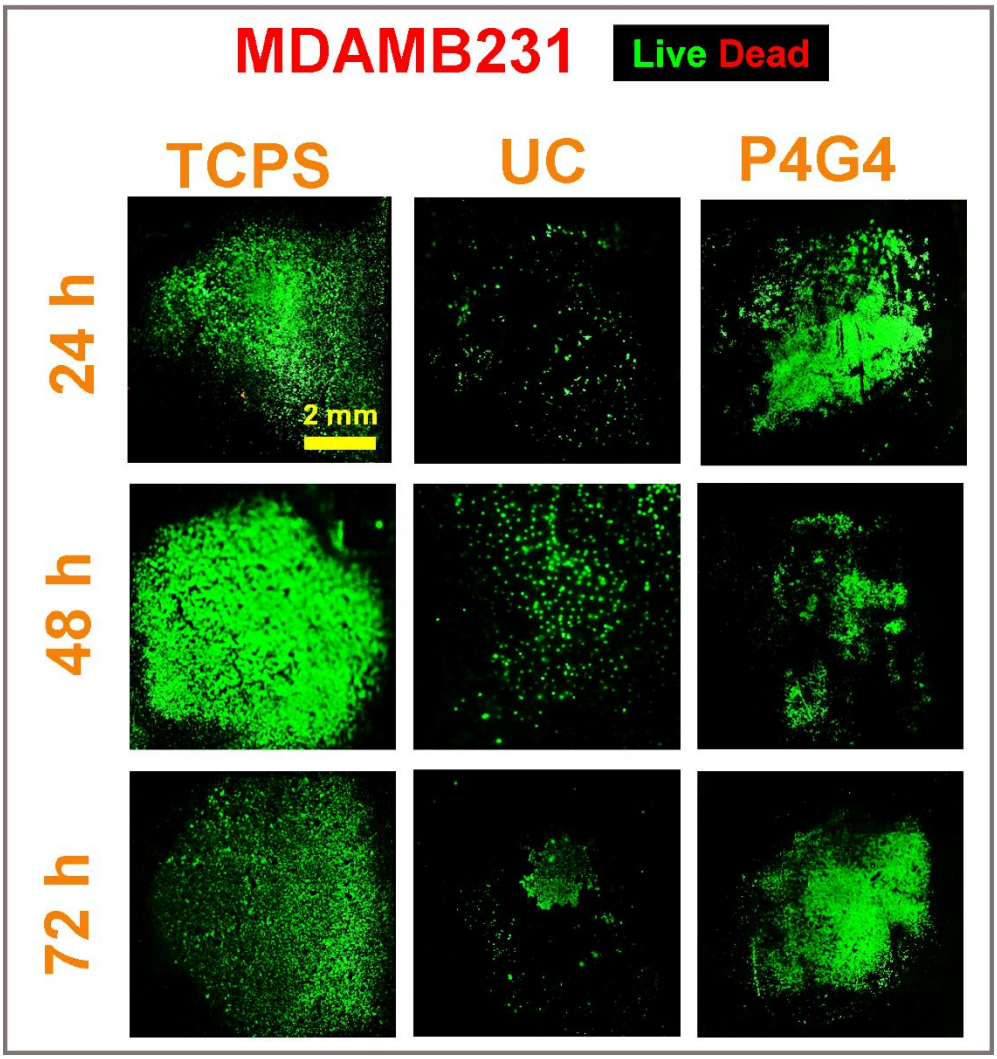

Figure 3.18. Live-Dead assay of MDAMB231 cells. Cells on the TCPS, unpatterned (UC) and micropatterned (P4G4) PMMA surfaces were stained for Live-Dead assay using Calcein (green, Live) and Propidium Iodide (red, Dead) upon 24, 48 and 72 h culture duration (Cell seeding density: 50,000 cells/sample, Scale bars: 2 mm).

3.3. Influence of Actin Inhibiting Drugs on Breast Cancer Cell Properties

3.3.1. Drug Dose Optimization on Cells by Alamar Blue Assay

Actin inhibiting drugs were chosen in this study to understand the role of mechanotransduction event on the deformability of the cells because there is a coordination between the mechanosensory (integrins) and force transmission elements, the actin cytoskeleton, that direct mechanotransduction event and so the deformability of the cell (DuFort et al, 2011). Two drugs used in this study were: Cytochalasin D and Jasplakinolide. Cytochalasin D acts by inhibiting actin polymerization by binding to monomers and capping the filaments and it is selective for actin (Otto et al, 2015; Glenn et al, 2016). Jasplakinolide, on the other hand, stimulates actin polymerization and shows its growth inhibition effect on breast cancer cells by disrupting F-actin fibers by blocking FAK signaling pathway (Shankar and Nabi, 2015). Action mechanisms of these two drugs were presented in Chapter 2 (Figure 2.4). In the test, the cells were cultured for 24 h (day 1) on the tissue culture plate, and then they were treated with drugs for another 24 h (day 2). Serial dilutions were used: For Cytochalasin D 0, 0.01, 0.05, 0.1, 0.5, 1, 5, 10 μM and for Jasplakinolide 0, 0.01, 0.05, 0.1, 0.5, 1, 5 μM. Effect of Cytochalasin D and Jasplakinolide on the cell metabolic activity was determined by Alamar Blue assay.

Dose-Response curves show that when either Cytochalasin D (CytoD) or Jasplakinolide (Jasp) (Figures 3.19 and 3.20) were used with their highest concentration (10 μM and 5 μM, respectively), they did not decrease the metabolic activity of the cells by more than 50% for all cell types. Cytotoxic levels of these drugs were reported to be above 100-200 μM on breast cancer cells (Hayot et al, 2006; Shankar and Nabi, 2015).

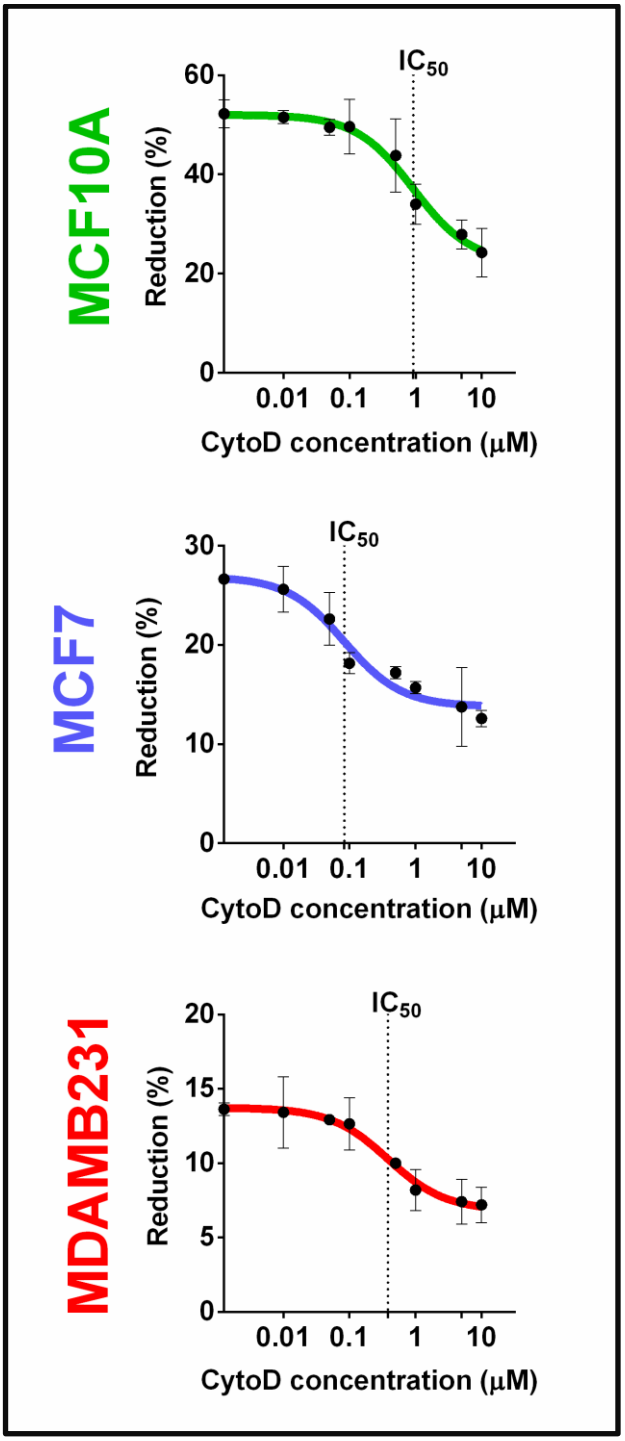

Figure 3.19. Drug dose-response curves of Cytochalasin D (CytoD) on 3 cell lines. Serial dilution of drug concentrations on TCPS are shown by using reduction (%) calculated from Alamar Blue Assay. Dose axis is logarithmic. IC_{50} indicated the drug dose needed to decrease the drug activity to its 50%.

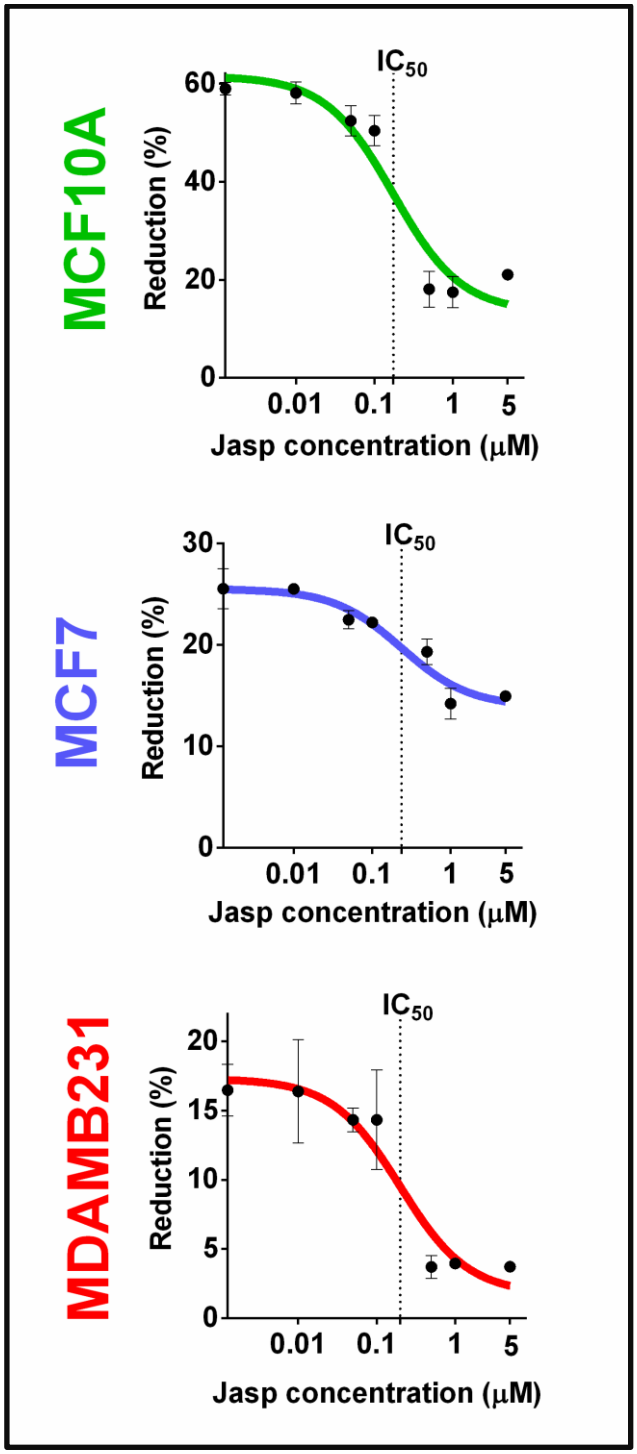

Figure 3.20. Drug dose-response curves of Jasplakinolide (Jasp) on 3 cell lines. Serial dilution of drug concentrations on TCPS are shown by using reduction (%) calculated from Alamar Blue Assay. Dose axis is logarithmic. IC_{50} indicated the drug dose needed to decrease the drug activity to its 50%.

3.3.2. Effect of Drugs on Cytoskeletal and Nuclear Deformation of Cells by Fluorescence Microscopy

Fluorescence micrographs of the cytoskeletons of the 3 cells after drug treatment while on TCPS are shown in Figures 3.21-3.23. It is observed that increasing the concentrations of drugs caused a progressive shrinking of the cells and reduced actin contents as shown by actin-specific stain (Alexa Fluor 488 Phalloidin). This observation is same as the literature that states increasing CytoD concentration from 10 to 200 μM resulted in progressive shrinking of the cells and reduced F-actin content when metastatic human cancer cell lines were used (Shankar and Nabi, 2015).

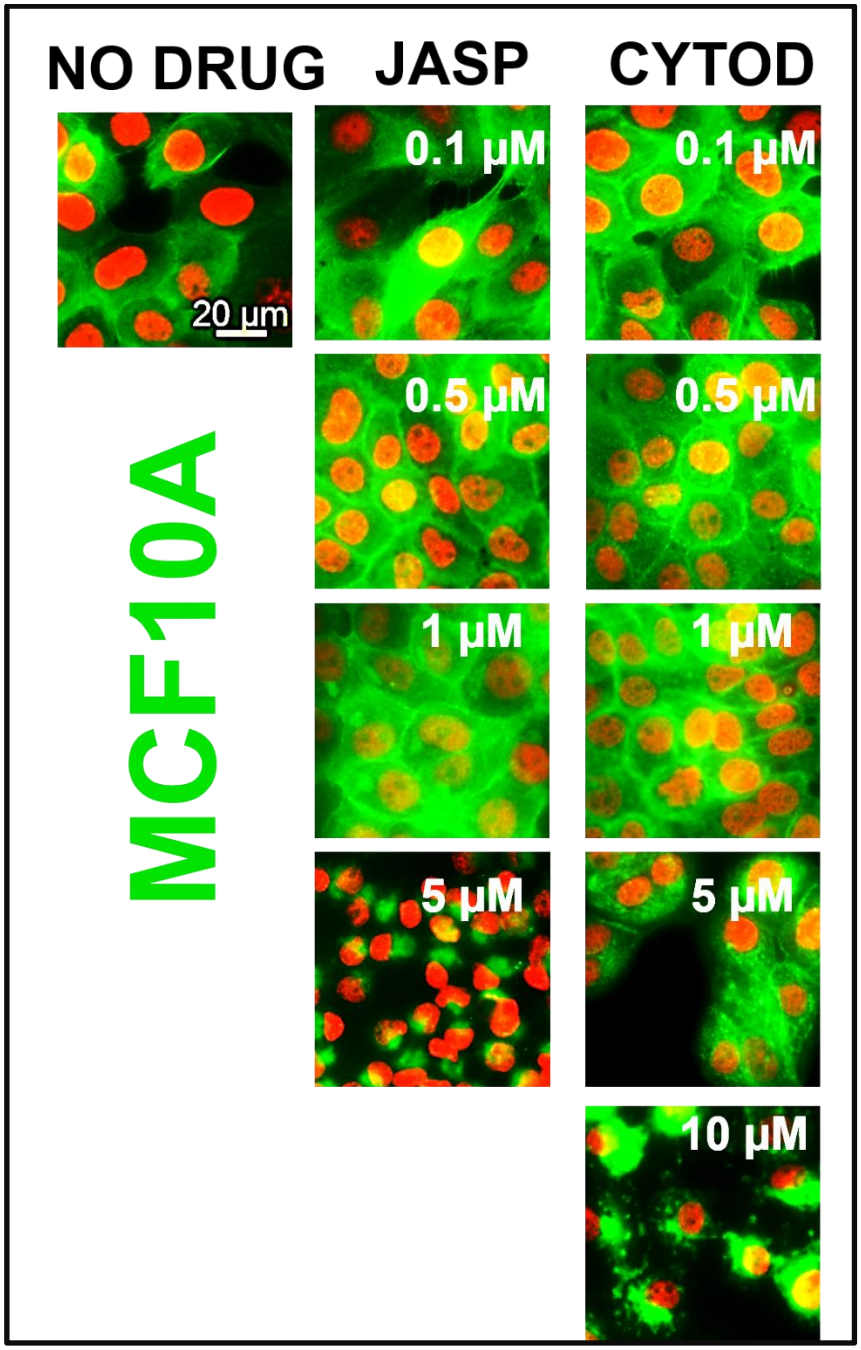

Figure 3.21. Drug treatments of MCF10A cells seeded on TCPS. Serial dilutions were used. For Cytochalasin D: 0, 0.01, 0.05, 0.1, 0.5, 1, 5, 10 µM and for Jasplakinolide: 0, 0.01, 0.05, 0.1, 0.5, 1, 5 µM. Fluorescence micrographs of MCF10A cells are shown under the treatment of CytoD and Jasp. (Scale bar: 20 µm)

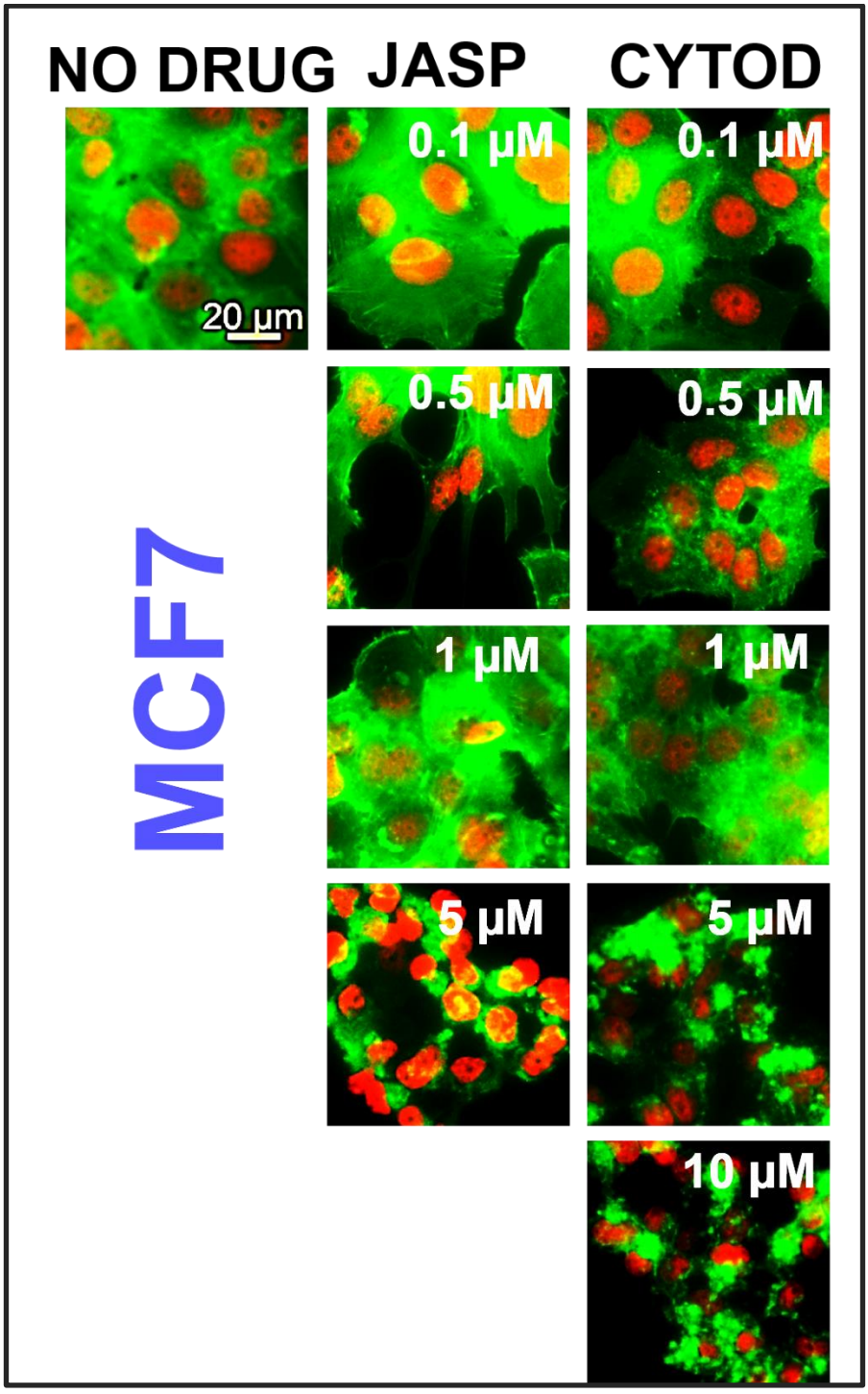

Figure 3.22. Drug treatments of MCF7 cells seeded on TCPS. Serial dilutions were used. For Cytochalasin D: 0, 0.01, 0.05, 0.1, 0.5, 1, 5, 10 µM and for Jasplakinolide: 0, 0.01, 0.05, 0.1, 0.5, 1, 5 µM. Fluorescence micrographs of MCF7 cells are shown under the treatment of CytoD and Jasp (Scale bar: 20 µm).

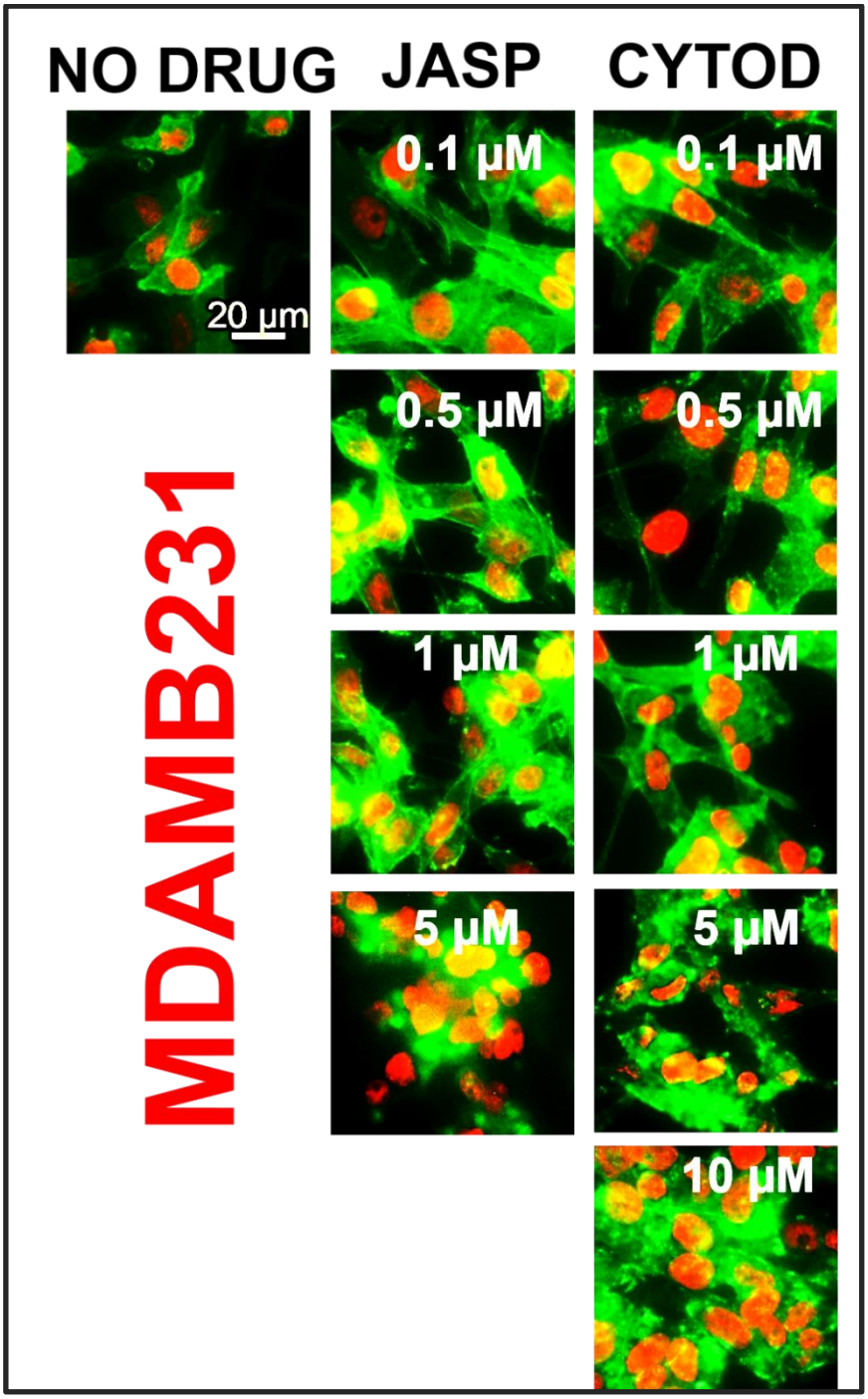

Figure 3.23. Drug treatments of MDAMB231 cells seeded on TCPS. Serial dilutions were used. For Cytochalasin D: 0, 0.01, 0.05, 0.1, 0.5, 1, 5, 10 µM and for Jasplakinolide: 0, 0.01, 0.05, 0.1, 0.5, 1, 5 µM. Fluorescence micrographs of MDAMB231 cells are shown under the treatment of CytoD and Jasp (Scale bar: 20 µm).

After showing that the highest concentrations used did not decrease the metabolic activity of the cells by more than 50% (Figure 3.19 and 3.20) and showed a distinct effect on actins of the cells (Figure 3.21, 3.22 and 3.23), only two highest drug doses (10 μM for CytoD and 5 μM for Jasp) were used to perform nuclear deformation analysis. In Figures 3.24-3.26 fluorescence micrographs of cells are presented. Upper and middle micrographs show cells with no drug treatment up to 48 h. Lower micrographs show the cells upon drug treatment and incubation for 24 h of culture. Drugs were added after 24 h culture duration and cells were cultured for 24 h with drugs. It is observed that nuclei of benign cells (Figure 3.24) were not deformed whereas nuclei of malignant cells (Figure 3.25 and 3.26) were highly deformed after 24 h culture. After 48 h culture, nuclei of all cells were deformed. However, nuclei of cells upon drug treatment were less deformed (Figure 3.24, bottom) or not deformed (Figure 3.25 and 3.26, bottom) at all after 24 h culture with the drug. This shows that nuclear deformability is directly related to the presence or absence of actins. In several studies, it was observed that loss or disruption of actins caused undeformed, force-free state of cells and a loss of actin-myosin contractility (Koch et al, 2012; Shankar and Nabi, 2015). Actin is one of the principal components of the cytoskeleton and forms a network of filaments with a class of molecular motors called myosins. The actomyosin network is best known for its role in contractility and force generation. Coordination between the mechanosensors (integrins) and response elements (actin cytoskeleton) guides mechanotransduction event and the deformability of the cell (DuFort et al, 2011). As a result, in this study, depolymerization of actin by CytoD caused a decrease or loss in deformability of the 3 cells. On the other hand, Jasp did not change nuclear deformation of MCF10A and MCF7 cells but only decreased the nuclear deformation of MDAMB231 cells only. So fluorescence micrographs of Jasp treatment are not shown here but quantification results for nuclear deformations are shown for both drugs in the next section.

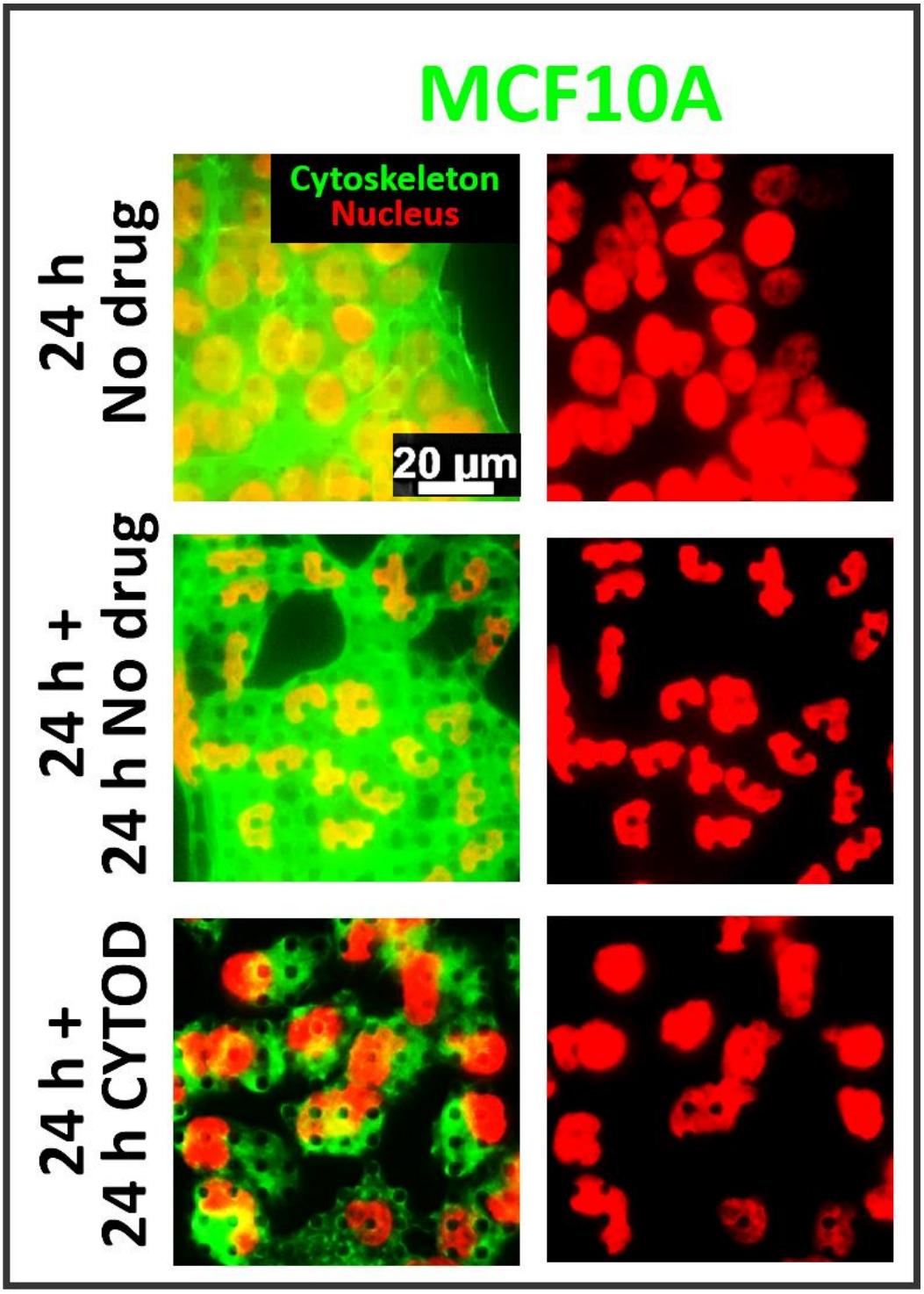

Figure 3.24. CytoD (10 µM) drug treatment on MCF10A (benign) cells on P4G4 PMMA. Fluorescence micrographs of MCF10A cells are shown with and without CytoD treatment (Scale bar: 20 µm).

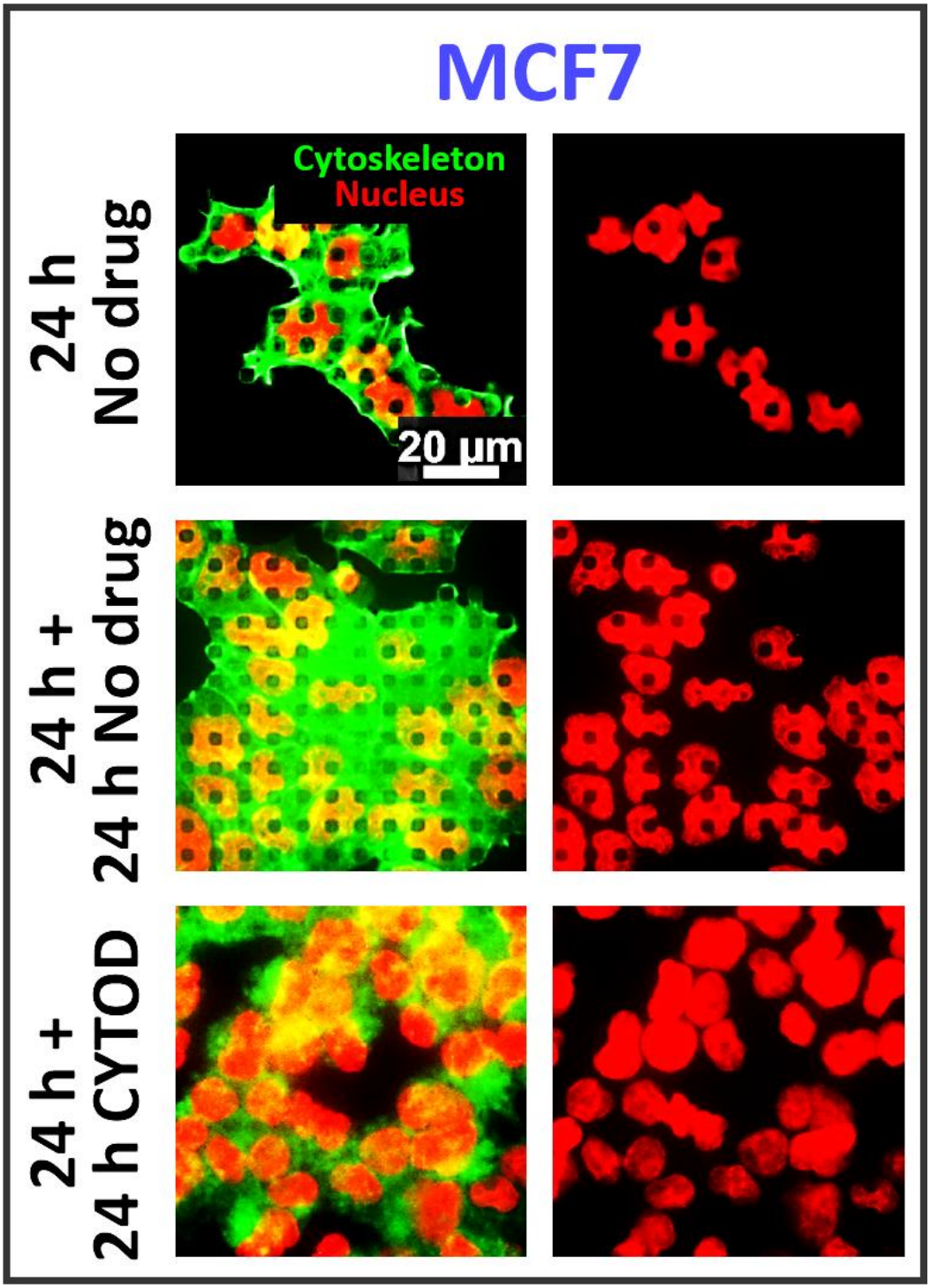

Figure 3.25. CytoD (10 µM) drug treatment on MCF7 (malignant) cells on P4G4 PMMA. Fluorescence micrographs of MCF7 cells are shown with and without CytoD treatment (Scale bar: 20 µm).

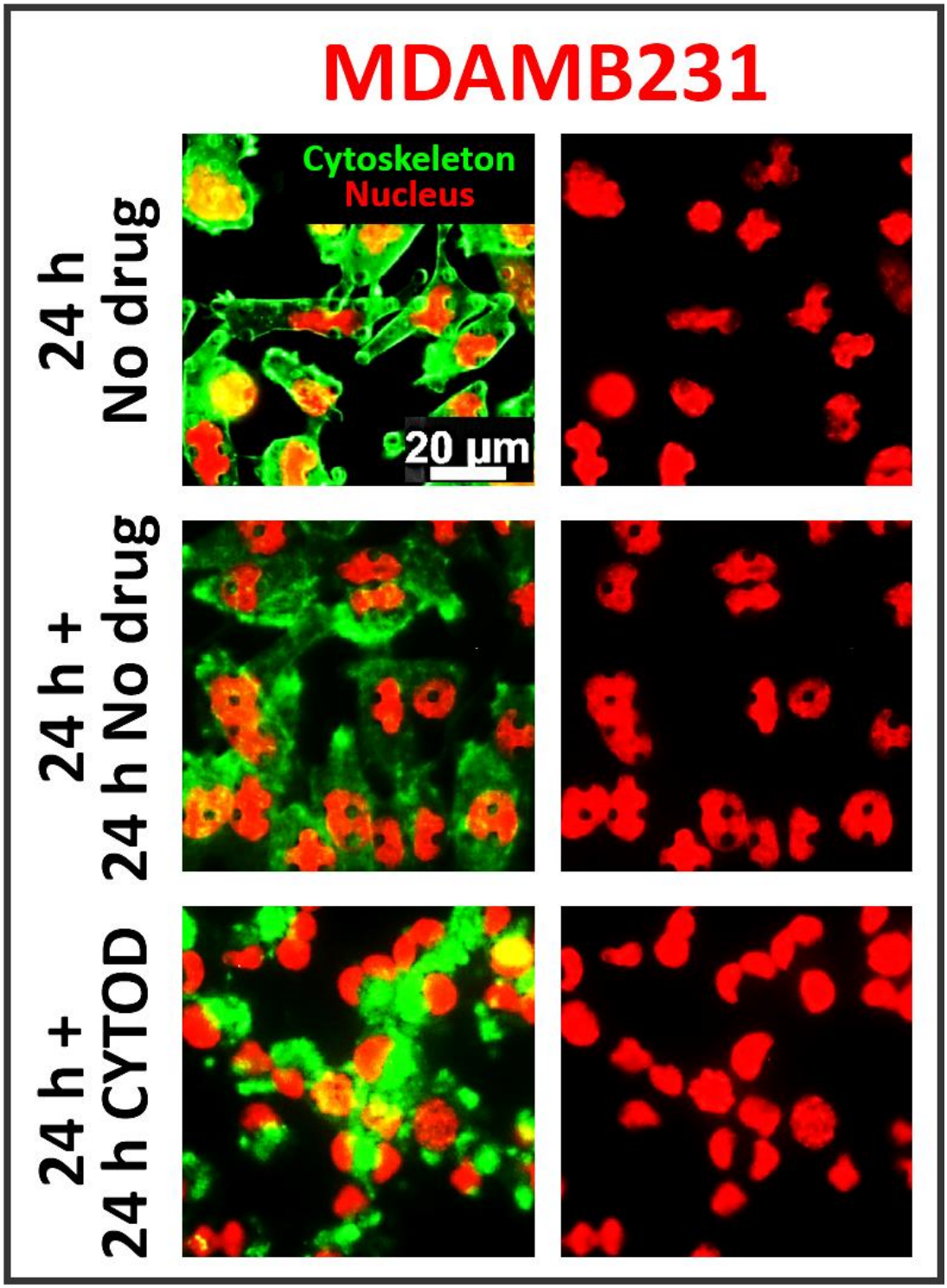

Figure 3.26. CytoD (10 µM) drug treatment on MDAMB231 (malignant) cells on P4G4 PMMA. Fluorescence micrographs of MDAMB231 cells are shown with and without CytoD treatment (Scale bar: 20 µm).

3.4. Quantification of the Nuclear Deformation

3.4.1. Analysis of Nuclear Deformation Before Drug Treatment

In the earlier sections, the influence of hydrophilicity of micropatterned surfaces and stiffness of different cell lines on the morphologies of the cells was investigated and conformational changes in nuclei were observed. In this section, they are quantified by the digital analysis of the fluorescence micrographs of the cells. Nucleus deformation analysis of the cells on different surfaces was done by using ImageJ (NIH) software. As an indicator of deformation, certain dimensional properties of the cells were needed. Circularity is one of them and is a measure of how close a cell nucleus to a perfect circle. A circularity of 1.0 indicates a perfect circle whereas a zero indicates significantly elongated shape. The equation for its calculation was given in Section 2.2.7.

In Figure 3.27, deformation analysis for the nuclei of cells is shown for the three cells on plasma treated and micropatterned PMMA surfaces and their controls. The circularity values shown in Figure 3.27 correlated with the results of the fluorescence micrographs that distortions in the shape of the cancer cells were not observed in benign cells in Figure 3.11-3.13.

On smooth (unpatterned) surfaces, circularity values were around 0.80 for all cells which is almost a perfect circle value meaning that there is no nuclear deformation. This was valid for both O_2 plasma treated and untreated surfaces. On plasma treated P4G4 surfaces, circularity values of the nuclei of cells were 0.57, 0.41, and 0.40 for MCF10A, MCF7 and MDAMB231 cells respectively. These values indicate that all types of cells have nuclei deformed to some extent on plasma treated micropatterned surfaces. On untreated P4G4 surfaces, circularity values were 0.78 for MCF10A cells whereas 0.43 for both MCF7 and MDAMB231 cells. This means that the nuclei of benign MCF10A cells had almost no conformational change whereas nuclei of the cancer cells were severely deformed. This result correlates with the stiffness of these cells; Young's Modulus were 0.7 kPa, 0.5 kPa and 0.3 kPa for MCF10A, MCF7 and MDAMB231 cells, respectively showing that the softer cancer cells were also most

deformed on micropatterned but plasma treated surfaces. In addition, it supports the notion that tumor cells are able to move and spread through dense ECM (Lekka et al, 1999; Huang et al, 2005).

As a result, on untreated P4G4 surfaces there was a significant difference between the circularity values of benign (MCF10A) and malignant (noninvasive MCF7 and invasive MDAMB231) cells but there was not a significant difference between the two malignant cells indicating that this kind of a surface can be used as an alternative identification method to the current proteomic techniques in order to discriminate the benign and malignant cells.

Since plasma treated surfaces were found that they were not able to discriminate benign and malignant cells, untreated P4G4 surfaces were used to study deformation analysis of the cells for the rest of the study.

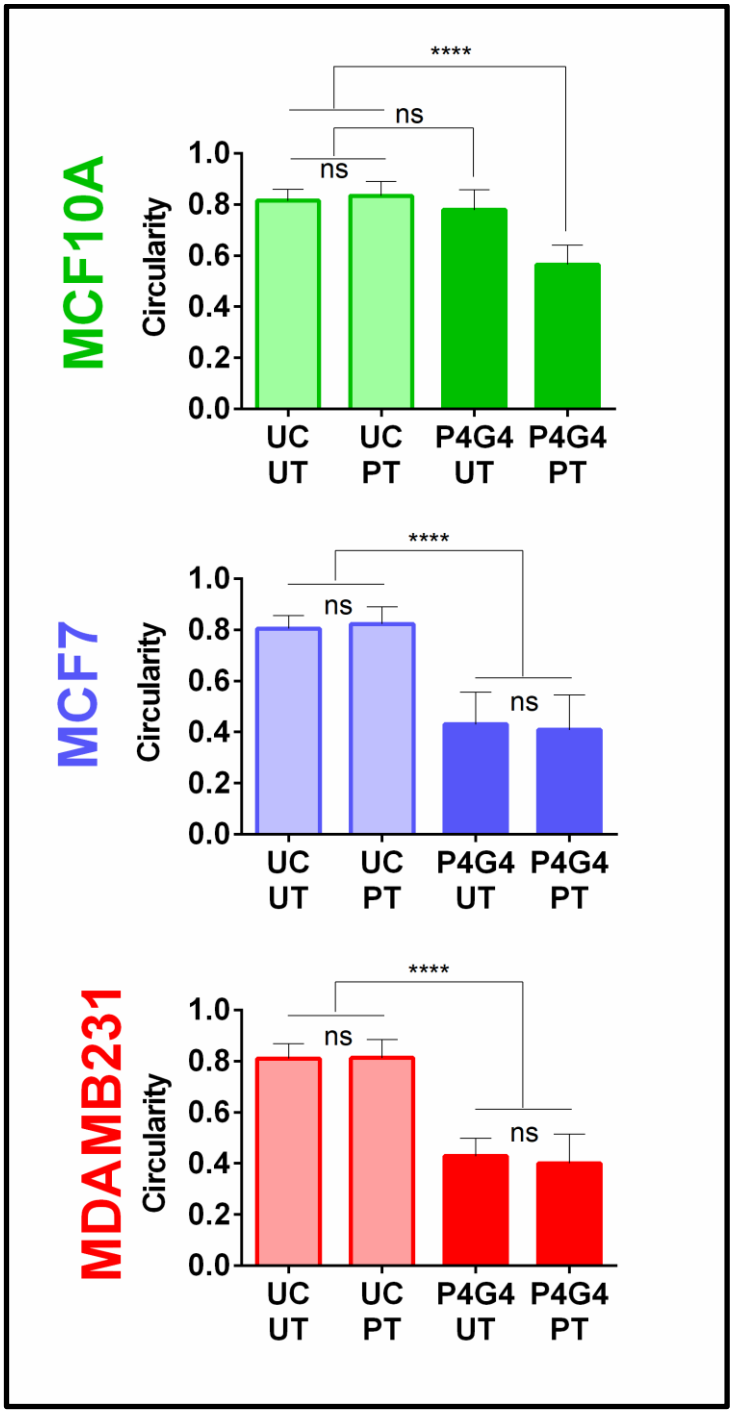

Figure 3.27. Nucleus deformation analysis by measuring circularity of the nuclei of three breast cell lines (Culture duration: 24 h). (one-way ANOVA, n=100, $p<0.0001$, Tukey post-hoc test *$p<0.005$, **$p<0.001$, ***$p<0.0005$, ****$p<0.0001$).

In order to further support our observations on cell, descriptors of deformability such as perimeter, nucleus area and roundness were also included in the study.

In Figure 3.28, nuclei of malignant and benign cells and the quantification parameters are shown. The deformed nuclei were selected to show how differences between cells could be quantified. Figure 3.28 shows the representative average values calculated from the 4 descriptors. When the deformation of nuclei of malignant cells (MCF7 and MDAMB231) were analyzed with "perimeter", results are 50 μm whereas for the benign cell (MCF10A) it is 40 μm. Perimeter increases when the nuclei deform. "Nucleus area" of malignant cells are lower (80 μm^2) than that of benign cells (100 μm^2). "Circularity" and "roundness" values are lower for the more deformable cells. All of the descriptors are useful for the discrimination of the benign and malignant cells but only the "circularity" shows significant differences.

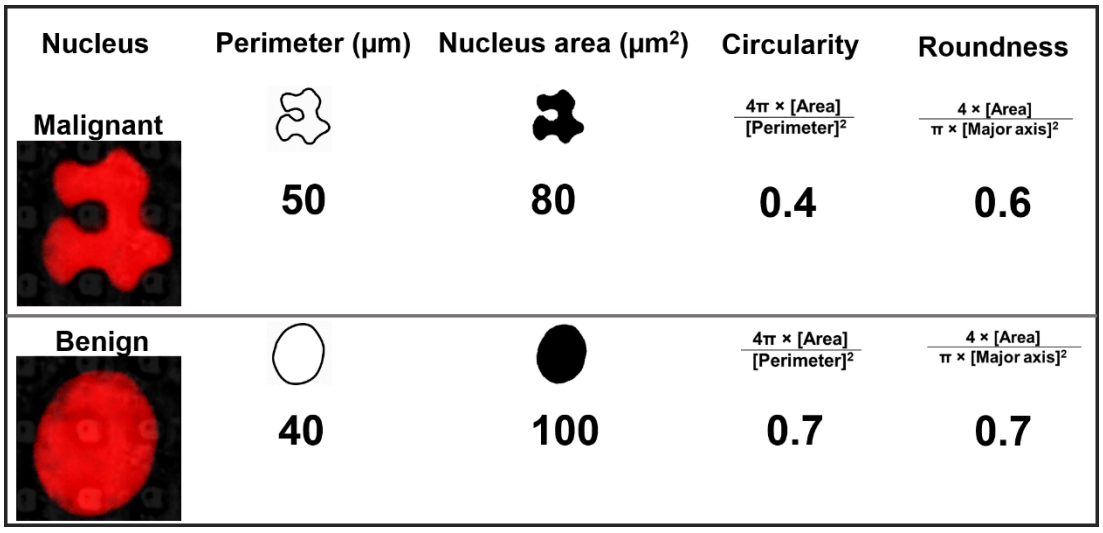

Figure 3.28. Fluorescence micrographs of the nuclei of malignant and benign cells and representative values from the quantification of nuclear deformations of cells. Nuclear deformation on P4G4 PMMA were quantified by using four descriptors: Perimeter, nucleus area, circularity and roundness.

Next, the effect of culture duration and substrate stiffness were studied on P4G4 and smooth PMMA films by using these 4 descriptors. Cells were cultured on PMMA for up to 48 hours (Figure 3.29 and 3.30).

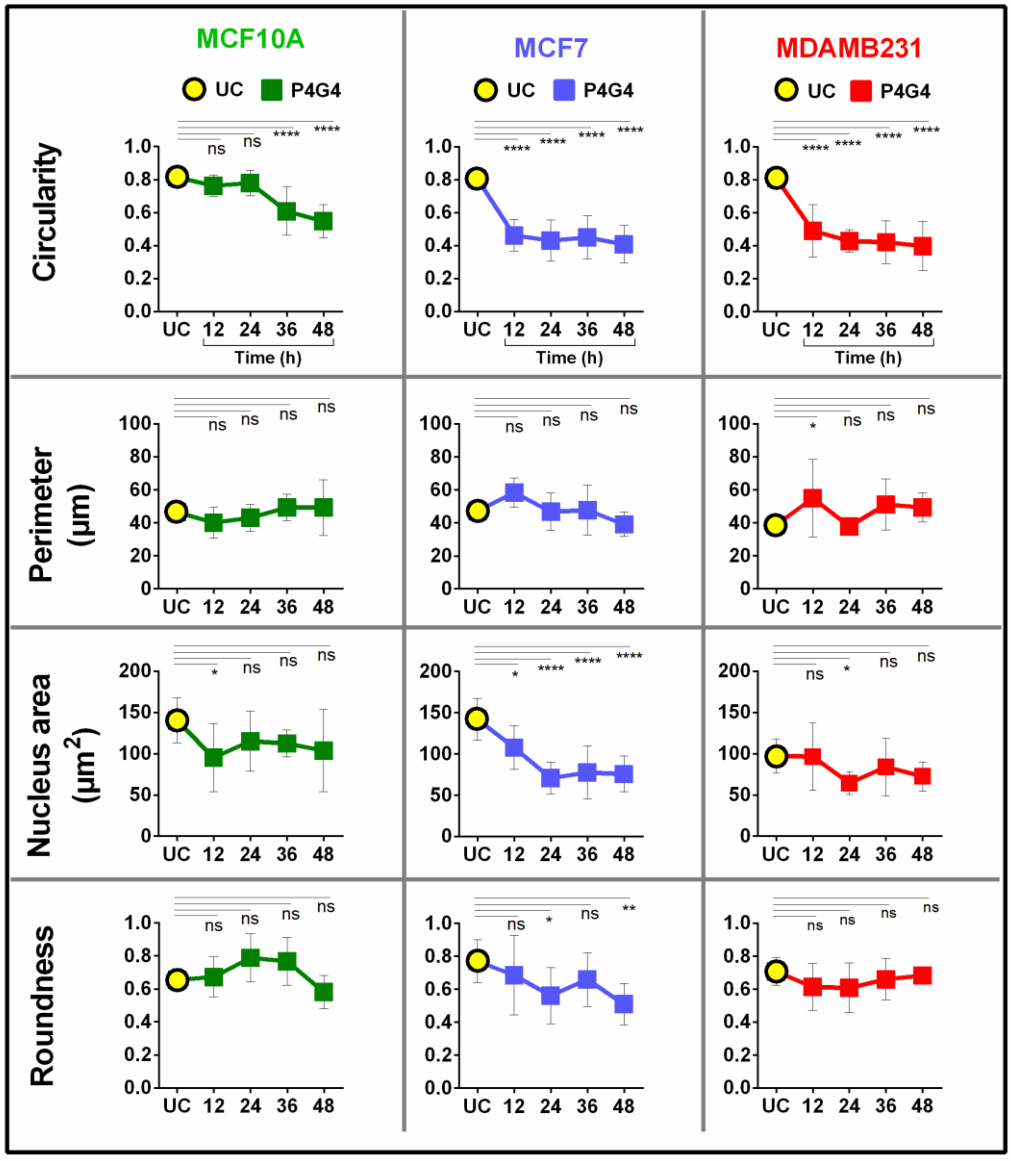

Figure 3.29. Digital analysis of nuclear deformation of breast cells (MCF10A, MCF7, MDAMB231) on stiffer (higher molecular weight) PMMA. Nuclear deformation analysis of cells was performed by calculating 4 descriptors (perimeter, circularity, nucleus area, roundness) on P4G4 PMMA (n=100) (Mw: 996K).

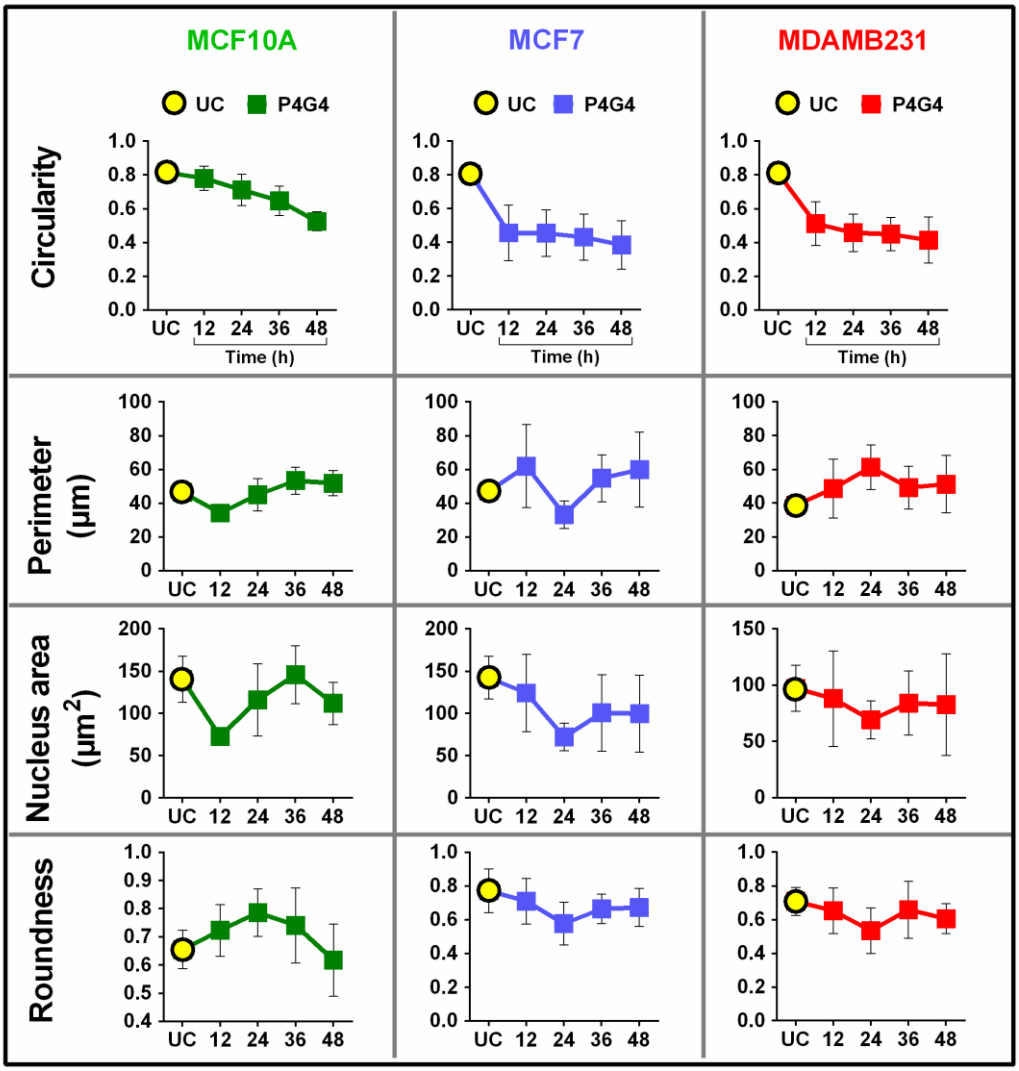

Figure 3.30. Digital analysis of nuclear deformation of breast cells (MCF10A, MCF7, MDAMB231) on softer (lower molecular weight) PMMA. Nuclear deformation analysis of cells was performed by calculating 4 descriptors (perimeter, circularity, nucleus area, roundness) on P4G4 PMMA (n=100) (Mw: 120K).

Two types of PMMA with different molecular weights and stiffnesses were used to study the effect of different mechanical properties (PMMA MW: 120K and 996K). Results obtained on higher molecular weight PMMA are shown in Figure 3.29. Lower molecular weight PMMA showed similar results with the higher and shown in Figure 3.30.

Mechanical properties of the two PMMAs were measured and tensile test results were presented in Figure 3.1. PMMA with lower molecular weight (Mw: 120K) has a Young's Modulus around 850 MPa whereas PMMA with higher molecular weight (Mw: 996K) has Young's Modulus around 1200 MPa. It was observed that nuclear deformation levels were not significantly different as shown by the four descriptors.

In Figure 3.29 how the cell deformation change with time is studied. It was observed that when the culture duration increased, a gradual increase in nuclear deformation of MCF10A cells was observed when "circularity" was used. Nuclei of MCF10A (benign) cells were not deformed for the first 24 h of culture. Upon longer culturing, their nuclei were deformed and the ability to discriminate between the non-cancerous and cancerous decreased significantly. On the other hand, malignant cells (MCF7 and MDAMB231) were deformed even on 12 h culture on P4G4 PMMA films since they had higher plasticity and lower stiffness than the benign ones (Li et al, 2008). When the cells were deformable (lower stiffness) such as malignant cells, they attach and adhere to the surface and the nucleus changes shape rapidly and drastically. This phenomenon was also reported for stem cells seeded on nanotopographical surfaces (Chalut et al, 2010). In this study, the most effective descriptor was circularity with a lower value than on smooth films for 3 cells.

"Perimeter" was the same for all cell types on 4 time points. Only MDAMB231 showed an increase in perimeter initially (12 h) since the nucleus of that cell deformed more than the other cells.

"Nucleus area" results were not correlated with the deformability of any of the cell types since it was affected by the adhesion properties of the cells. When culture duration was increased, cells adhered to the surface more and nucleus area increased whereas increase in deformation caused a decrease in nucleus area. However, at 24 h, due to the deformability of the malignant cell, they could conform to the gap between the pillars and this decreased the nucleus area while the opposite was observed for the benign cells.

"Roundness" values were almost the same for all cell types.

As a conclusion, results show that only the “circularity” descriptor can be used for the discrimination between benign and malignant cells since it gives significantly different result obtained from the statistical analysis.

Figure 3.30 shows almost the same results with the Figure 3.29 and different molecular weight of PMMA did not change the results in terms of deformability of the cell.

3.4.2. Analysis of Nuclear Deformation After Drug Treatment

Nuclear deformation extent was quantified using the 4 descriptors including circularity. After testing these on deformation of breast cell nuclei, the influence of drugs affecting actin polymerization was tested before and after CytoD and Jasp treatments were done by using only the circularity descriptor (Figure 3.31 and 3.32). Results obtained from processing the fluorescence micrographs of cells are presented in Figures 3.24-3.26.

After using the highest concentration of CytoD, circularity values of all cells were found to approach the circularity on smooth control surfaces indicating minimal distortion even though they were seeded on micropatterned surfaces which were not treated with O_2 plasma. However, benign (MCF10A) cells retained its deformation significantly since they were the stiffest cell line and were not affected by drug as much as malignant cells (MCF7 and MDAMB231). On the other hand, malignant cells lost deformability completely upon treatment with the highest concentration of CytoD because actin is one of the main components of mechanotransduction and CytoD is specific for actin polymerization. On the other hand, Jasp could affect only one cell type and caused the disappearance of nuclear deformation (the same circularity value on P4G4 and smooth PMMA after drug treatment) and this was the most malignant and softest cell type, MDAMB231, among the three.

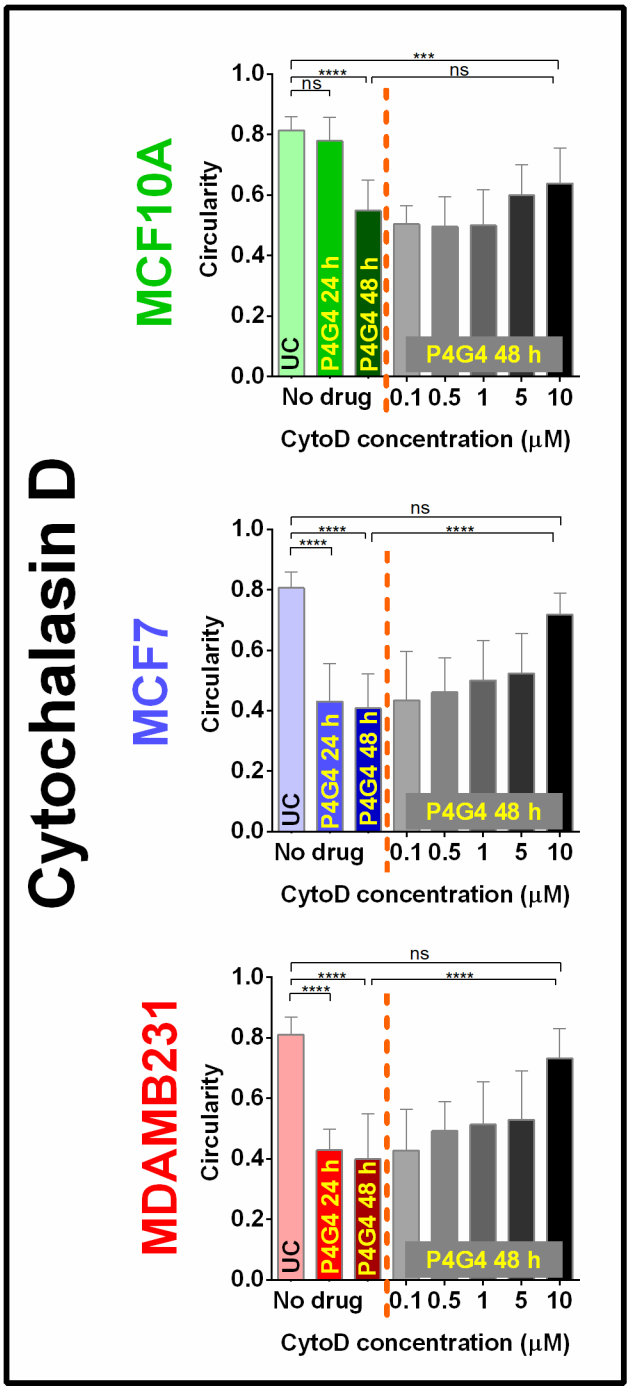

Figure 3.31. Quantification of nuclear deformation by the circularity value before and after CytoD (10 μM) drug treatment. Fluorescence micrographs of MCF10A, MCF7 and MDAMB231 cells on unpatterned (UC) and micropatterned (P4G4) PMMA are used for the circularity analysis.

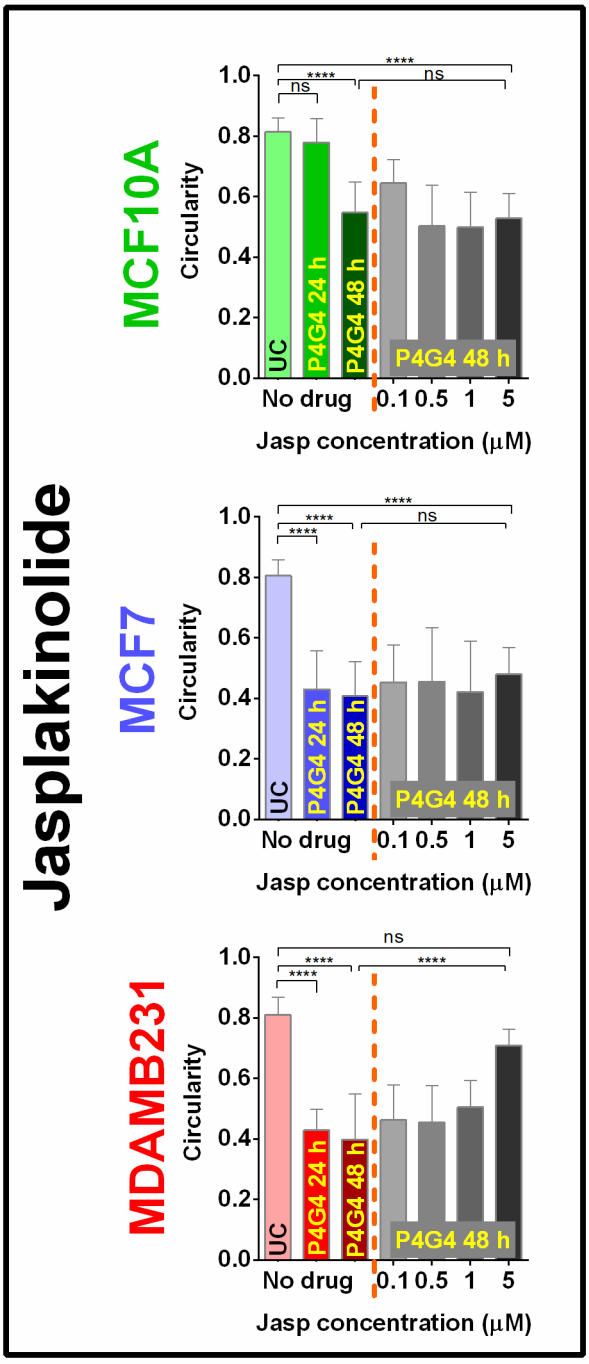

Figure 3.32. Quantification of nuclear deformation by the circularity value before and after Jasp (5 μM) drug treatment. Fluorescence micrographs of MCF10A, MCF7 and MDAMB231 cells on unpatterned (UC) and micropatterned (P4G4) PMMA are used for the circularity analysis.

3.5. Molecular Level Changes: Expression of Lamin A/C, Nesprin-2 and Ki-67 Before and After Drug Treatment

Three proteins, Ki-67, Lamin A/C and Nesprin-2, were detected and studied with immunohistochemistry.

The expression of the human Ki-67 protein is associated with cell proliferation. During interphase, the antigen can be detected within the nucleus, whereas in mitosis most of this protein is relocated to the surface of the chromosomes (Scholzen and Gerdes, 2000). Ki-67 is present during all active phases of the cell cycle (G1, S, G2, and mitosis), but is absent only in resting cells (G0) and cannot be detected at protein level, so its presence can be used as a marker to determine the growth fraction (the proportion of cells committed to the cell cycle) of a given cell population. For this reason, antibodies against Ki-67 are increasingly used as a diagnostic tool in different types of neoplasms (Scholzen and Gerdes, 2000).

Other important cancer markers are nuclear lamina component Lamin A/C and components of the LINC complex SUN1, SUN2, and Nesprin-2. The latter are downregulated in human breast cancer tissues (Matsumoto et al, 2015). Since the nuclear lamina and LINC complex play roles in nuclear organization and nuclear mechanical stiffness, their loss decreases nuclear and cellular rigidity, and consequently increases tissue fluidity, a property important for invasive activity (Matsumoto et al, 2015).

Lamins are the components of the nuclear lamina and they are in a fibrous layer on the nucleoplasmic side of the inner nuclear membrane. They also work as a framework for the nuclear envelope and may also interact with chromatin. Lamin A and C are present in equal amounts in the lamina of mammals. They have important role in nuclear assembly, chromatin organization, nuclear membrane and telomere dynamics (De Vos et al, 2010).

Nesprin-2 proteins form a linkage between organelles and the actin cytoskeleton to maintain the subcellular organization. They are one of the components of LINC

complexes which link the nucleoskeleton and cytoskeleton by providing outer nuclear membrane attachment sites for cytoskeletal filaments. They are also involved in the maintenance of nuclear organization and structural integrity and they connect nuclei to the cytoskeleton by interacting with the nuclear envelope and with F-actin in the cytoplasm and take role in actin-dependent nuclear movement (Gutiérrez-Fernández et al, 2015).

For this reason, in this study Ki-67 marker was used to study the proliferation of cells and Lamin A/C and Nesprin-2 proteins were used to study the relation between deformability and the malignancy of the cells.

Since the expression levels of these proteins change drastically in the cancer tissues and the deformability is a property of only cancer cells, one malignant cell line (MCF7) was chosen for ICC staining. The cells were seeded on micropatterned (P4G4) PMMA films and on tissue culture plates (TCPS) and (unpatterned (UC) controls. Their cytoskeletal and nuclear morphologies were shown by the Confocal Laser Scanning Microscopy (CLSM) after 24 h incubation in the normal medium followed by another 24 h with drug (CytoD). Protein expression levels were deduced from the intensity levels of the CLSM micrographs (Figures 3.33-3.38).

In CLSM micrographs for cells before the drug addition show that nuclei of cells were deformed on P4G4 surfaces but not on TCPS and UC surfaces as expected from the results earlier presented (Figures 3.33-3.35).

Lamin A/C staining was almost all around the nucleus since this protein is in the nuclear envelope (Figure 3.33).

Since Nesprin-2 molecules are in outer membrane of nucleus, staining pattern of these proteins were around the nucleus (Figure 3.34).

In Figure 3.35, yellow chevrons show the cells in mitotic phase and Ki-67 staining patterns are the most distinct ones in these cells. Since Ki-67 is mostly localized in the nucleolus and can be seen only in mitosis, their staining pattern were observed only in the dividing cells.

After the addition of drug CytoD, the actin cytoskeleton of the cells decreased in area (shrunk) and nuclei lost their deformability on P4G4 surfaces (Figure 3.36-3.38). Signal intensities of ICC stains for actins of the cells cultured with drugs seem to be higher than the ones without drug. However, it is not easy to assess the difference in the signal intensities of the CLSM and intensity of each antibody was measured and quantified using ImageJ (NIH) software (Figure 3.39). Results were given as optimized to the cell number by dividing signal intensities by the number of cells counted from the same surface. Only the intensities of Lamin A/C and Nesprin-2 could be measured but Ki-67 was not detectable because it was stained only in the dividing cells.

According to the results, when the nuclear deformability was lost after drug treatment, signal intensities of Lamin A/C and Nesprin-2 for these cells increased on P4G4 surfaces which means that expression levels of these proteins increased (Figure 3.39). As stated before, Lamin A/C and Nesprin-2 are in a direct contact with actin filaments of the cell. Actin inhibitor drug CytoD caused the loss of actin filaments by depolymerization and cells lost their deformability. As a result, after the drug treatment, expression of two mechanotransduction proteins (Lamin A/C and Nesprin-2) were increased. It was shown that these proteins were overexpressed in normal state of the nucleus whereas the reverse was seen for the deformed states of the nucleus. In summary, the lower the expression of these proteins indicated that the cells were more deformable. On TCPS and unpatterned control (UC) surfaces, intensities of the proteins did not change as much and the deformability of the nuclei did not change on these surfaces.

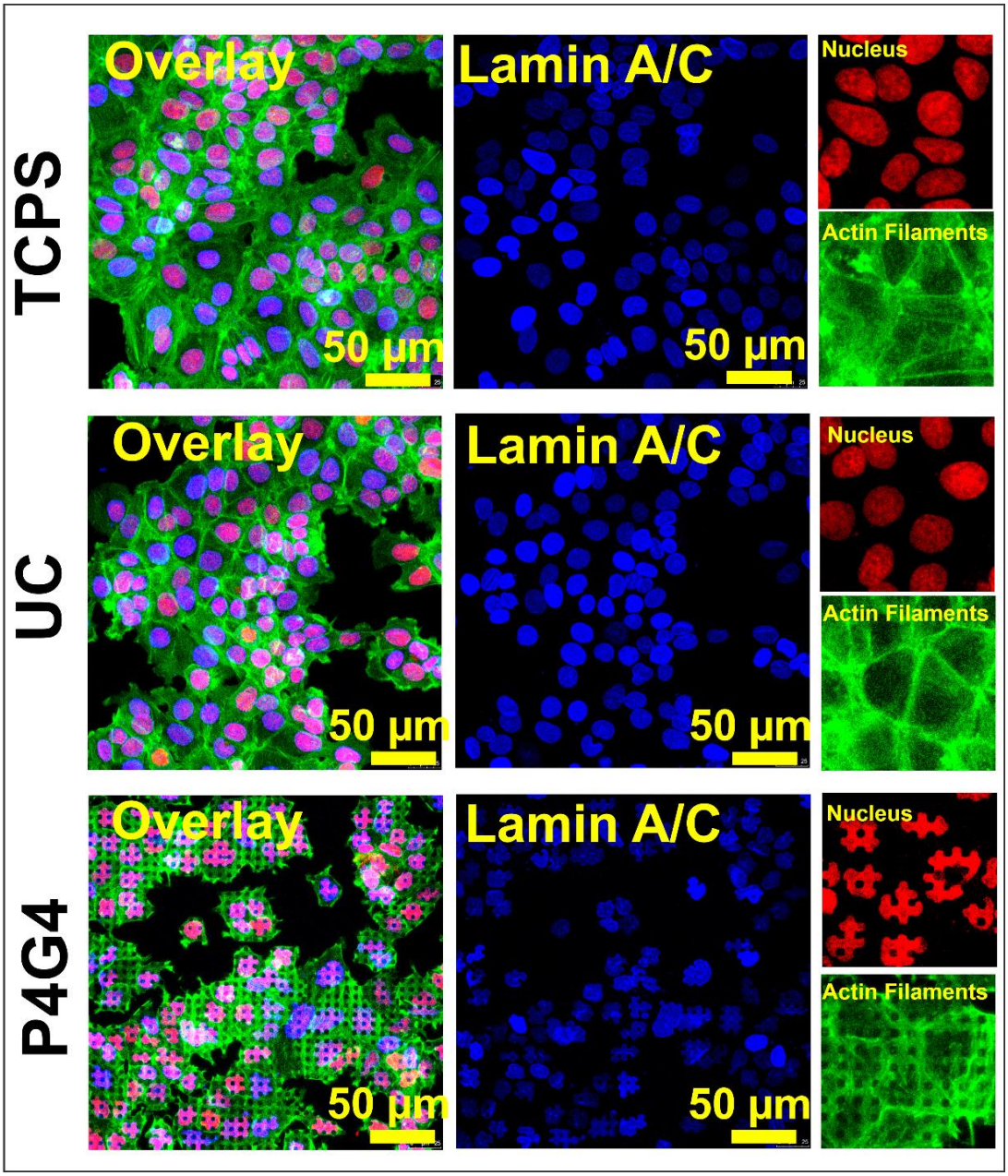

Figure 3.33. CLSM images of MCF7 cells for ICC staining of Lamin A/C before drug treatment. Cells are cultured on tissue culture plate (TCPS), unpatterned control (UC) and micropatterned (P4G4) surfaces. Cells were stained for Lamin A/C (blue: Anti Lamin A), nucleus (red: TOPRO-3) and actin filaments (green: Alexa Fluor 532 Phalloidin). (X40 objective, Scale bars: 50 µm).

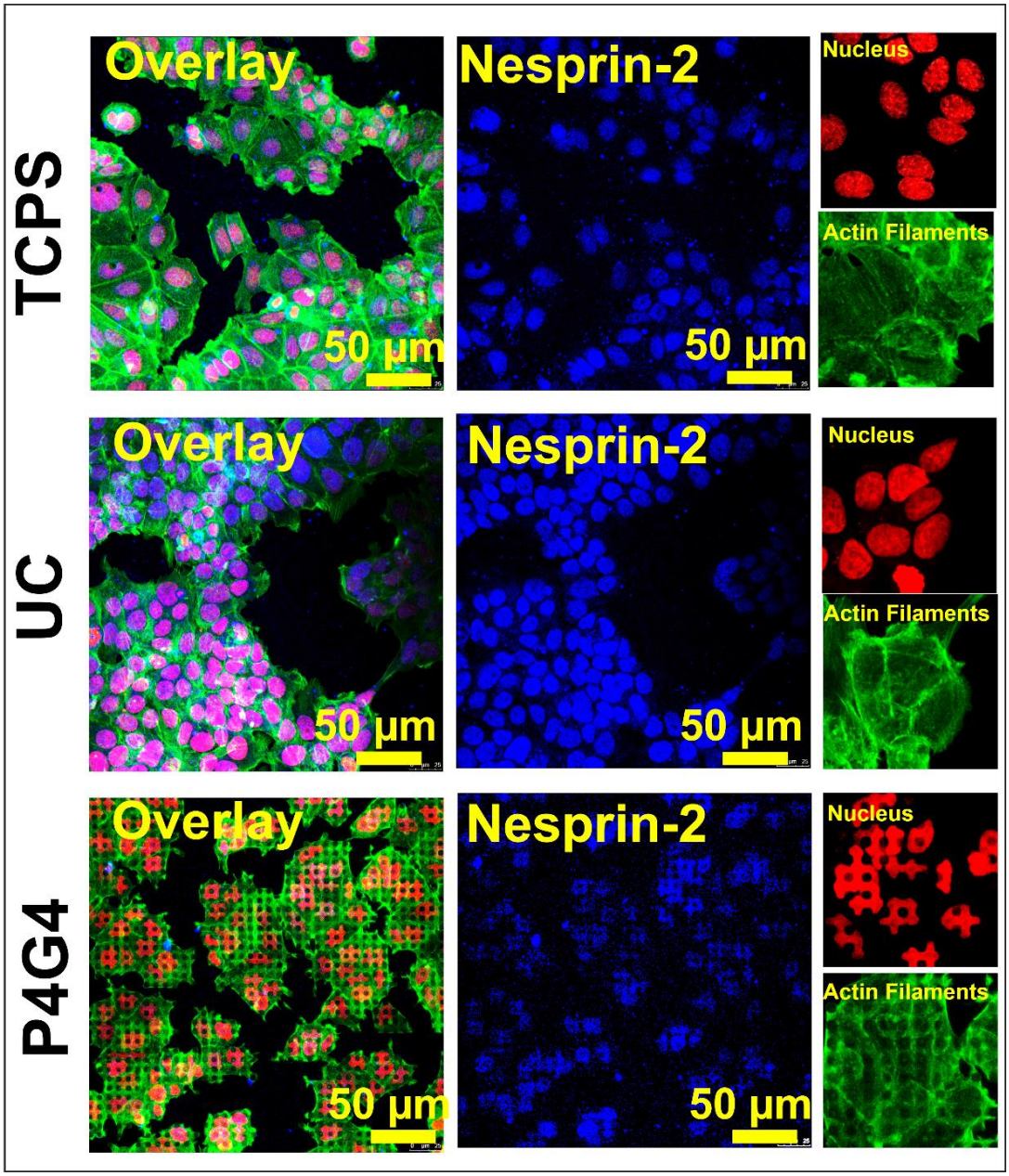

Figure 3.34. CLSM images of MCF7 cells for ICC staining of Nesprin-2 before drug treatment. Cells are cultured on tissue culture plate (TCPS), unpatterned control (UC) and micropatterned (P4G4) surfaces. Cells were stained for Nesprin-2 (blue: Anti Nesprin-2), nucleus (red: TOPRO-3) and actin filaments (green: Alexa Fluor 532 Phalloidin). (X40 objective, Scale bars: 50 µm).

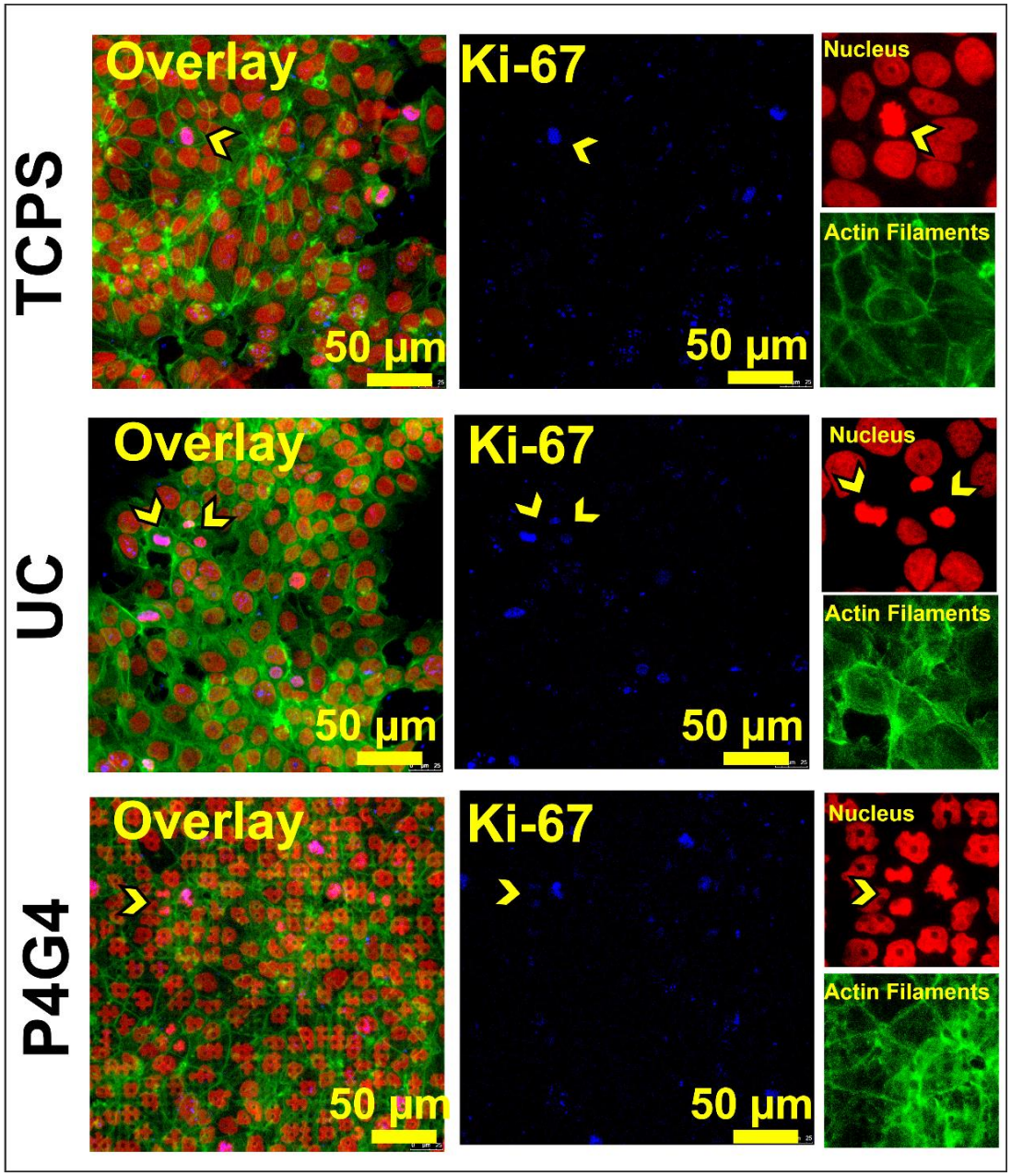

Figure 3.35. CLSM images of MCF7 cells for ICC staining of Ki-67 before drug treatment. Cells are cultured on tissue culture plate (TCPS), unpatterned control (UC) and micropatterned (P4G4) surfaces. Cells were stained for Ki-67 (blue: Anti Ki-67), nucleus (red: TOPRO-3) and actin filaments (green: Alexa Fluor 532 Phalloidin). (Yellow chevrons show dividing mitotic cells) (X40 objective, Scale bars: 50 µm).

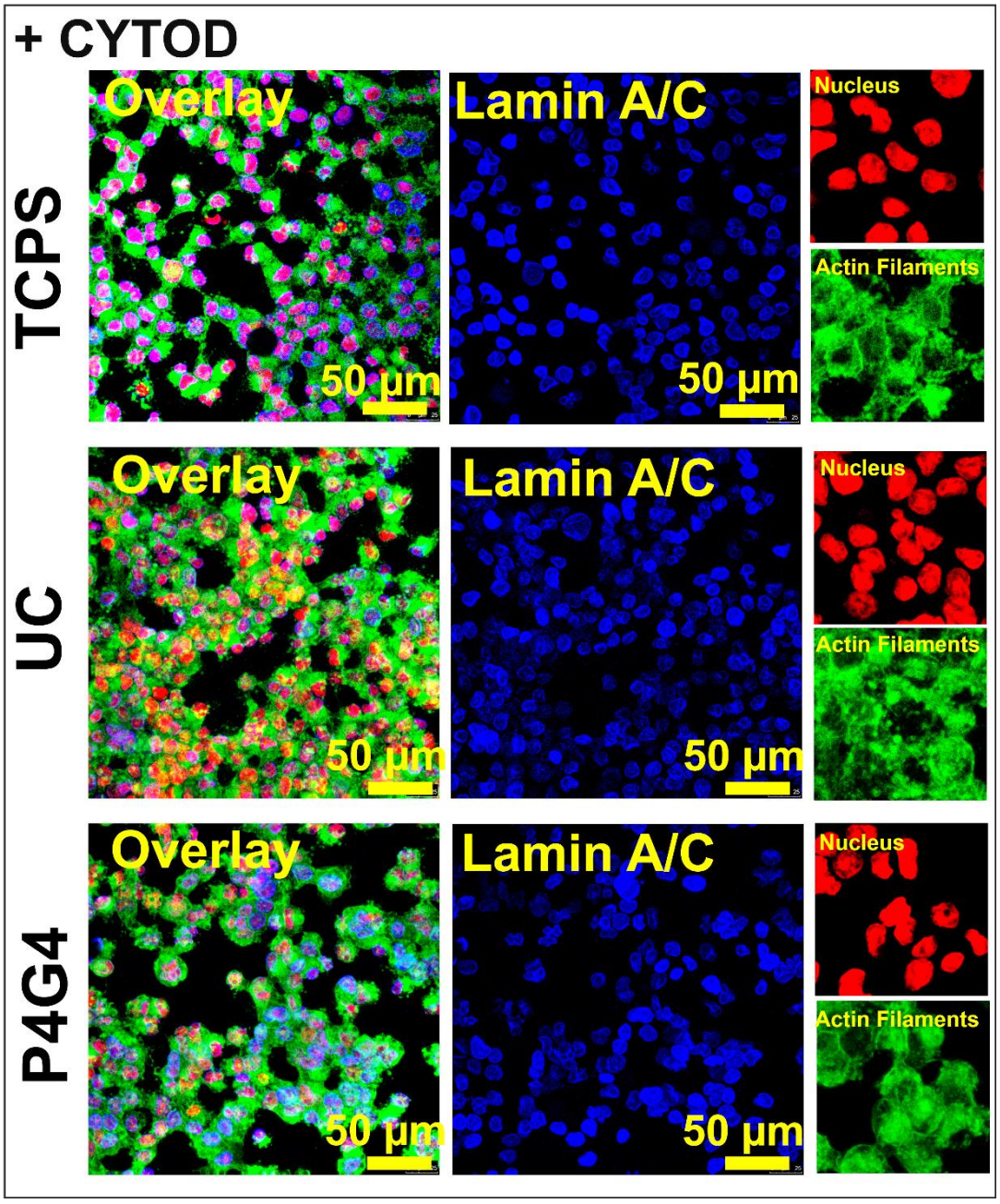

Figure 3.36. CLSM images of MCF7 cells for ICC staining of Lamin A/C after drug (CytoD: 10 µM) treatment. Cells are cultured on tissue culture plate (TCPS), unpatterned control (UC) and micropatterned (P4G4) surfaces. Cells were stained for Lamin A/C (blue: Anti Lamin A), nucleus (red: TOPRO-3) and actin filaments (green: Alexa Fluor 532 Phalloidin). (X40 objective, Scale bars: 50 µm).

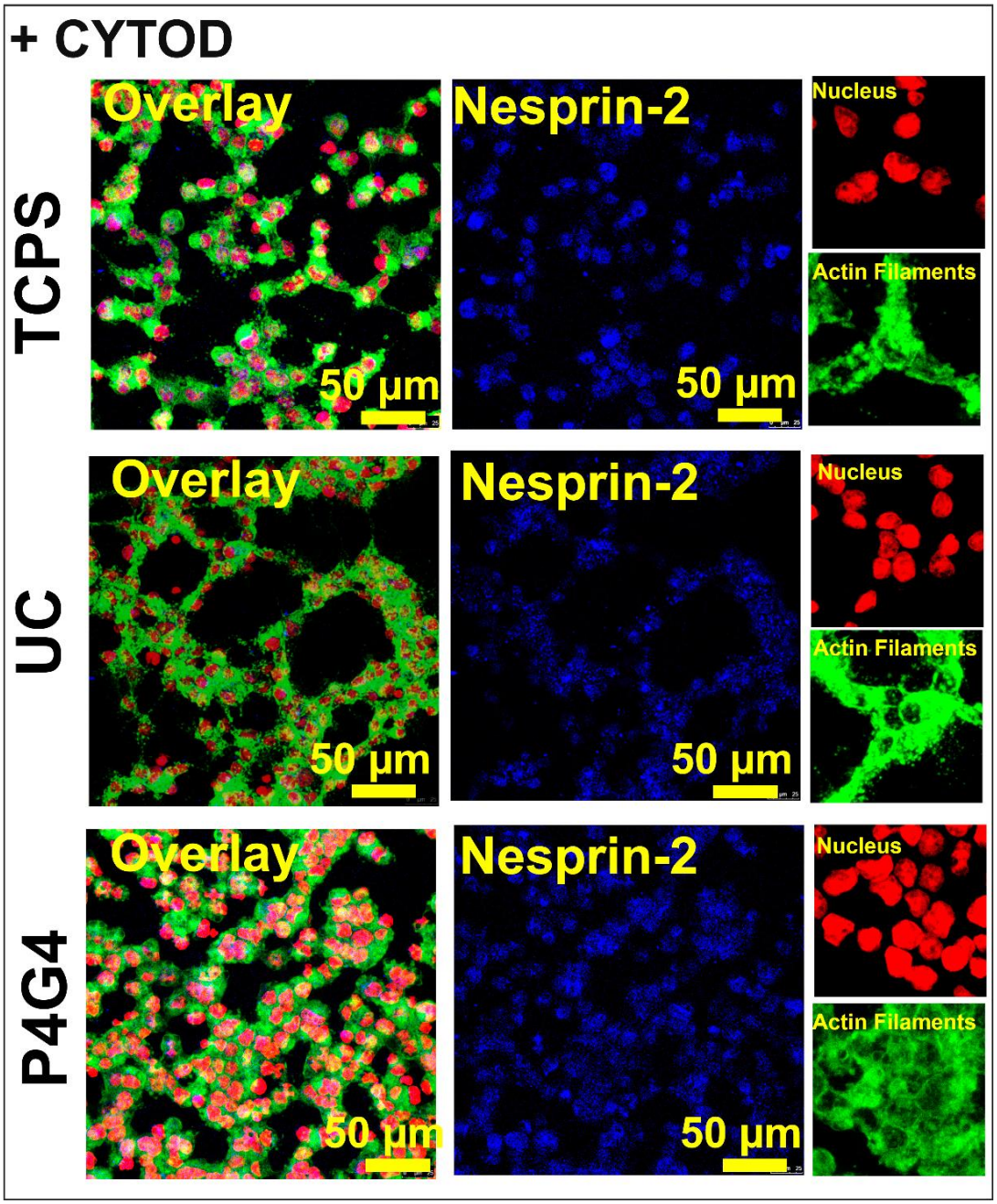

Figure 3.37. CLSM images of MCF7 cells for ICC staining of Nesprin-2 after drug (CytoD: 10 µM) treatment. Cells are cultured on tissue culture plate (TCPS), unpatterned control (UC) and micropatterned (P4G4) surfaces. Cells were stained for Nesprin-2 (blue: Anti Nesprin-2), nucleus (red: TOPRO-3) and actin filaments (green: Alexa Fluor 532 Phalloidin). (X40 objective, Scale bars: 50 µm).

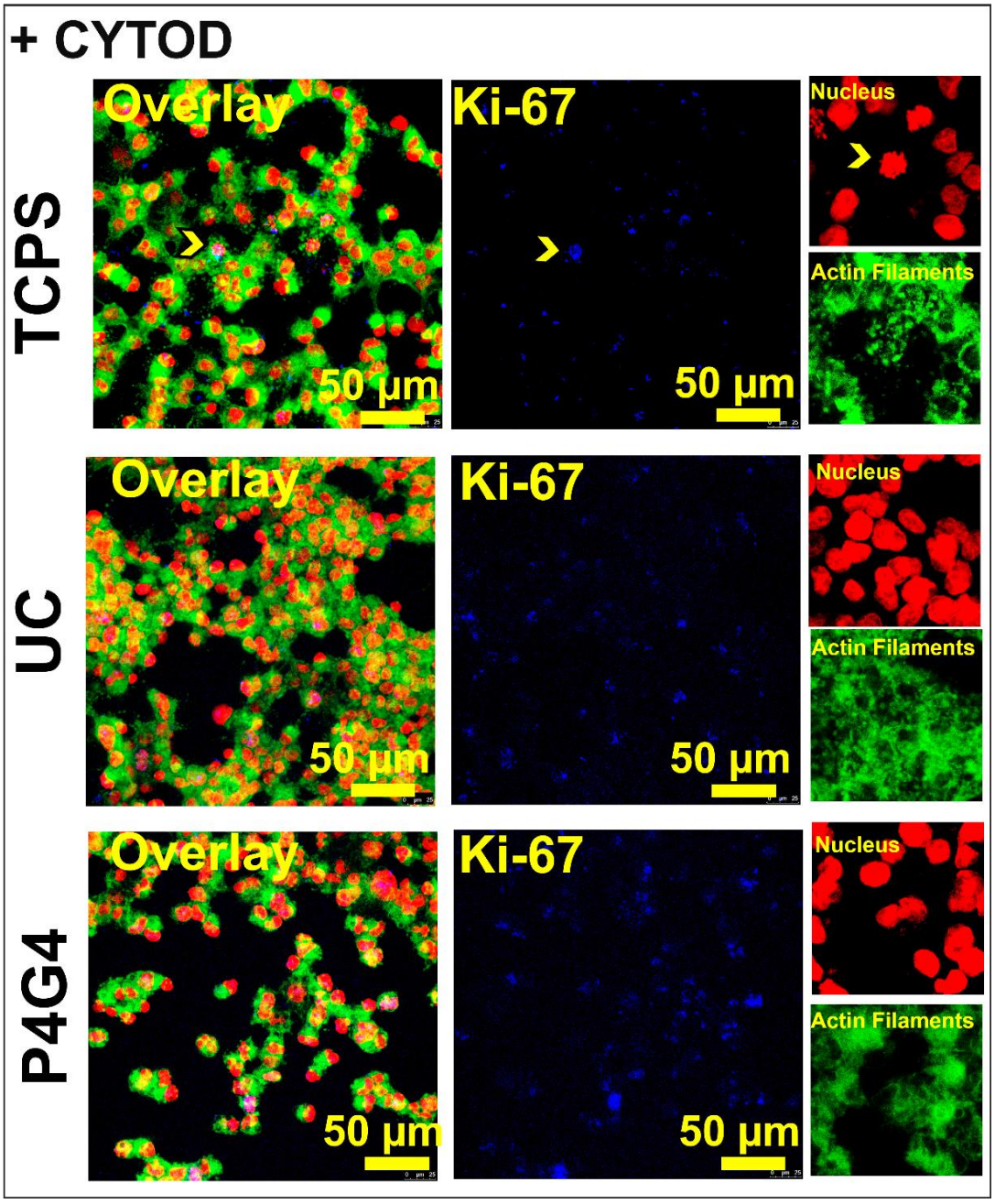

Figure 3.38. CLSM images of MCF7 cells for ICC staining of Ki-67 after drug (CytoD: 10 µM) treatment. Cells are cultured on tissue culture plate (TCPS), unpatterned control (UC) and micropatterned (P4G4) surfaces. Cells were stained for Ki-67 (blue: Anti Ki-67), nucleus (red: TOPRO-3) and actin filaments (green: Alexa Fluor 532 Phalloidin). (X40 objective, Scale bars: 50 µm).

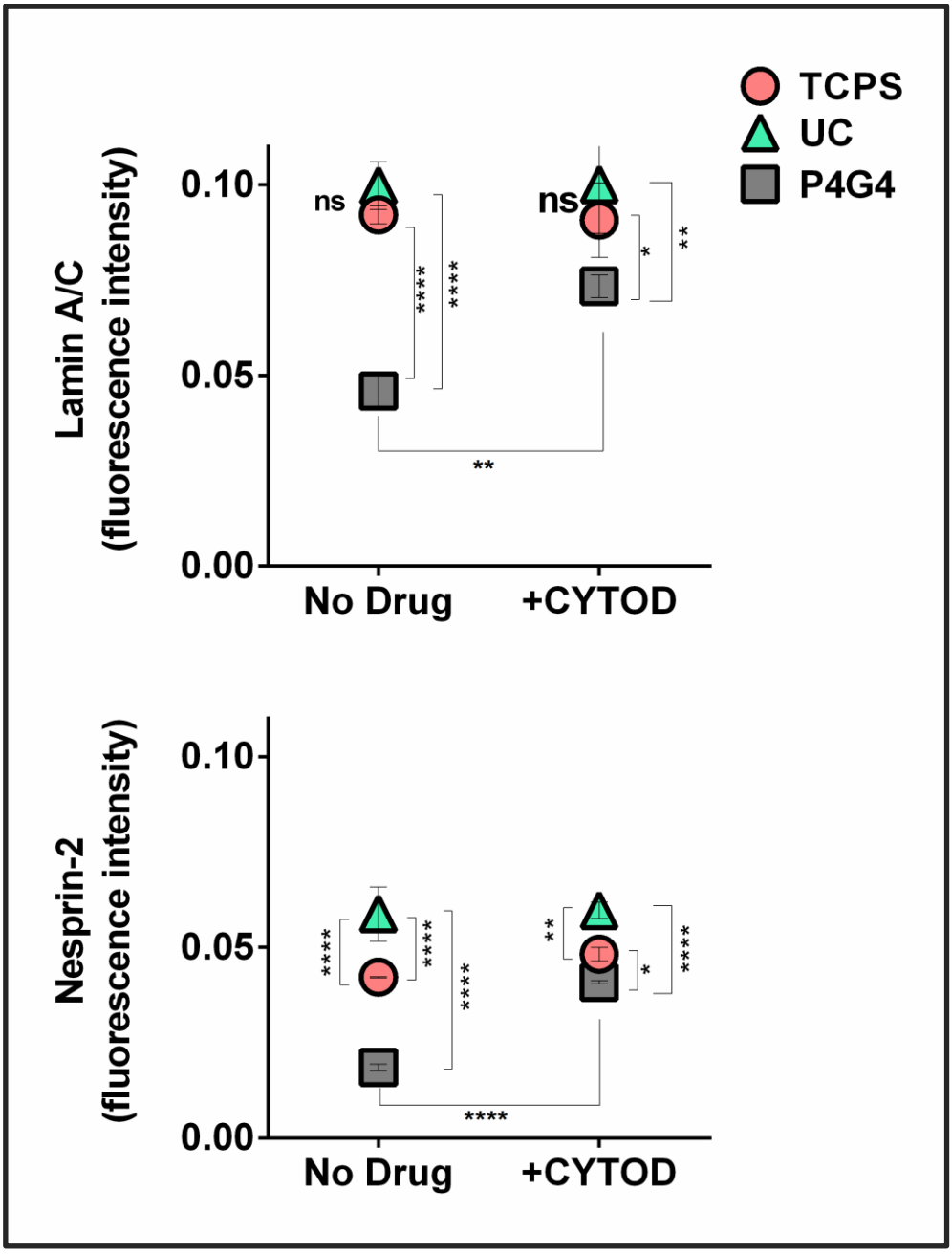

Figure 3.39. Lamin A/C and Nesprin-2 expression levels of MCF7 cells before and after drug treatment as determined from their fluorescence intensities on tissue micropatterned (P4G4) surfaces. Fluorescence intensities were calculated using ImageJ (NIH) software. Results were given as optimized to the cell number by dividing signal intensities by the number of cells counted from the same surface. (One-way ANOVA, $p<0.001$, Tukey test for pairwise comparison, * $p<0.05$, ** $p<0.01$, *** $p<0.005$, ****, n=3)

3.6. Gene Expression Studies

Expression levels of the genes for Ki-67, Lamin A/C and Nesprin-2 were studied with qPCR for cells cultured on micropatterned PMMA films.

Both malignant cells MCF7 and MDAMB231 showed a downregulation of Nesprin-2 and Lamin A/C genes but benign cells MCF10A showed an increase in the expression of these genes on P4G4 surfaces (Figures 3.40 and 3.41). The downregulation by the invasive MDAMB231 cells was higher than the non-invasive cells. This proves that the cancer state of the cells correlates well with the downregulation of these LINC complex and nuclear lamin component genes.

Another result is that Ki-67 was also downregulated in MCF7 and MDAMB231 cells but upregulated in MCF10A cells (Figure 3.42). It also correlates well with the attachment and nuclear deformation of the cells. Since MDA-MB231 is a more aggressive carcinoma cell type, a faster response to physical cues were expected as observed. However, the results were not found significant by the statistical analysis at gene expression level.

As a conclusion, nucleus deformation analysis (nucleus circularity) and gene and protein expression studies show that there is a correlation between them when seeded on P4G4 PMMA surfaces. It can be said that biomechanical properties (rigidity, elasticity, deformability) of cells can provide in depth information about the state of the cancer and they can they can serve as an alternative identification method to current proteomic techniques in the specific example of breast cancer model.

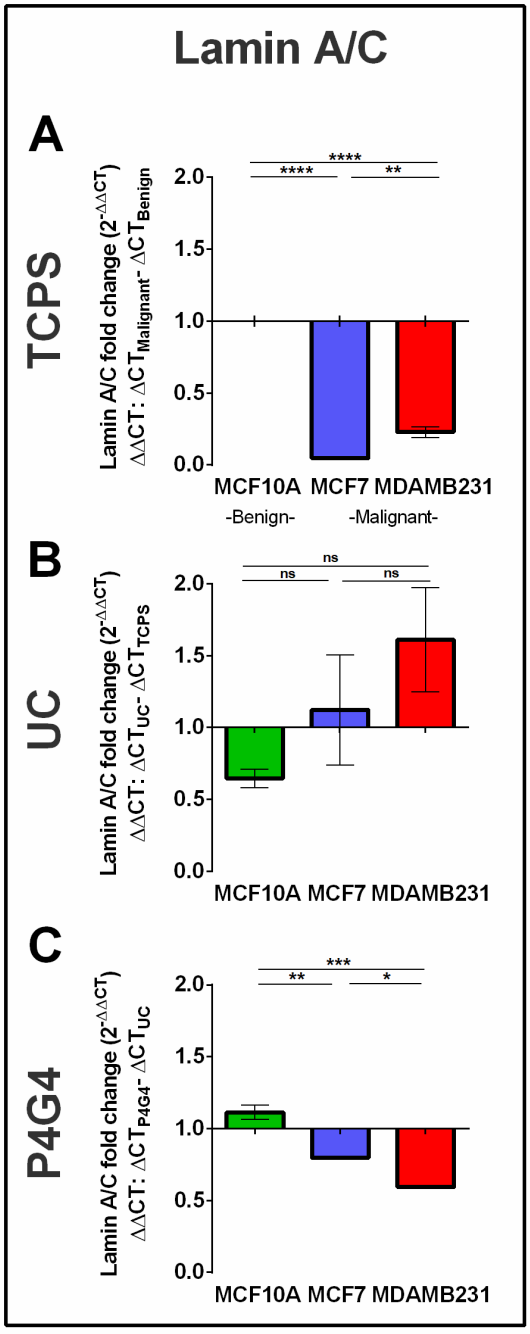

Figure 3.40. Lamin A/C mRNA levels of MCF10A, MCF7 and MDAMB231 cells. Cells are cultured on tissue culture plate (TCPS), unpatterned control (UC) and micropatterned (P4G4) substrates for 24 h. mRNA CT values were normalized to GAPDH (ΔCT) and to unpatterned control (ΔΔCT). (One-Way ANOVA, $p<0.001$, Tukey test for pairwise comparison, * $p<0.05$, ** $p<0.01$, *** $p<0.005$, **** $p<0.001$, n=2).

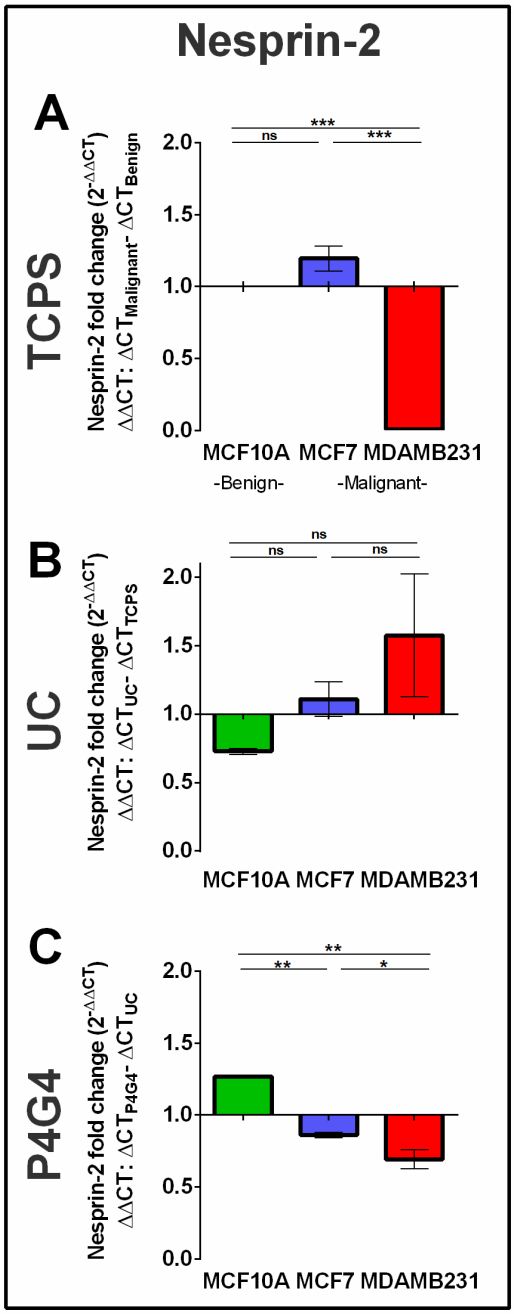

Figure 3.41. Nesprin-2 mRNA levels of MCF10A, MCF7 and MDAMB231 cells. Cells are cultured on tissue culture plate (TCPS), unpatterned control (UC) and micropatterned (P4G4) substrates for 24 h. mRNA CT values were normalized to GAPDH (ΔCT) and to unpatterned control (ΔΔCT). (One-Way ANOVA, $p<0.001$, Tukey test for pairwise comparison, * $p<0.05$, ** $p<0.01$, *** $p<0.005$, **** $p<0.001$, n=2).

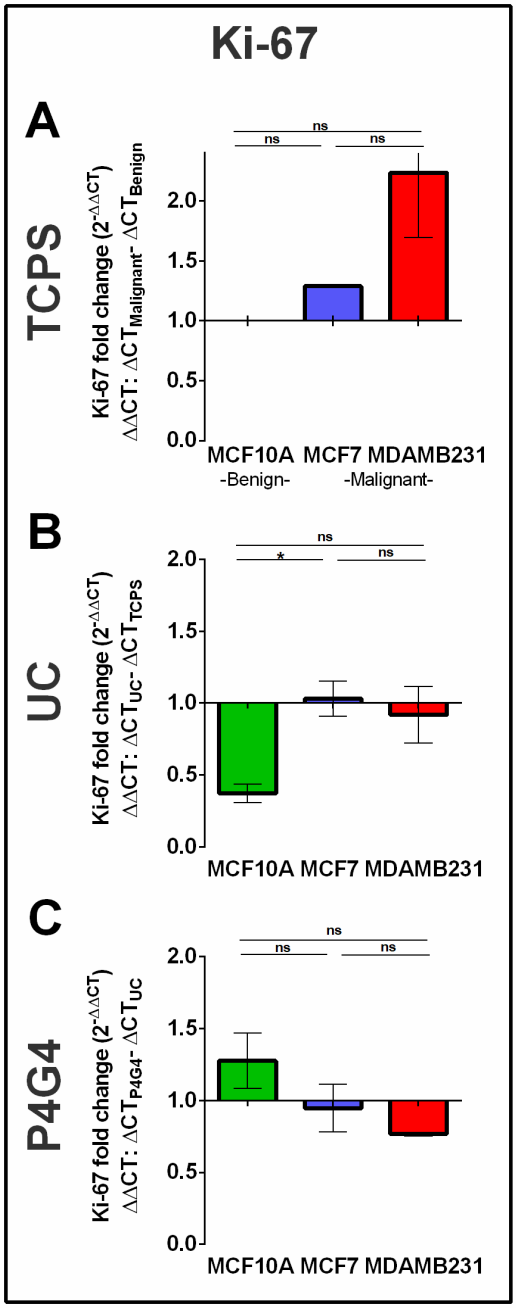

Figure 3.42. Ki-67 mRNA levels of MCF10A, MCF7 and MDAMB231 cells. Cells are cultured on tissue culture plate (TCPS), unpatterned control (UC) and micropatterned (P4G4) substrates for 24 h. mRNA CT values were normalized to GAPDH (ΔCT) and to unpatterned control (ΔΔCT). (One-Way ANOVA, $p<0.001$, Tukey test for pairwise comparison, * $p<0.05$, ** $p<0.01$, *** $p<0.005$, **** $p<0.001$, n=2).

CHAPTER 4

CONCLUSION

Cancer and healthy cells placed on micropatterned surfaces show differences in their attachment, migration, proliferation and nucleus deformation. Nuclear deformation is a result of both the inherent properties of the cells and the topography of the environment. Deformability property belongs only to cancer or diseased cells and so it is important to understand the mechanism underlying this behavior since it gives a clue about the malignancy of the cells. In this study, the main assumption was that the difference in mechanical properties of malignant and benign breast cancer cells could be used as a simple and direct tool in cancer detection. For this reason, three breast cancer cell lines with different malignancy levels were used and cultured on micropatterned surfaces. They were analyzed in terms of their circularity value of the nucleus, expression levels of the mechanotransduction proteins and F-actin contents before and after the use of actin inhibiting drugs. PMMA was used as substrate material and it was designed with the topographies having the dimensions optimal for the highest nucleus deformation. PCR and ICC were used as detection methods for the expression levels of the genes and proteins. Quantification of the measurements was done by the help of image analysis software. It was shown that both the actin filaments and the mechanotransduction proteins take role in the deformation of the nuclei. Moreover, designed surfaces with the desired topographies could be used to discriminate benign and malignant cells by using the deformability capacity of them. In summary, it can be said that biomechanical properties (rigidity, elasticity, deformability) of cells can provide useful information about cancer state and they can be viewed as biological markers, which suggest an alternative identification method to current proteomic techniques.

REFERENCES

Ali, U., Karim, K. J. B. A., & Buang, N. A. (2015). A Review of the Properties and Applications of Poly (Methyl Methacrylate)(PMMA). Polymer Reviews,55(4), 678-705.

Arnaout, M. A., Goodman, S. L., & Xiong, J. P. (2007). Structure and mechanics of integrin-based cell adhesion. Current opinion in cell biology, 19(5), 495-507.

Bao, G., & Suresh, S. (2003). Cell and molecular mechanics of biological materials. Nature materials, 2(11), 715-725.

Barthes, J., Özçelik, H., Hindié, M., Ndreu-Halili, A., Hasan, A., & Vrana, N. E. (2014). Cell microenvironment engineering and monitoring for tissue engineering and regenerative medicine: the recent advances. BioMed research international, 2014.

Bettinger, C. J., Langer, R., & Borenstein, J. T. (2009). Engineering substrate topography at the micro-and nanoscale to control cell function. Angewandte Chemie International Edition, 48(30), 5406-5415.

Bie, L., Zhao, G., Cheng, P., Rondeau, G., Porwollik, S., Ju, Y., ... & McClelland, M. (2011a). The accuracy of survival time prediction for patients with glioma is improved by measuring mitotic spindle checkpoint gene expression. PloS one, 6(10), e25631.

Bie, L., Zhao, G., Ju, Y., & Zhang, B. (2011b). Integrative genomic analysis identifies CCNB1 and CDC2 as candidate genes associated with meningioma recurrence. Cancer genetics, 204(10), 536-540. B

Bie, L., Zhao, G., Wang, Y. P., & Zhang, B. (2012). Kinesin family member 2C (KIF2C/MCAK) is a novel marker for prognosis in human gliomas. Clinical neurology and neurosurgery, 114(4), 356-360.

Bissell, M. J., Weaver, V. M., Lelièvre, S. A., Wang, F., Petersen, O. W., & Schmeichel, K. L. (1999). Tissue structure, nuclear organization, and gene expression in normal and malignant breast. Cancer Research, 59(7 Supplement), 1757s-1764s.

Bruinink, A., & Wintermantel, E. (2001). Grooves affect primary bone marrow but not osteoblastic MC3T3-E1 cell cultures. Biomaterials, 22(18), 2465-2473.

Burke, B., & Ellenberg, J. (2002). Remodelling the walls of the nucleus. Nature reviews molecular cell biology, 3(7), 487-497.

Caille, N., Thoumine, O., Tardy, Y., & Meister, J. J. (2002). Contribution of the nucleus to the mechanical properties of endothelial cells. Journal of biomechanics, 35(2), 177-187.

Calzado-Martín, A., Encinar, M., Tamayo, J., Calleja, M., & San Paulo, A. (2016). Effect of Actin Organization on the Stiffness of Living Breast Cancer Cells Revealed by Peak-Force Modulation Atomic Force Microscopy. ACS nano, 10(3), 3365-3374.

Cassie, A. B. D., & Baxter, S. (1944). Wettability of porous surfaces.Transactions of the Faraday Society, 40, 546-551.

Chai, J., Lu, F., Li, B., & Kwok, D. Y. (2004). Wettability interpretation of oxygen plasma modified poly (methyl methacrylate). Langmuir, 20(25), 10919-10927.

Chalut, K. J., Kulangara, K., Giacomelli, M. G., Wax, A., & Leong, K. W. (2010). Deformation of stem cell nuclei by nanotopographical cues. Soft Matter, 6(8), 1675-1681.

Chen, C. S., Mrksich, M., Huang, S., Whitesides, G. M., & Ingber, D. E. (1997). Geometric control of cell life and death. Science, 276(5317), 1425-1428.

Chomczynski, P., Mackey, K., Drews, R., & Wilfinger, W. (1997). DNAzol (R): A reagent for the rapid isolation of genomic DNA. Biotechniques, 22(3), 550-553.

Chu, P. K., Chen, J. Y., Wang, L. P., & Huang, N. (2002). Plasma-surface modification of biomaterials. Materials Science and Engineering: R: Reports, 36(5), 143-206.

Clark, P., Connolly, P., Curtis, A. S., Dow, J. A., & Wilkinson, C. D. (1987). Topographical control of cell behaviour. I. Simple step cues. Development,99(3), 439-448.

Clark, P., Connolly, P., Curtis, A. S., Dow, J. A., & Wilkinson, C. D. (1990). Topographical control of cell behaviour: II. Multiple grooved substrata. Development, 108(4), 635-644.

Coceano, G. (2015). Local measurement of breast cancer cells mechanical properties.

Collas, P., Lund, E. G., & Oldenburg, A. R. (2014). Closing the (nuclear) envelope on the genome: how nuclear lamins interact with promoters and modulate gene expression. Bioessays, 36(1), 75-83.

Coradeghini, R., Barboro, P., Rubagotti, A., Boccardo, F., Parodi, S., Carmignani, G., ... & Balbi, C. (2006). Differential expression of nuclear lamins in normal and cancerous prostate tissues. Oncology reports, 15(3), 609-613.

Coutinho, D., Costa, P., Neves, N., Gomes, M. E., & Reis, R. L. (2011). Micro-and nanotechnology in tissue engineering. In Tissue Engineering (pp. 3-29). Springer Berlin Heidelberg.

Curtis, A. S. G., & Varde, M. (1964). Control of cell behavior: topological factors. Journal of the National Cancer Institute, 33(1), 15-26.

Curtis, A. S., Dalby, M., & Gadegaard, N. (2006). Cell signaling arising from nanotopography: implications for nanomedical devices.

Cvelbar, U., Pejovnik, S., Mozetie, M., & Zalar, A. (2003). Increased surface roughness by oxygen plasma treatment of graphite/polymer composite. Applied surface science, 210(3), 255-261.

Dahl, K. N., Ribeiro, A. J., & Lammerding, J. (2008). Nuclear shape, mechanics, and mechanotransduction. Circulation research, 102(11), 1307-1318.

Dalby, M. J. (2005). Topographically induced direct cell mechanotransduction. Medical engineering & physics, 27(9), 730-742.

Dalby, M. J., Riehle, M. O., Sutherland, D. S., Agheli, H., & Curtis, A. S. (2004). Fibroblast response to a controlled nanoenvironment produced by colloidal lithography. Journal of Biomedical Materials Research Part A, 69(2), 314-322.

De Vos, W. H., Houben, F., Hoebe, R. A., Hennekam, R., van Engelen, B., Manders, E. M., ... & Van Oostveldt, P. (2010). Increased plasticity of the nuclear envelope and hypermobility of telomeres due to the loss of A–type lamins. Biochimica et Biophysica Acta (BBA)-General Subjects, 1800(4), 448-458.

Deguchi, S., Maeda, K., Ohashi, T., & Sato, M. (2005). Flow-induced hardening of endothelial nucleus as an intracellular stress-bearing organelle. Journal of biomechanics, 38(9), 1751-1759.

Denais, C., & Lammerding, J. (2014). Nuclear mechanics in cancer. In Cancer Biology and the Nuclear Envelope (pp. 435-470). Springer New York.

Dhandayuthapani, B., Yoshida, Y., Maekawa, T., & Kumar, D. S. (2011). Polymeric scaffolds in tissue engineering application: a review. International Journal of Polymer Science, 2011.

Dhowre, H. S., Rajput, S., Russell, N. A., & Zelzer, M. (2015). Responsive cell–material interfaces. Nanomedicine, 10(5), 849-871.

Discher, D. E., Janmey, P., & Wang, Y. L. (2005). Tissue cells feel and respond to the stiffness of their substrate. Science, 310(5751), 1139-1143.

DuFort, C. C., Paszek, M. J., & Weaver, V. M. (2011). Balancing forces: architectural control of mechanotransduction. Nature reviews Molecular cell biology, 12(5), 308-319.

Ermis, M. (2016). Influence of micropatterned polymeric substrates on cancer cell behavior (Doctoral dissertation, Middle East Technical University).

Ermis, M., Akkaynak, D., Chen, P., Demirci, U., & Hasirci, V. (2016). A high throughput approach for analysis of cell nuclear deformability at single cell level. Scientific reports, 6.

Evans, M. D., Pavon-Djavid, G., Hélary, G., Legeais, J. M., & Migonney, V. (2004). Vitronectin is significant in the adhesion of lens epithelial cells to PMMA polymers. Journal of Biomedical Materials Research Part A, 69(3), 469-476.

Flemming, R. G., Murphy, C. J., Abrams, G. A., Goodman, S. L., & Nealey, P. F. (1999). Effects of synthetic micro-and nano-structured surfaces on cell behavior. Biomaterials, 20(6), 573-588.

Fletcher, D. A., & Mullins, R. D. (2010). Cell mechanics and the cytoskeleton. Nature, 463(7280), 485-492.

Flitney, E. W., Kuczmarski, E. R., Adam, S. A., & Goldman, R. D. (2009). Insights into the mechanical properties of epithelial cells: the effects of shear stress on the assembly and remodeling of keratin intermediate filaments. The FASEB Journal, 23(7), 2110-2119.

Friedl, P., Wolf, K., & Lammerding, J. (2011). Nuclear mechanics during cell migration. Current opinion in cell biology, 23(1), 55-64.

Geiger, B., Bershadsky, A., Pankov, R., & Yamada, K. M. (2001). Transmembrane crosstalk between the extracellular matrix and the cytoskeleton. Nature Reviews Molecular Cell Biology, 2(11), 793-805.

Geltmeier, A., Rinner, B., Bade, D., Meditz, K., Witt, R., Bicker, U., ... & Maier, P. (2015). Characterization of dynamic behaviour of MCF7 and MCF10A cells in ultrasonic field using modal and harmonic analyses. PloS one, 10(8), e0134999.

Georges, P. C., & Janmey, P. A. (2005). Cell type-specific response to growth on soft materials. Journal of applied physiology, 98(4), 1547-1553.

Ghibaudo, M., Trichet, L., Le Digabel, J., Richert, A., Hersen, P., & Ladoux, B. (2009). Substrate topography induces a crossover from 2D to 3D behavior in fibroblast migration. Biophysical journal, 97(1), 357-368.

Glenn, H. L., Messner, J., & Meldrum, D. R. (2016). A simple non-perturbing cell migration assay insensitive to proliferation effects. Scientific reports, 6.

Green, A. M., Jansen, J. A., Van der Waerden, J. P. C. M., & Von Recum, A. F. (1994). Fibroblast response to microtextured silicone surfaces: texture orientation into or out of the surface. Journal of Biomedical Materials Research Part A, 28(5), 647-653.

Greiner, A. M., Sales, A., Chen, H., Biela, S. A., Kaufmann, D., & Kemkemer, R. (2016). Nano-and microstructured materials for in vitro studies of the physiology of vascular cells. Beilstein journal of nanotechnology, 7, 1620.

Gruenbaum, Y., Margalit, A., Goldman, R. D., Shumaker, D. K., & Wilson, K. L. (2005). The nuclear lamina comes of age. Nature reviews Molecular cell biology, 6(1), 21-31.

Guck, J., Schinkinger, S., Lincoln, B., Wottawah, F., Ebert, S., Romeyke, M., ... & Käs, J. (2005). Optical deformability as an inherent cell marker for testing

malignant transformation and metastatic competence. Biophysical journal,88(5), 3689-3698.

Guilak, F. (1995). Compression-induced changes in the shape and volume of the chondrocyte nucleus. Journal of biomechanics, 28(12), 1529-1541.

Guilak, F., Tedrow, J. R., & Burgkart, R. (2000). Viscoelastic properties of the cell nucleus. Biochemical and biophysical research communications, 269(3), 781-786.

Gunatillake, P. A., & Adhikari, R. (2003). Biodegradable synthetic polymers for tissue engineering. Eur Cell Mater, 5(1), 1-16.

Gutiérrez-Fernández, A., Soria-Valles, C., Osorio, F. G., Gutiérrez-Abril, J., Garabaya, C., Aguirre, A., ... & López-Otín, C. (2015). Loss of MT1-MMP causes cell senescence and nuclear defects which can be reversed by retinoic acid. The EMBO journal, 34(14), 1875-1888.

Halliday, N. L., & Tomasek, J. J. (1995). Mechanical properties of the extracellular matrix influence fibronectin fibril assembly in vitro. Experimental cell research, 217(1), 109-117.

Harrison, R. G. (1911). On the stereotropism of embryonic cells. Science, 34(870), 279-281.

Hasirci, V., & Kenar, H. (2006). Novel surface patterning approaches for tissue engineering and their effect on cell behavior.

Hasirci, V., Vrana, E., Zorlutuna, P., Ndreu, A., Yilgor, P., Basmanav, F. B., & Aydin, E. (2006). Nanobiomaterials: a review of the existing science and technology, and new approaches. Journal of Biomaterials Science, Polymer Edition, 17(11), 1241-1268.

Hasturk, O., Sivas, A., Karasozen, B., Demirci, U., Hasirci, N., & Hasirci, V. (2016). Quantification of Type, Timing, and Extent of Cell Body and Nucleus

Deformations Caused by the Dimensions and Hydrophilicity of Square Prism Micropillars. Advanced healthcare materials, 5(23), 2972-2982.

Hayot, C., Debeir, O., Van Ham, P., Van Damme, M., Kiss, R., & Decaestecker, C. (2006). Characterization of the activities of actin-affecting drugs on tumor cell migration. Toxicology and applied pharmacology, 211(1), 30-40.

Huang, H., Sylvan, J., Jonas, M., Barresi, R., So, P. T., Campbell, K. P., & Lee, R. T. (2005). Cell stiffness and receptors: evidence for cytoskeletal subnetworks. American Journal of Physiology-Cell Physiology, 288(1), C72-C80.

Hudson, M. E., Pozdnyakova, I., Haines, K., Mor, G., & Snyder, M. (2007). Identification of differentially expressed proteins in ovarian cancer using high-density protein microarrays. Proceedings of the National Academy of Sciences,104(44), 17494-17499.

Ingber, D. E. (1998). The architecture of life. Scientific American, 278(1), 48-57.

Ingber, D. E. (2003). Tensegrity I. Cell structure and hierarchical systems biology. Journal of cell science, 116(7), 1157-1173.

Ingber, D. E., Prusty, D., Sun, Z., Betensky, H., & Wang, N. (1995). Cell shape, cytoskeletal mechanics, and cell cycle control in angiogenesis. Journal of biomechanics, 28(12), 1471-1484.

Isermann, P., & Lammerding, J. (2013). Nuclear mechanics and mechanotransduction in health and disease. Current Biology, 23(24), R1113-R1121.

Katti, K. S. (2004). Biomaterials in total joint replacement. Colloids and Surfaces B: Biointerfaces, 39(3), 133-142.

Kawaguchi, T., Lassila, L. V., Tokue, A., Takahashi, Y., & Vallittu, P. K. (2011). Influence of molecular weight of polymethyl (methacrylate) beads on the

properties and structure of cross-linked denture base polymer. Journal of the mechanical behavior of biomedical materials, 4(8), 1846-1851.

Keselowsky, B. G., Wang, L., Schwartz, Z., Garcia, A. J., & Boyan, B. D. (2007). Integrin α5 controls osteoblastic proliferation and differentiation responses to titanium substrates presenting different roughness characteristics in a roughness independent manner. Journal of Biomedical Materials Research Part A, 80(3), 700-710.

Khorasani, M. T., Mirzadeh, H., & Irani, S. (2008). Plasma surface modification of poly (L-lactic acid) and poly (lactic-co-glycolic acid) films for improvement of nerve cells adhesion. Radiation Physics and Chemistry, 77(3), 280-287.

Kim, E. J., Boehm, C. A., Mata, A., Fleischman, A. J., Muschler, G. F., & Roy, S. (2010). Post microtextures accelerate cell proliferation and osteogenesis. Acta biomaterialia, 6(1), 160-169.

Koch, T. M., Münster, S., Bonakdar, N., Butler, J. P., & Fabry, B. (2012). 3D traction forces in cancer cell invasion. PloS one, 7(3), e33476.

Kollmannsberger, P., & Fabry, B. (2011). Linear and nonlinear rheology of living cells. Annual review of materials research, 41, 75-97.

Krause, M., & Wolf, K. (2015). Cancer cell migration in 3D tissue: Negotiating space by proteolysis and nuclear deformability. Cell adhesion & migration, 9(5), 357-366.

Kumar, P., Zamani Esteki, M., Van der Aa, N., & Voet, T. (2013). How to analyse a single blastomere? Application of whole-genome technologies: micro-arrays and next generation sequencing.

Landel, R. F., & Nielsen, L. E. (1993). Mechanical properties of polymers and composites. CRC Press.

Latz, C., Migonney, V., Pavon-Djavid, G., Rieck, P., Hartmann, C., Latz, C., ... & Legeais, J. M. (2000). Inhibition of lens epithelial cell proliferation by substituted PMMA intraocular lenses. Graefe's archive for clinical and experimental ophthalmology, 238(8), 696-700.

Lecuit, T., & Lenne, P. F. (2007). Cell surface mechanics and the control of cell shape, tissue patterns and morphogenesis. Nature Reviews Molecular Cell Biology, 8(8), 633-644.

Lekka, M., Laidler, P., Gil, D., Lekki, J., Stachura, Z., & Hrynkiewicz, A. Z. (1999). Elasticity of normal and cancerous human bladder cells studied by scanning force microscopy. European Biophysics Journal, 28(4), 312-316.

Li, J., Han, D., & Zhao, Y. P. (2014). Kinetic behaviour of the cells touching substrate: the interfacial stiffness guides cell spreading. Scientific reports, 4, 3910.

Li, Q. S., Lee, G. Y. H., Ong, C. N., & Lim, C. T. (2008). AFM indentation study of breast cancer cells. Biochemical and biophysical research communications,374(4), 609-613.

Lodish, H., Berk, A., Zipursky, S. L., Matsudaira, P., Baltimore, D., & Darnell, J. (2003). Molecular cell biology 5th edition. National Center for Biotechnology Informations Bookshelf.

Ma, Z., Mao, Z., & Gao, C. (2007). Surface modification and property analysis of biomedical polymers used for tissue engineering. Colloids and Surfaces B: Biointerfaces, 60(2), 137-157.

Macaulay, I. C., & Voet, T. (2014). Single cell genomics: advances and future perspectives. PLoS Genet, 10(1), e1004126.

Maniotis, A. J., Chen, C. S., & Ingber, D. E. (1997). Demonstration of mechanical connections between integrins, cytoskeletal filaments, and nucleoplasm that

stabilize nuclear structure. Proceedings of the National Academy of Sciences, 94(3), 849-854.

Mathur, A. B., Reichert, W. M., & Truskey, G. A. (2007). Flow and high affinity binding affect the elastic modulus of the nucleus, cell body and the stress fibers of endothelial cells. Annals of biomedical engineering, 35(7), 1120-1130.

Matsumoto, A., Hieda, M., Yokoyama, Y., Nishioka, Y., Yoshidome, K., Tsujimoto, M., & Matsuura, N. (2015). Global loss of a nuclear lamina component, lamin A/C, and LINC complex components SUN1, SUN2, and nesprin-2 in breast cancer. Cancer medicine, 4(10), 1547-1557.

Matsuzaka, K., Walboomers, X. F., Yoshinari, M., Inoue, T., & Jansen, J. A. (2003). The attachment and growth behavior of osteoblast-like cells on microtextured surfaces. Biomaterials, 24(16), 2711-2719.

Mattila, P. K., & Lappalainen, P. (2008). Filopodia: molecular architecture and cellular functions. Nature reviews Molecular cell biology, 9(6), 446-454.

McDonald, E. S., Mankoff, D. A., & Mach, R. H. (2016). Novel strategies for breast cancer imaging: new imaging agents to guide treatment. Journal of Nuclear Medicine, 57(Supplement 1), 69S-74S.

McGregor, A. L., Hsia, C. R., & Lammerding, J. (2016). Squish and squeeze—the nucleus as a physical barrier during migration in confined environments. Current opinion in cell biology, 40, 32-40.

Melnikov, A. A., Gartenhaus, R. B., Levenson, A. S., Motchoulskaia, N. A., & Levenson, V. V. (2005). MSRE-PCR for analysis of gene-specific DNA methylation. Nucleic acids research, 33(10), e93-e93.

Michaelis, S., Robelek, R., & Wegener, J. (2011). Studying cell–surface interactions in vitro: a survey of experimental approaches and techniques. In Tissue engineering III: cell-surface interactions for tissue culture (pp. 33-66). Springer Berlin Heidelberg.

Miller, D. C., Thapa, A., Haberstroh, K. M., & Webster, T. J. (2004). Endothelial and vascular smooth muscle cell function on poly (lactic-co-glycolic acid) with nano-structured surface features. Biomaterials, 25(1), 53-61.

Mitra, S. K., Hanson, D. A., & Schlaepfer, D. D. (2005). Focal adhesion kinase: in command and control of cell motility. Nature reviews Molecular cell biology, 6(1), 56-68.

Moroni, L., & Lee, L. P. (2009). Micropatterned hot-embossed polymeric surfaces influence cell proliferation and alignment. Journal of Biomedical Materials Research Part A, 88(3), 644-653.

Naderi, H., Matin, M. M., & Bahrami, A. R. (2011). Critical issues in tissue engineering: biomaterials, cell sources, angiogenesis, and drug delivery systems. Journal of biomaterials applications, 26(4), 383-417.

Nagayama, K., Hamaji, Y., Sato, Y., & Matsumoto, T. (2015). Mechanical trapping of the nucleus on micropillared surfaces inhibits the proliferation of vascular smooth muscle cells but not cervical cancer HeLa cells. Journal of biomechanics, 48(10), 1796-1803.

Neuman, K. C., & Nagy, A. (2008). Single-molecule force spectroscopy: optical tweezers, magnetic tweezers and atomic force microscopy. Nature methods, 5(6), 491-505.

Nikkhah, M., Edalat, F., Manoucheri, S., & Khademhosseini, A. (2012). Engineering microscale topographies to control the cell–substrate interface.Biomaterials, 33(21), 5230-5246.

O'Brien, F. J. (2011). Biomaterials & scaffolds for tissue engineering. Materials today, 14(3), 88-95.

Otto, O., Rosendahl, P., Mietke, A., Golfier, S., Herold, C., Klaue, D., ... & Wobus, M. (2015). Real-time deformability cytometry: on-the-fly cell mechanical phenotyping. Nature methods, 12(3), 199-202.

Ozcan, C., & Hasirci, N. (2007). Plasma modification of PMMA films: surface free energy and cell-attachment studies. Journal of Biomaterials Science, Polymer Edition, 18(6), 759-773.

Özçelik, H., Padeste, C., & Hasirci, V. (2014). Systematically organized nanopillar arrays reveal differences in adhesion and alignment properties of BMSC and Saos-2 cells. Colloids and Surfaces B: Biointerfaces, 119, 71-81.

Paszek, M. J., Zahir, N., Johnson, K. R., Lakins, J. N., Rozenberg, G. I., Gefen, A., ... & Hammer, D. A. (2005). Tensional homeostasis and the malignant phenotype. Cancer cell, 8(3), 241-254.

Piskin, E. (1995). Biodegradable polymers as biomaterials. Journal of Biomaterials Science, Polymer Edition, 6(9), 775-795.

Popat, K. C., Chatvanichkul, K. I., Barnes, G. L., Latempa, T. J., Grimes, C. A., & Desai, T. A. (2007). Osteogenic differentiation of marrow stromal cells cultured on nanoporous alumina surfaces. Journal of Biomedical Materials Research Part A, 80(4), 955-964.

Punet, X., Mauchauffe, R., Rodríguez-Cabello, J. C., Alonso, M., Engel, E., & Mateos-Timoneda, M. A. (2015). Biomolecular functionalization for enhanced cell–material interactions of poly (methyl methacrylate) surfaces. Regenerative biomaterials, 2(3), 167-175.

Ranella, A., Barberoglou, M., Bakogianni, S., Fotakis, C., & Stratakis, E. (2010). Tuning cell adhesion by controlling the roughness and wettability of 3D micro/nano silicon structures. Acta biomaterialia, 6(7), 2711-2720.

Recknor, J. B., Recknor, J. C., Sakaguchi, D. S., & Mallapragada, S. K. (2004). Oriented astroglial cell growth on micropatterned polystyrene substrates. Biomaterials, 25(14), 2753-2767.

Roach, P., Eglin, D., Rohde, K., & Perry, C. C. (2007). Modern biomaterials: a review—bulk properties and implications of surface modifications. Journal of Materials Science: Materials in Medicine, 18(7), 1263-1277.

Roach, P., Shirtcliffe, N. J., & Newton, M. I. (2008). Progess in superhydrophobic surface development. Soft matter, 4(2), 224-240.

Rother, J., Nöding, H., Mey, I., & Janshoff, A. (2014). Atomic force microscopy-based microrheology reveals significant differences in the viscoelastic response between malign and benign cell lines. Open biology, 4(5), 140046.

Rowat, A. C., Lammerding, J., Herrmann, H., & Aebi, U. (2008). Towards an integrated understanding of the structure and mechanics of the cell nucleus. Bioessays, 30(3), 226-236.

Schindelin, J., Arganda-Carreras, I., Frise, E., Kaynig, V., Longair, M., Pietzsch, T., ... & Tinevez, J. Y. (2012). Fiji: an open-source platform for biological-image analysis. Nature methods, 9(7), 676-682.

Schindelin, J., Rueden, C. T., Hiner, M. C., & Eliceiri, K. W. (2015). The ImageJ ecosystem: An open platform for biomedical image analysis. Molecular reproduction and development, 82(7-8), 518-529.

Scholzen, T., & Gerdes, J. (2000). The Ki-67 protein: from the known and the unknown. Journal of cellular physiology, 182(3), 311-322.

Schulze, C., Lochner, K., Jonitz, A., Lenz, R., Duettmann, O., Hansmann, D., & Bader, R. (2013). Cell viability, collagen synthesis and cytokine expression in human osteoblasts following incubation with generated wear particles using different bone cements. International journal of molecular medicine, 32(1), 227-234.

Serth, J., Kuczyk, M. A., Paeslack, U., Lichtinghagen, R., & Jonas, U. (2000). Quantitation of DNA extracted after micropreparation of cells from frozen and

formalin-fixed tissue sections. The American journal of pathology, 156(4), 1189-1196.

Shankar, J., & Nabi, I. R. (2015). Actin cytoskeleton regulation of epithelial mesenchymal transition in metastatic cancer cells. PloS one, 10(3), e0119954.

Shirtcliffe, N. J., McHale, G., Newton, M. I., & Perry, C. C. (2005). Wetting and wetting transitions on copper-based super-hydrophobic surfaces. Langmuir,21(3), 937-943.

Sieminski, A. L., Hebbel, R. P., & Gooch, K. J. (2004). The relative magnitudes of endothelial force generation and matrix stiffness modulate capillary morphogenesis in vitro. Experimental cell research, 297(2), 574-584.

Staunton, J. R., Doss, B. L., Lindsay, S., & Ros, R. (2016). Correlating confocal microscopy and atomic force indentation reveals metastatic cancer cells stiffen during invasion into collagen I matrices. Scientific reports, 6, 19686.

Subik, K., Lee, J. F., Baxter, L., Strzepek, T., Costello, D., Crowley, P., ... & Tang, P. (2010). The expression patterns of ER, PR, HER2, CK5/6, EGFR, Ki-67 and AR by immunohistochemical analysis in breast cancer cell lines. Breast cancer: basic and clinical research, 4, 35.

Suresh, S. (2007). Biomechanics and biophysics of cancer cells. Acta Materialia, 55(12), 3989-4014.

Swift, J., & Discher, D. E. (2014). The nuclear lamina is mechano-responsive to ECM elasticity in mature tissue. J Cell Sci, 127(14), 3005-3015.

Tsimbouri, P. M. (2015). Adult Stem Cell Responses to Nanostimuli. Journal of functional biomaterials, 6(3), 598-622.

Unal, M., Alapan, Y., Jia, H., Varga, A. G., Angelino, K., Aslan, M., ... & Gurkan, U. A. (2014). Micro and nano-scale technologies for cell mechanics. Nanobiomedicine, 1, 5.

Uzer, G., Rubin, C. T., & Rubin, J. (2016). Cell Mechanosensitivity Is Enabled by the LINC Nuclear Complex. Current Molecular Biology Reports, 2(1), 36-47.

Van Diest, P. J., Brugal, G., & Baak, J. P. (1998). Proliferation markers in tumours: interpretation and clinical value. Journal of clinical pathology, 51(10), 716.

Versaevel, M., Grevesse, T., & Gabriele, S. (2012). Spatial coordination between cell and nuclear shape within micropatterned endothelial cells. Nature communications, 3, 671.

Vesel, A., & Mozetic, M. (2012). Surface modification and ageing of PMMA polymer by oxygen plasma treatment. Vacuum, 86(6), 634-637.

Wang, L., & Carrier, R. L. (2011). Biomimetic topography: bioinspired cell culture substrates and scaffolds. INTECH Open Access Publisher.

Watt, F. M., Jordan, P. W., & O'Neill, C. H. (1988). Cell shape controls terminal differentiation of human epidermal keratinocytes. Proceedings of the National Academy of Sciences, 85(15), 5576-5580.

Webb, K., Hlady, V., & Tresco, P. A. (1998). Relative importance of surface wettability and charged functional groups on NIH 3T3 fibroblast attachment, spreading, and cytoskeletal organization. Journal of biomedical materials research, 41(3), 422.

Wenzel, R. N. (1936). Resistance of solid surfaces to wetting by water.Industrial & Engineering Chemistry, 28(8), 988-994.

Wojciak-Stothard, B., Curtis, A., Monaghan, W., Macdonald, K., & Wilkinson, C. (1996). Guidance and activation of murine macrophages by nanometric scale topography. Experimental cell research, 223(2), 426-435.

Yang, Y., Wang, K., Gu, X., & Leong, K. W. (2017). Biophysical Regulation of Cell Behavior—Cross Talk between Substrate Stiffness and Nanotopography. Engineering, 3(1), 36-54.

Yuan, Y., He, H., & Lee, L. J. (2009). Protein A-based antibody immobilization onto polymeric microdevices for enhanced sensitivity of enzyme-linked immunosorbent assay. Biotechnology and bioengineering, 102(3), 891-901.

Zambonin, G., Colucci, S., Cantatore, F., & Grano, M. (1998). Response of human osteoblasts to polymethylmetacrylate in vitro. Calcified tissue international, 62(4), 362-365.

Zhu, C., Bao, G., & Wang, N. (2000). Cell mechanics: mechanical response, cell adhesion, and molecular deformation. Annual review of biomedical engineering, 2(1), 189-226.

Zink, D., Fischer, A. H., & Nickerson, J. A. (2004). Nuclear structure in cancer cells. Nature reviews cancer, 4(9), 677-687.

APPENDIX A

ALAMAR BLUE ASSAY

Reduction (%) = (((ε "ox")"λ_2" x A "λ_1")-((ε "ox")"λ_1" x A "λ_2"))/(((ε "red")"λ_1" x A’ "λ_2")-((ε "red")"λ_2" x A’ "λ_1")) x 100

where,

λ_1 = 570 nm

λ_2 = 595 nm

Aλ_1 and Aλ_2 = Absorbance of cell seeded films,

A'λ_1 and A'λ_2 = Absorbance of the negative control (unseeded unpatterned film)

Molar Extinction Coefficients were:

(Ɛox)λ_1= 80.586 (Ɛred)λ_1= 155.677

(Ɛox)λ_2= 117.216 (Ɛred)λ_2= 14.652

APPENDIX B

STANDARD CURVE FOR DNA QUANTIFICATION

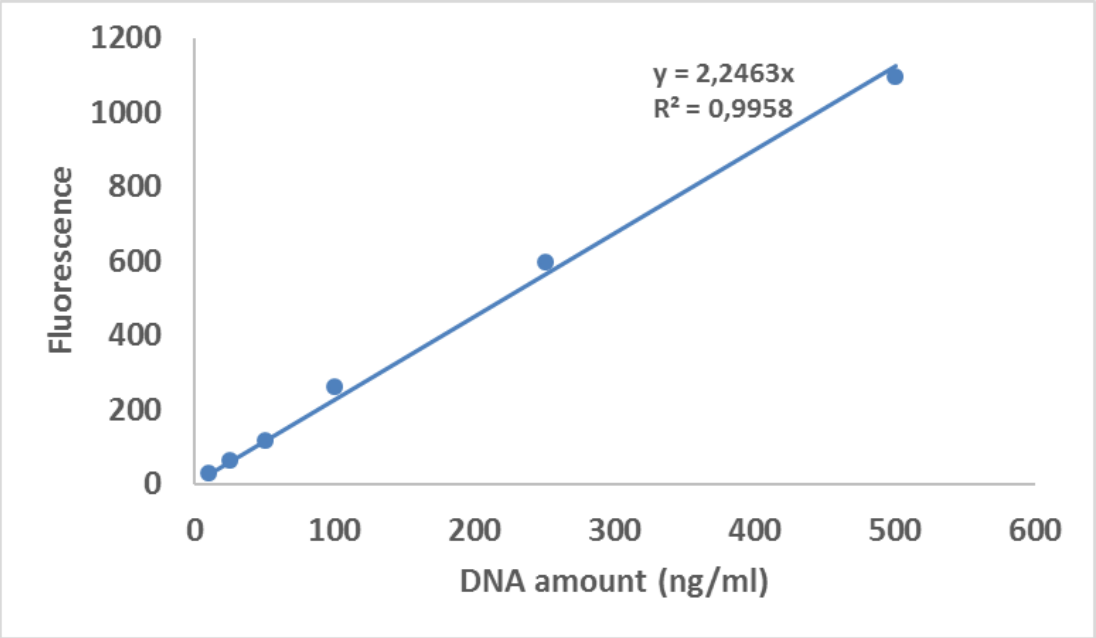

Figure B.1. Standard curve for DNA quantification with PicoGreen.

APPENDIX C

STANDARD AND MELT CURVES OF PRIMERS

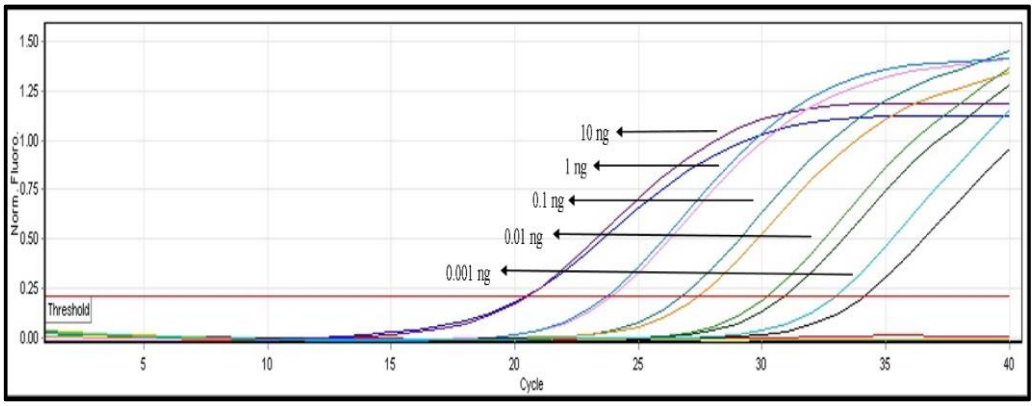

Figure C.1. The amplification of Ki-67 (yellow line: Non-template control)

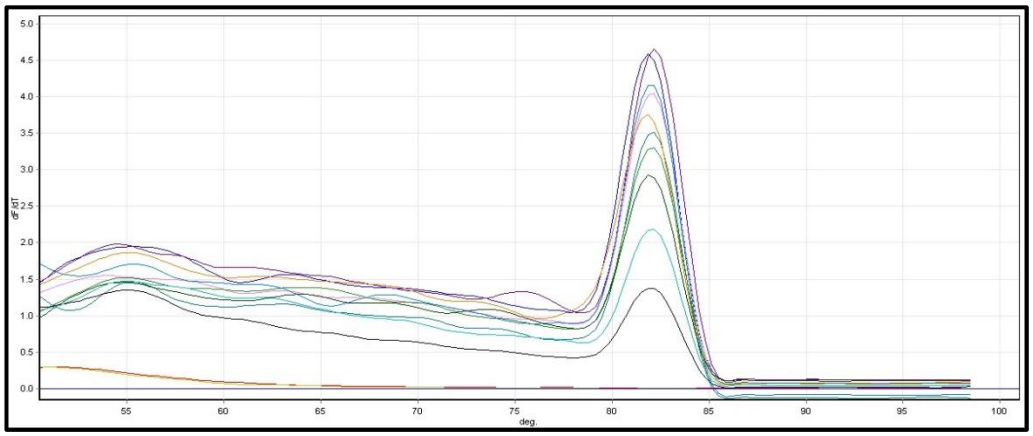

Figure C.2. The melt curve of Ki-67 (yellow line: Non-template control)

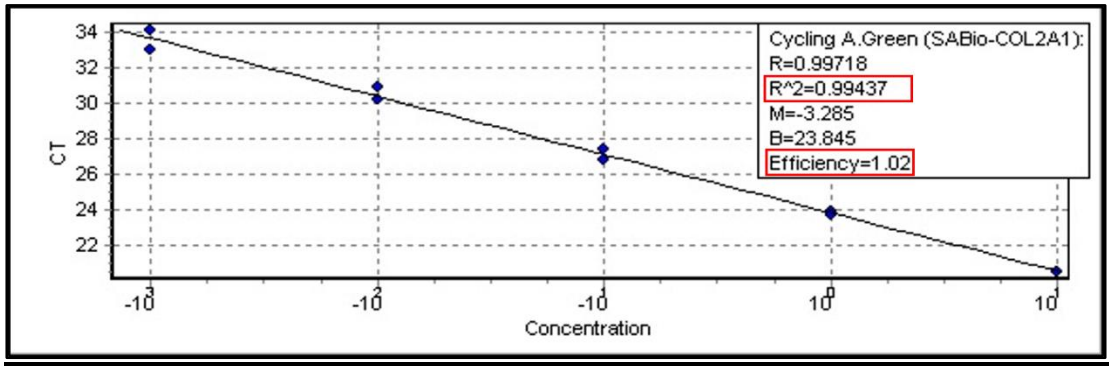

Figure C.3. The standard curve of Ki-67

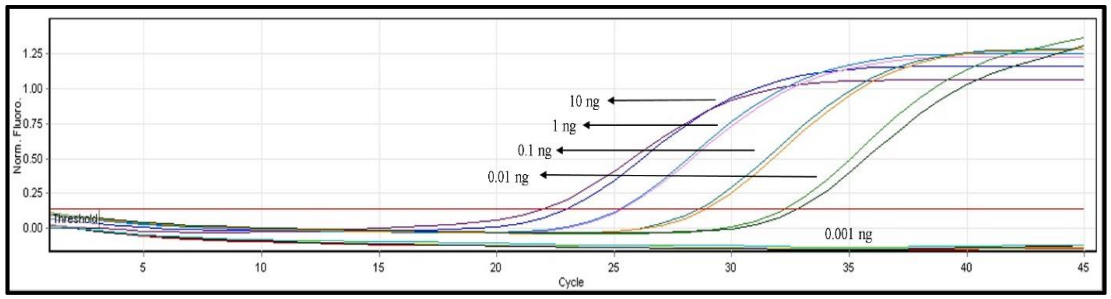

Figure C.4. The amplification of Nesprin-2 reaction (yellow line: Non-template control, blue line: 0.001 ng cDNA template)

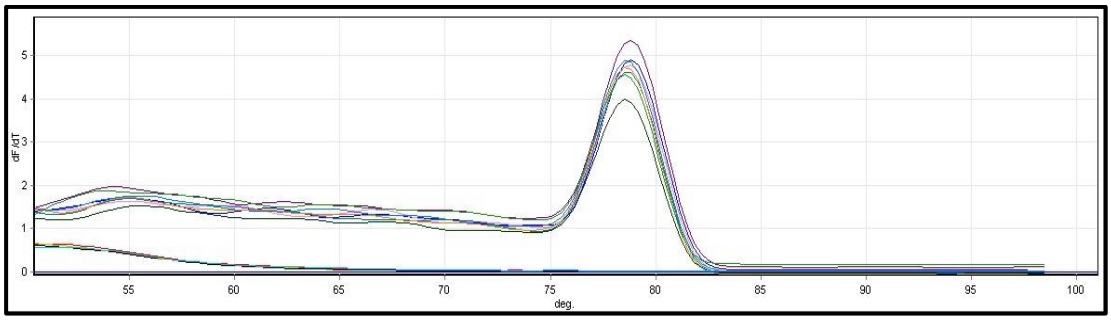

Figure C.5. The melt curve of Nesprin-2 reaction (yellow line: Non-template control, blue line: 0.001 ng cDNA template)

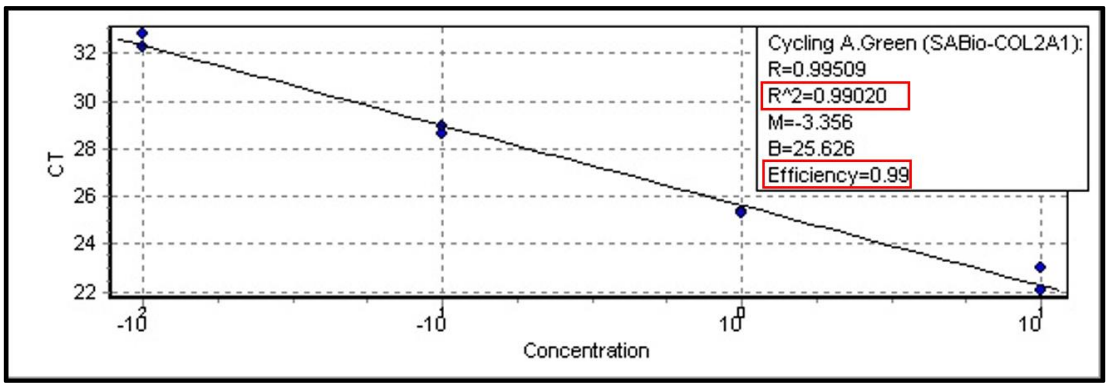

Figure C.6. The standard curve of Nesprin-2.

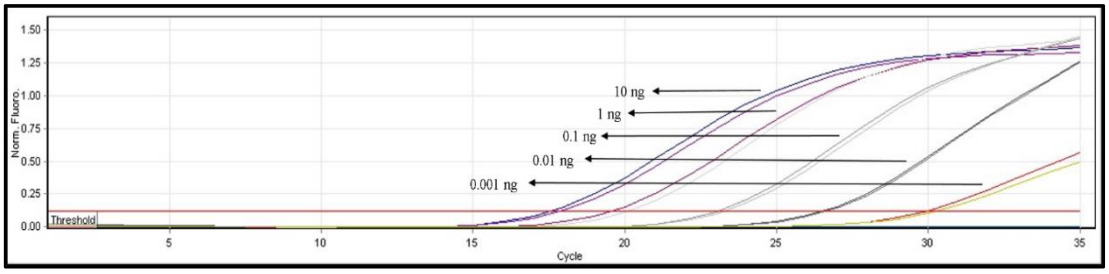

Figure C.7. The amplification of Lamin A/C reaction (blue line: Non-template control)

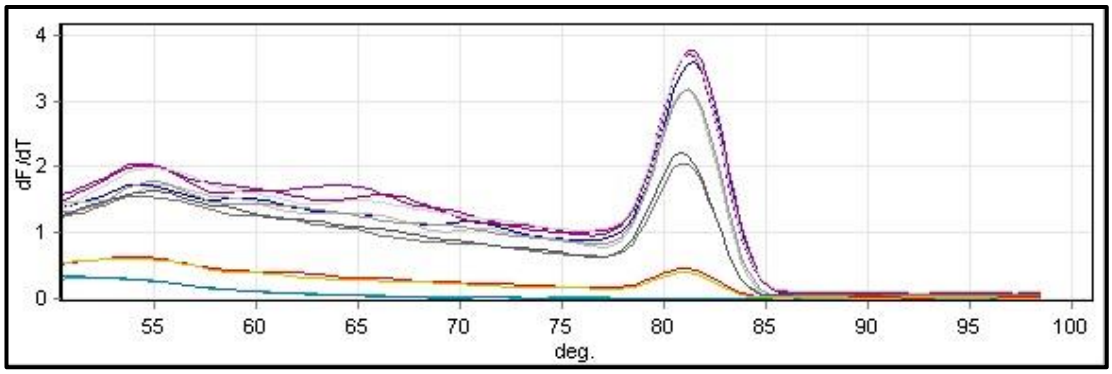

Figure C.8. The melt curve of Lamin A/C reaction (blue line: Non-template control)

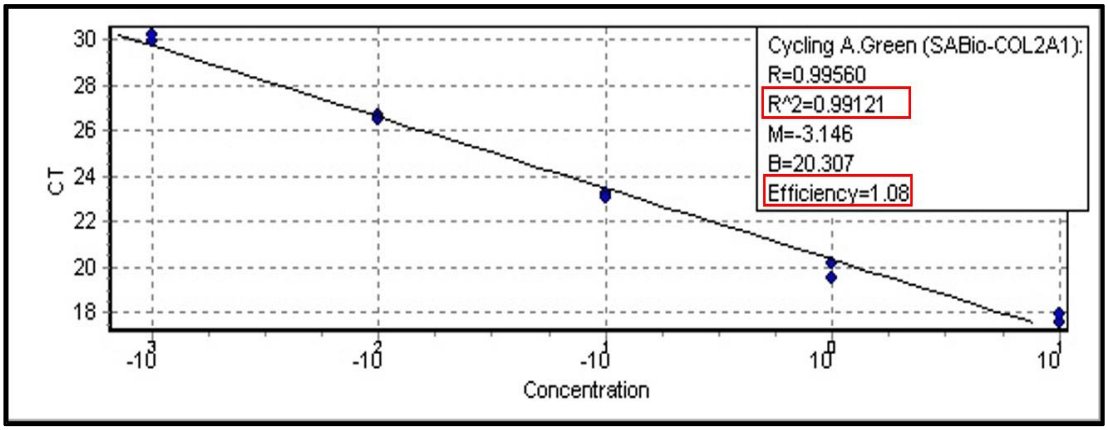

Figure C.9. The standard curve of Lamin A/C

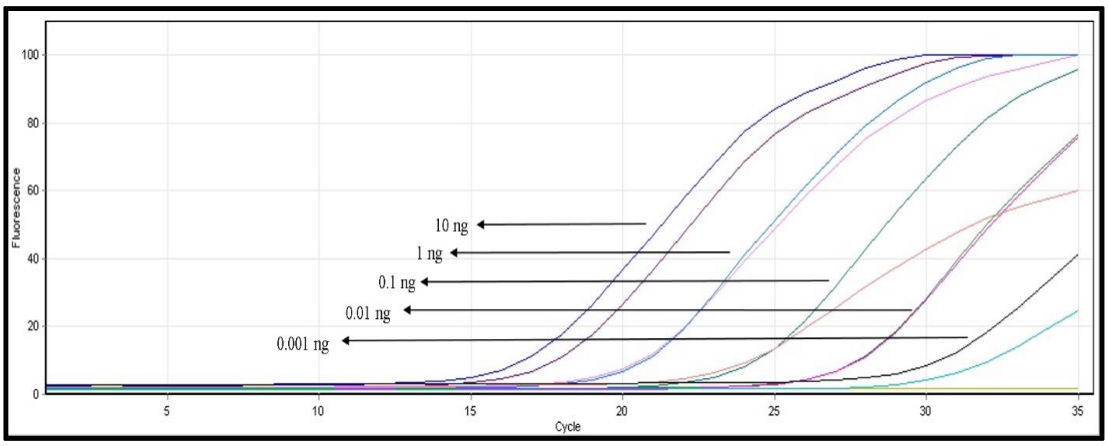

Figure C.10. The amplification of GAPDH reaction (yellow line: Non-template control)

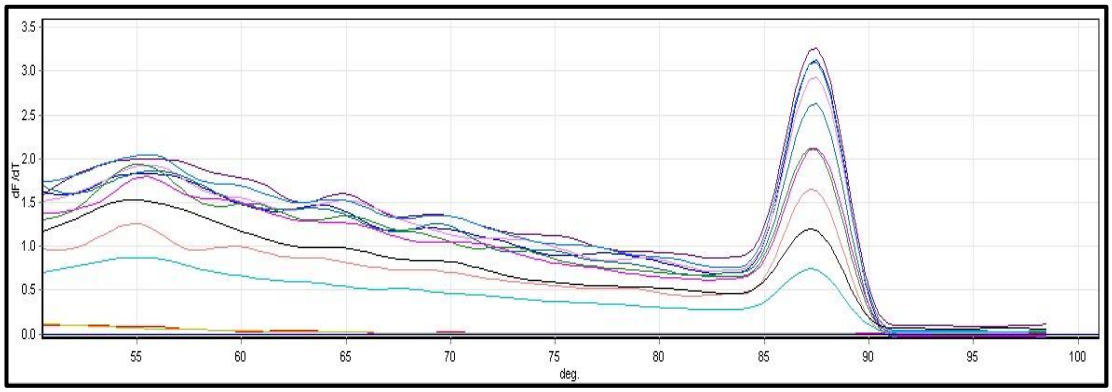

Figure C.11. The melt curve of GAPDH reaction (yellow line: Non-template control)

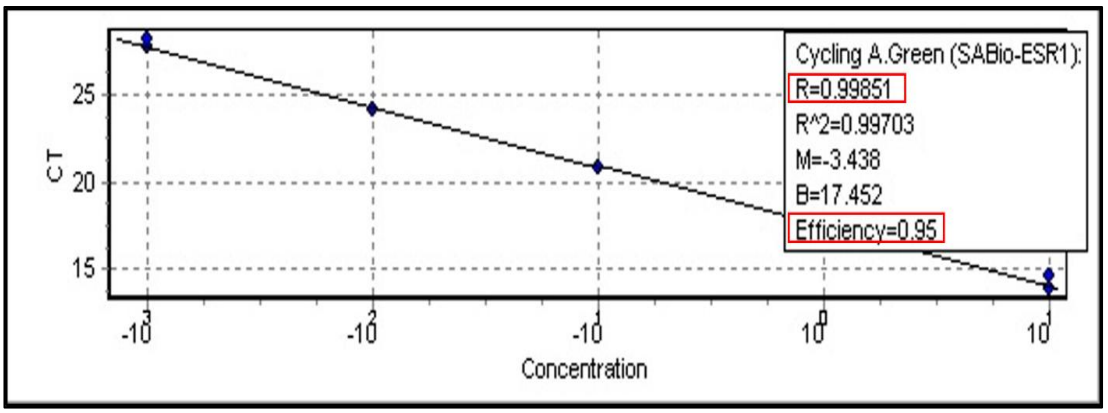

Figure C.12. The standard curve of GAPDH

APPENDIX D

AGAROSE GEL ELECTROPHORESIS

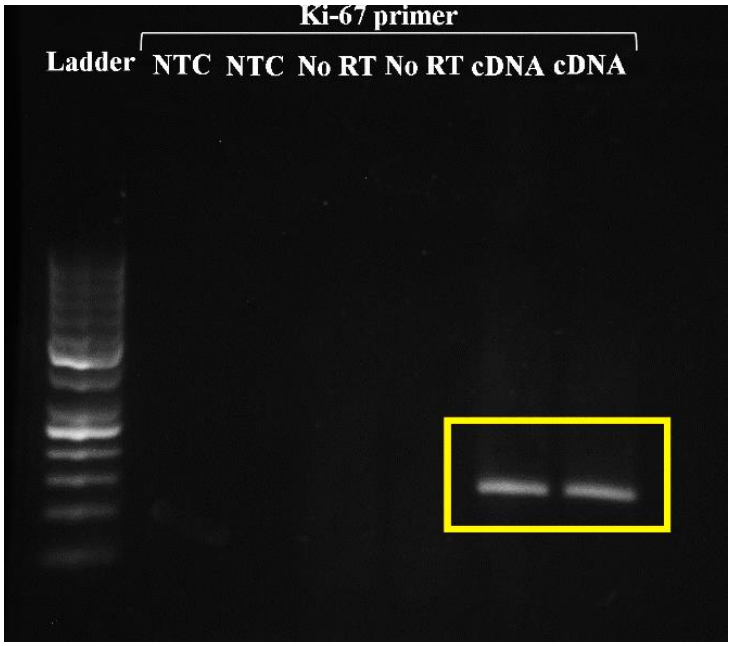

Figure D.1. Agarose gel electrophoresis micrograph of PCR products of Ki-67 primer (NTC: Non-template control, No RT: Negative control (No Reverse Transcriptase (RT) enzyme))

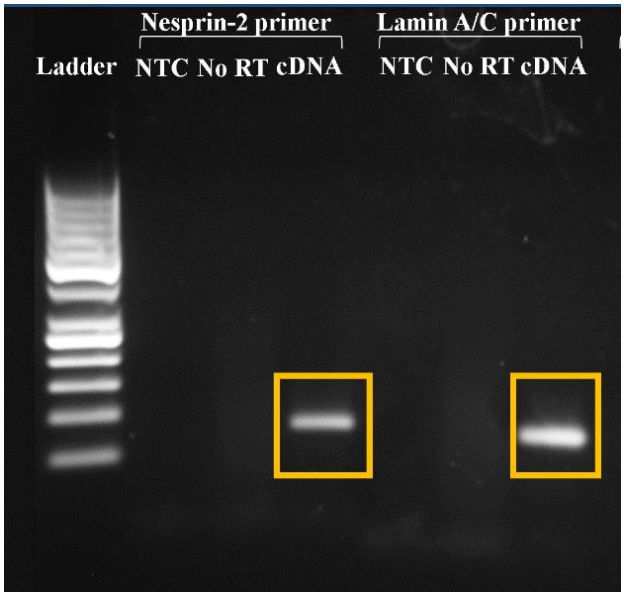

Figure D.2. Agarose gel electrophoresis micrograph of PCR products of Nesprin-2 and Lamin A/C primers (NTC: Non-template control, No RT: Negative control (No Reverse Transcriptase (RT) enzyme))

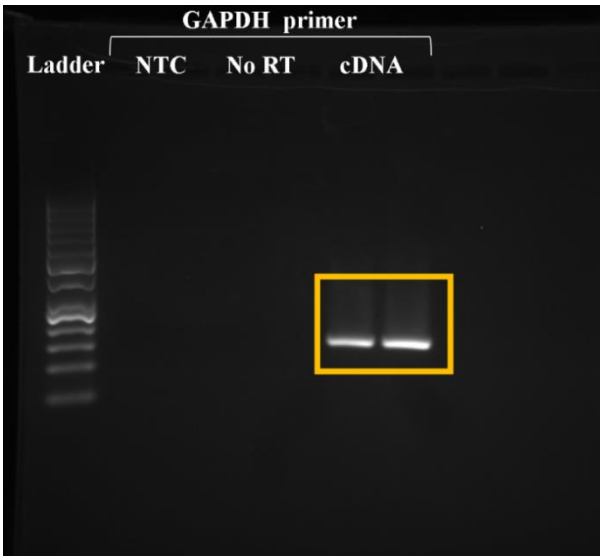

Figure D.3. Agarose gel electrophoresis micrograph of PCR products of GAPDH primer (NTC: Non-template control, No RT: Negative control (No Reverse Transcriptase (RT) enzyme))

CURRICULUM VITAE

PERSONAL INFORMATION

Surname, Name: Antmen, Ezgi
Nationality: Turkish (T.C.)
Date and Place of Birth: 01 July 1988, Adana
Marital Status: Single
Phone: +905051402594
Email: ezgiantmenn@gmail.com, ezgi.antmen@metu.edu.tr

EDUCATION

Degree	Institution	Year of Graduation
MS	METU Biology	2013
BS	METU Molecular Biology and Genetics	2011
High School	Icel Anatolian High School	2006

WORK EXPERIENCE

Year	Place	Enrollment
2010	BAMM Labs, Harvard – MIT Health Sciences and Technology	Visiting Scholar

FOREIGN LANGUAGES

Advanced English

PUBLICATIONS

1. Antmen E., Ermis M., Demirci U., Hasirci V. Engineered Natural and Synthetic Polymer Surfaces Induce Nuclear Deformation in Osteosarcoma Cells. (Submitted to J Biomed Mater Res B Appl Biomater).

2. Antmen E., Demirci U., Hasirci V. Micropatterned Surfaces to Screen Breast Tumor Cells. (In Preparation)

3. Antmen E., Demirci U., Hasirci V. Role of Actin Filaments in the Nuclear Deformability of Breast Tumor Cells. (In Preparation)

4. Ermis, M., Baran, E. T., Dursun, T., Antmen, E., & Hasirci, V. (2014). Contribution of Physical Forces on the Design of Biomimetic Tissue Substitutes. Bio-inspired Materials for Biomedical Engineering, 59-76.

HOBBIES

Scuba diving, Fencing, Badminton, Painting, Reading